

Universidade do Minho
Escola de Engenharia

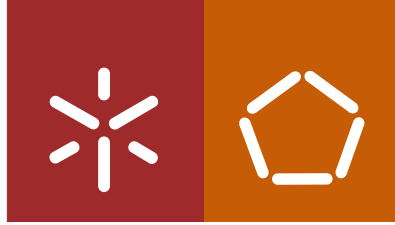
Óscar José Maciel Barros

**Development of Hyaluronic
Acid-Doxorubicin nanogels**

Óscar José Maciel Barros **Development of Hyaluronic Acid-Doxorubicin nanogels**

UMinho | 2016

outubro de 2016



Universidade do Minho
Escola de Engenharia

Óscar José Maciel Barros

**Development of Hyaluronic
Acid-Doxorubicin nanogels**

Dissertação de Mestrado
Mestrado em Bioengenharia

Trabalho efetuado sob a orientação da

Doutora Catarina Gonçalves

e do

Professor Doutor Francisco Miguel Portela da Gama

AGRADECIMENTOS

Gostaria de agradecer a toda a gente que diretamente ou indiretamente me ajudaram na escrita desta tese:

à minha orientadora Doutora Catarina Gonçalves, por todo o conhecimento transmitido neste último ano, por toda a paciência, pela orientação e pela preciosa ajuda na tese para que a mesma chegasse a bom porto;

ao Professor Miguel Gama pela oportunidade que me deu, por tudo o que tive oportunidade de aprender, por fazer parte do seu grupo de trabalho e pela disponibilização do laboratório e equipamentos para a realização desta tese;

aos meus colegas de laboratório, Ana Cristina, Daniela, Dina, Isabel, Ricardo e Salomé, pelas conversas, pelos conselhos, pela boa disposição e em especial por toda a ajuda prestada;

ao Doutor Yoann Lalatonne da Universidade de Paris 13 por gentilmente ter cedido as nanopartículas de ferro e os ensaios que realizou nos meus compostos;

a toda a minha família, em especial aos meus pais, por toda a paciência que tiveram e todos os conselhos e conversas que tivemos durante este último ano;

e por fim a todos os meus colegas de mestrado que de uma forma ou de outra me ajudaram neste último ano.

A todos o meu mais sincero obrigado.

RESUMO

O cancro é a principal causa de morte no mundo. A investigação na área do cancro está em evolução contínua, e tem como objetivo alcançar terapias mais eficientes e diagnósticos precoces. Diferentes desafios vão surgindo, relativamente ao desenvolvimento de sistemas de entrega de fármacos eficientes em comparação com as terapias convencionais, como a quimioterapia. Têm sido desenvolvidas novas formulações que promovam uma distribuição controlada do fármaco, potenciando uma ação farmacêutica seletiva e eficiente. Os nanogéis, produzidos por auto-organização de polímeros naturais quimicamente modificados, são adequados para este objetivo, uma vez que permitem encapsular fármacos hidrofóbicos, de forma física ou química. O uso de ligações lábeis, para estabilizar os fármacos, permite uma libertação seletiva, tais como as ligações hidrazona, sensíveis ao pH. A doxorubicina é um fármaco usado atualmente em quimioterapia, contudo, o seu maior problema é a toxicidade em tecidos saudáveis, quando usada em doses elevadas, e o desenvolvimento de multirresistência durante tratamentos prolongados. A doxorubicina pode ser conjugada ao ácido hialurónico, que é um polímero natural abundante no corpo humano, através de uma ligação hidrazona ou amida. Os principais objetivos deste projeto consistem no desenvolvimento de nanogéis de ácido hialurónico e doxorubicina para tratamento do cancro, assim como a incorporação de $\gamma\text{-Fe}_2\text{O}_3$ nos nanogéis, para o desenvolvimento de formulações teranósticas.

O ácido hialurónico foi modificado quimicamente para se obter um polímero anfifílico, o qual foi conjugado com a doxorubicina por ligação hidrazona ou amida. A quantidade de doxorubicina ligada, o tamanho médio e o índice de polidispersidade foram avaliados. Os nanogéis mais promissores foram ainda estudados em ensaios de libertação a diferentes pH, citotoxicidade e incorporação de $\gamma\text{-Fe}_2\text{O}_3$.

Os conjugados de ácido hialurónico e doxorubicina por ligação hidrazona foram produzidos em tampão PBS pH 7,4, contendo 22 μg DOX/mg, tamanho médio de 100 nm e um índice de polidispersidade de cerca de 0,5. A conjugação por ligação amida foi efetuada em DMSO, o que conduziu a um conteúdo de doxorubicina de 29 μg DOX/mg, tamanho médio de 70 nm e um índice de polidispersidade de cerca de 0,45. Os estudos de libertação indicam uma libertação satisfatória a pH 5,0 (pH dos lisossomas), contudo a pH 7,4 (pH extracelular) verificou-se também alguma libertação. A estabilização de $\gamma\text{-Fe}_2\text{O}_3$ nos nanogéis, designados de nanomagnetogéis, levou à estabilização de 0,6 a 0,9 mM de $\gamma\text{-Fe}_2\text{O}_3$. Os ensaios de citotoxicidade foram realizados com a linha celular A549, e o conjugado

de ácido hialurónico por ligação amida apresentou uma atuação rápida e levou a um decréscimo na viabilidade celular.

Em suma, foram produzidos nanogéis de ácido hialurónico e doxorrubicina usando uma ligação sensível ao pH, hidrazona, e ligação amida. Os nanogéis mostraram características interessantes para sistemas de entrega de fármacos, permitindo assim terapias mais eficientes, apesar de ainda serem necessárias algumas otimizações. A incorporação de $\gamma\text{-Fe}_2\text{O}_3$ foi conseguida nos nanogéis, o que pode permitir a sua deteção por técnicas de imagem para diagnóstico ou para avaliação da terapêutica, ao mesmo tempo que se faz a libertação controlada do fármaco.

Palavras-Chave: Ácido Hialurónico; Doxorrubicina; Nanogéis auto-organizados; $\gamma\text{-Fe}_2\text{O}_3$; Teranósticos.

ABSTRACT

Cancer is the leading cause of death in the world. Cancer research is continuously growing aiming to achieve more efficient therapies and early diagnostics. Different challenges arise, concerning the development of efficient drug delivery systems compared to conventional therapies, such as chemotherapy. New formulations promoting a controlled drug distribution, potentiating selective and efficient pharmaceutical actions, have been developed. Nanogels, produced by self-assembly of chemical modified natural polymers, are suitable for this purpose since they are able to encapsulate the hydrophobic drugs, physically or chemically. The use of labile linkages, to stabilize drugs, allows a selective drug release, such as pH-sensitive hydrazone. Doxorubicin is a drug currently used in chemotherapy, however, a major drawback remains its toxicity to healthy tissues, when used in high dosages, and the development of multi-drug resistance during prolonged treatment. Doxorubicin can be conjugated with hyaluronic acid, a natural polymer abundant in the human body, via hydrazone or amide linkages. The main goals of this work consist in the development of hyaluronic acid-based nanogels for cancer therapy with doxorubicin, as well as the incorporation of $\gamma\text{-Fe}_2\text{O}_3$ into the nanogels to develop a theranostic formulation.

Chemical modifications were performed on the hyaluronic acid to obtain an amphiphilic polymer grafted with doxorubicin via hydrazone or amide linkage. Doxorubicin content, average size and polydispersity index were evaluated. The most promising nanogels were further characterized concerning release profile at different pH, cytotoxicity and physical incorporation of $\gamma\text{-Fe}_2\text{O}_3$.

Hyaluronic acid-doxorubicin conjugates, via hydrazone, were produced in PBS pH 7.4, containing 22 μg DOX/mg, an average size of 100 nm and a polydispersity index around 0.5. The conjugation, via amide, was performed in DMSO, leading to a doxorubicin content of 29 μg DOX/mg, an average size of 70 nm and a polydispersity index around 0.45. The release studies indicated a satisfactory release at pH 5.0 (lysosomal pH) although exhibiting some release at pH 7.4 (extracellular pH). $\gamma\text{-Fe}_2\text{O}_3$ stabilization into nanogels, designed as nanomagnetogels, lead to 0.6-0.9 mM of stabilized $\gamma\text{-Fe}_2\text{O}_3$. Concerning the cytotoxicity assay performed using A549 cell line, hyaluronic acid-doxorubicin conjugate via amide presented a fast action and promoted a decrease in cell viability.

In summary, hyaluronic acid-doxorubicin nanogels were produced using a pH-sensitive linkage, hydrazone, and amide linkage. The nanogels exhibited interesting characteristics for drug delivery applications envisaging more effective therapies, even though further optimizations are required. $\gamma\text{-Fe}_2\text{O}_3$

incorporation was accomplished allowing imaging detection for diagnostic purposes or therapy evaluation along with the controlled drug release.

KEYWORDS: Hyaluronic Acid; Doxorubicin; Self-assembled nanogels; γ -Fe₂O₃; Theranostics;

TABLE OF CONTENT

Agradecimientos.....	iii
Resumo.....	v
Abstract.....	vii
List of Figures.....	xi
List of Tables.....	xv
List of Schemes.....	xvii
List of Abbreviations	xviii
1. Introduction	1
1.1 Nanomedicines in cancer therapy.....	1
1.2 Hyaluronic Acid based nanogels	8
1.3 Doxorubicin.....	10
1.4 Theranostic formulations	12
2. Objectives.....	15
3. Materials and Methods.....	17
3.1 Materials.....	17
3.2 Chemical Reactions.....	17
3.2.1 Amphiphilic HA production.....	17
3.2.2 Doxorubicin conjugation.....	18
3.3 ¹ H NMR.....	22
3.4 Size Distribution	22
3.5 DOX quantification.....	22
3.6 DOX release studies	23
3.7 γ -Fe ₂ O ₃ incorporation	23
3.7.1 γ -Fe ₂ O ₃ incorporation.....	23
3.7.2 γ -Fe ₂ O ₃ quantification	24
3.7.3 Size Distribution and Zeta Potential	24
3.7.4 Magnetic Characterization.....	24
3.8 Cytotoxicity assay	24
4. Results and Discussion	27

4.1	Synthesis of amphiphilic HA	27
4.1.1	Amphiphilic HA production with two different DS	27
4.1.2	Production of amphiphilic HA using theoretical DS 15 %	31
4.2	Production of HA-DOX nanogels.....	34
4.2.1	Hydrazone Linkage	34
4.2.2	Amide Linkage.....	39
4.3	Release Studies.....	42
4.4	γ -Fe ₂ O ₃ incorporation	44
4.5	Cytotoxicity.....	47
5.	Conclusions and Future Perspectives	51
	References	53
	Supplementary Data	59
	• Production of HA-DOX nanogels.....	59
	○ DOX Calibration curve	59
	○ Calculations examples I.....	59
	○ Calculations examples II	60
	• Release Studies.....	61
	• γ -Fe ₂ O ₃ incorporation	62
	• HA 4.0 kDa	63
	○ Amphiphilic HA	63
	○ Production of HA-DOX nanogels.....	64
	○ Release Studies.....	68
	○ γ -Fe ₂ O ₃ incorporation	69
	○ Cytotoxicity.....	72

LIST OF FIGURES

Chapter 1

Figure 1.1: Schematic representation of differences between normal (A) and cancer tissue (B) (Maeda et al., 1989).	2
Figure 1.2: Schematics representation of passive targeting, by exploration of the EPR effect (A), and active targeting (B) using surface decoration (Lammers et al., 2012).	3
Figure 1.3: Schematic diagram showing the relative size of some nanoparticles, biological entities and cells (van Rijt, Bein, & Meiners, 2014)	4
Figure 1.4: Schematic representation of free-drug elimination by a multidrug resistance process. The nanocarrier accumulates by the EPR effect and enters the cell, through endocytosis (mediated by the specific ligand). The increase of drug concentration inside the cell overcomes the efflux pump mediated by drug resistance (Davis et al., 2008).	5
Figure 1.5: Representation of some examples of nanoparticles that can be used. In gray is represented the liposomal bilayer; polymers and polymer-coatings in green; linkers for drug release in blue rectangles; targeting ligands in yellow arrows; imaging agents in orange suns and conjugated or entrapped (chemo-) therapeutic agents in red stars. A-D from Twan Lammers et al., 2012 and E from T. Lammers et al., 2008.	6
Figure 1.6: Chemical structure of HA, the arrows denote the principal places for modifications in the HA structure (Choi et al., 2012).	8
Figure 1.7: Chemical structure of DOX. Functional groups (amine and carbonyl), highlighted with red circles correspond to the coupling sites with the promoieties (Bildstein et al., 2011).	10

Chapter 3

Figure 3.1: Relation between DOX concentration (PBS) and optical absorbance (A) or fluorescence intensity (B) (Mohan & Rapoport, 2010).	23
---	----

Chapter 4

Figure 4.1: ^1H NMR spectra in D_2O of HA-TBA (A) and HA-C ₁₆ NH ₂ (B) for the theoretical DS 30 %	28
Figure 4.2: Average size distribution of a HA _{10.5} solution at 1 mg/mL, 10 consecutive measurements are represented.	29
Figure 4.3: Correlogram of HA _{10.5} with 10 consecutive measurements are represented.	29
Figure 4.4: Average Size (●) and Pdl (■) values obtained for HA _{10.5} (A) and HA _{26.0} (B) over time, with the respective standard deviation (n=10).	30
Figure 4.5: Average size (●) and Pdl (■) values obtained for HA _{8.0} (A), HA _{10.5} (B) and for HA _{12.6} (C) over time, with the respective standard deviation (n=10).	32
Figure 4.6: ^1H NMR of HA _{12.6} (A) and HA _{12.6} -ADH (B), in D_2O	35

Figure 4.7: Average size (●) and Pdl (■) values obtained for HA-ADH _{6.9} over time, with the respective standard deviation (n=10).	36
Figure 4.8: Absorbance spectra of free DOX at 25 µg/mL (●) and 50 µg/mL (○), HA _{Hidra1} 1.0 mg/mL (○), HA _{Hidra2} 1.0 mg/mL (●), HA _{Hidra3} 1.0 mg/mL (●) and HA-ADH 1.0 mg/mL with free DOX at 25 µg/mL (●) when dispersed at PBS buffer pH 7.4.	37
Figure 4.9: Average size (●) and Pdl (■) obtained for the HA-DOX nanogels over time, HA _{Hidra2} (A) and HA _{Hidra3} (B), with the respective standard deviation (n=10).	38
Figure 4.10: Absorbance spectra of free DOX at 25 µg/mL (●), HA _{Ami1} (○), HA _{Ami2} (●) and HA-C ₁₆ NH ₂ 1.0 mg/mL with free DOX 25 µg/mL (●) when dispersed at PBS buffer pH 7.4.	39
Figure 4.11: Average size (●) and Pdl values (■) for the HA-DOX nanogels, HA _{Ami1} (A), HA _{Ami2} (B), with the respective standard deviation (n=10).	40
Figure 4.12: Cumulative release (%) profiles for HA _{Ami2} (◆), HA _{Hidra3} (▲) and free DOX (●), at pH 7.4 (solid line) or pH 5.0 (dashed line), (n=3).	42
Figure 4.13: Result of the iron quantification after the incorporation of γ -Fe ₂ O ₃ into different NG, with the respective standard deviation (n=6).	44
Figure 4.14: Average size (■) and Pdl (■) distribution for HA-DOX conjugates after the incorporation with γ -Fe ₂ O ₃ , (nanomagnetogels), with the respective standard deviation (n=5).	45
Figure 4.15: Zeta Potential of free γ -Fe ₂ O ₃ (■), NG (■) and the nanomagnetogels (■), each value presents its standard deviation, (n=5).	45
Figure 4.16: Magnetization versus magnetic applied field of HA _{Hidra3} (■) and free γ -Fe ₂ O ₃ (■). Nanomagnetogels were dispersed in distilled water pH 7.4, while bare γ -Fe ₂ O ₃ in distilled water pH 2.0.	46
Figure 4.17: Cell viability of A549 cells was determined by MTT assay at 24 h (■), 48 h (■) and 72 h (■). For all nanogels the concentration is represented in mg/mL while for free DOX is expressed in µg/mL.	48

Supplementary Data

Figure S.1: Calibration curve for DOX dissolved in PBS buffer pH 7.4. Absorbance quantified at 488 nm. The curve obtained is $y = 0.0032x - 0.0135$, associated with a square error of 0.9986.	59
Figure S.2: Calibration curve obtained for Fe dissolved in HNO ₃ 2%. Absorbance quantified at 260 nm. The curve obtained is $y = 9708192,1x - 12347,638$, associated with a square error of 0.9999.	62
Figure S.3: Average size (●) and Pdl (■) values obtained for HA _{11.0} , over time, with the respective standard deviation (n=10).	63
Figure S.4: Absorbance spectra of free DOX at 25 µg/mL (●), HA _{Hidra4} 1.0 mg/mL (●) and HA-ADH 1.0 mg/mL with free DOX at 25 µg/mL (●) when dispersed at PBS buffer pH 7.4.	64
Figure S.5: Average size (●) and Pdl (■) values distribution for HA _{Hidra4} with the respective standard deviation (n=10). ...	65
Figure S.6: Absorbance spectra of free DOX at 150 µg/mL (●), HA _{Ami3} (●) and HA-C ₁₆ NH ₂ 1.0 mg/mL with free DOX 25 µg/mL (●) when dispersed at PBS buffer pH 7.4.	66

Figure S.7: Average size (●) and Pdl values (■) values distribution for HA _{Ami3} , with the respective standard deviation (n=10).	67
Figure S.8: Cumulative release (%) profiles for HA _{Ami3} (◆), HA _{Ami4} (▲) and free DOX (●), at pH of 7.4 (solid line) or pH 5.0 (dashed line), (n=3).	68
Figure S.9: Results for the iron quantification after γ -Fe ₂ O ₃ incorporation into the different NG using HA 4.0 kDa, with the respective standard deviation (n=6).	69
Figure S.10: Average size (■) and Pdl (■) distribution for the nanomagnetogels, with the respective standard deviation (n=5).	69
Figure S.11: Results from the Zeta Potential for the free γ -Fe ₂ O ₃ (■), for the nanogel (■) and for the nanomagnetogels (■), each value presents its own standard deviation, (n=5).....	70
Figure S.12: Magnetization versus magnetic applied field of HA _{Ami3} (■) and free γ -Fe ₂ O ₃ (■). Nanomagnetogel was dispersed in distilled water pH 7.4, while bare γ -Fe ₂ O ₃ in distilled water pH 2.0.....	70
Figure S.13: Cell viability of A549 cells was determined by MTT assay at 24 h (■), 48 h (■) and 72 h (■). For all nanogels the concentration is represented in mg/mL while for free DOX is expressed in μ g/mL.	73

LIST OF TABLES

Chapter 4

Table 4.1: Results of the different productions of amphiphilic HA.....	28
Table 4.2: Different batches of amphiphilic HA produced with a theoretical DS of 15 %.....	31
Table 4.3: Results obtained for HA-DOX nanogels, via hydrazone.....	36
Table 4.4: Results obtained for HA-DOX nanogels, via amide.....	39

Supplementary Data

Table S.1: Table containing the results for each NG used in the incorporation of the γ -Fe ₂ O ₃	62
Table S.2: Results from the conjugation of HA-ADH with DOX.....	64
Table S.3: Different conjugations of amphiphilic HA with DOX.....	66

LIST OF SCHEMES

Chapter 3

Scheme 3.1: Representation of the reaction between HA and C ₁₆ NH ₂ performed in DMSO with EDC, NHS and TEA.....	18
Scheme 3.2: Representation of the reaction between the amphiphilic HA and ADH performed with EDC.....	19
Scheme 3.3: Representation of the conjugation between HA-ADH and DOX through an hydrazone linkage.	20
Scheme 3.4: Representation of the conjugation of amphiphilic HA with DOX via amide linkage in DMSO with EDC, NHS and TEA.....	21

LIST OF ABBREVIATIONS

Others

λ_{\max} wavelength with the maximal absorbance

A

ADH Adipic Acid Dihydrazide

ADCs Antibody-Drug Conjugates

B

BD Biodistribution

C

$C_{16}NH_2$ hexadecylamine

D

DDS Drug Delivery Systems

DLS Dynamic Light Scattering

DMSO Dimethyl sulfoxide

DOX Doxorubicin

DS Substitution Degree

$DS_{C_{16}NH_2}$ (%) Substitution Degree for $C_{16}NH_2$

DS_{ADH} (%) Substitution Degree for ADH

E

ECM	extracellular matrix
EDC	1-Ethyl-3-(3-dimethylaminopropyl)carbodiimide

H

HA _{10.5}	Amphiphilic HA with a DS _{C16NH2} of 10.5 %
HA _{11.0}	Amphiphilic HA with a DS _{C16NH2} of 11.0 %, from HA with a MW of 4.0 kDa
HA _{26.0}	Amphiphilic HA with a DS _{C16NH2} of 26.0 %
HA _{8.0}	Amphiphilic HA with a DS _{C16NH2} of 8.0 %
HA-ADH _{6.9}	Amphiphilic HA with a DS _{C16NH2} of 12.6 % and a DS _{ADH} of 6.9%
HA _{Ami1}	HA-DOX conjugated through an amide linkage in DMSO, DS _{C16NH2} of 10.5 %
HA _{Ami2}	HA-DOX conjugated through an amide linkage in DMSO, DS _{C16NH2} of 12.6 %
HA _{Ami3}	HA-DOX conjugated through an amide linkage in DMSO, DS _{C16NH2} of 11.0 %, from HA with a MW of 4.0 kDa
HA _{Hidra1}	HA-DOX conjugated through a hydrazone linkage in DMSO, DS _{C16NH2} of 8.0 % and a DS _{ADH} of 8.7 %
HA _{Hidra2}	HA-DOX conjugated through a hydrazone linkage in PBS, DS _{C16NH2} of 8.0 % and a DS _{ADH} of 8.7 %
HA _{Hidra3}	HA-DOX conjugated through a hydrazone linkage in PBS, DS _{C16NH2} of 12.6 % and a DS _{ADH} of 6.9 %
HA _{Hidra4}	HA-DOX conjugated through a hydrazone linkage in PBS, DS _{C16NH2} of 11.0 % and a DS _{ADH} of 16.1 %, from HA with a MW of 4.0 kDa
HNO ₃	Nitric Acid

I

ICP Inductively Coupled Plasma

K

KBr Potassium Bromide

L

LYVE-1 Lymphatic Vessel Endothelial Hyaluronan receptor 1

M

MNPs Magnetic nanoparticles

MPS Mononuclear Phagocyte System

MRI Magnetic Resonance Imaging

MSME Multi-Slice-Multi-Echo

MW Molecular weight

MWCO Molecular Weight Cut-off

N

n Number of moles

Na⁺ Ion sodium

NaCl Sodium chloride

NG Nanogel

NHS N-Hydroxysuccinimide

NMR Nuclear Magnetic Resonance

P

PBS	Phosphate Buffered Saline
PdI	Polydispersity Index
PKs	Pharmacokinetics

R

RES	Reticuloendothelial system
RHAMM	Receptor for Hyaluronan Mediated motility

S

SPION	Superparamagnetic iron oxide nanoparticles
-------	--

T

TBA-F	Tetra-n-butylammonium fluoride
TEA	Triethanolamine
TSG-6	Tumor necrosis factor-simulator gene-6

1. INTRODUCTION

1.1 Nanomedicines in cancer therapy

Cancer is the leading cause of death in economically developed countries and the second in developing countries (World Health Organization, 2008). Due to the growth and aging of the population, in particular in less developed countries, where about 82 % of the world's populations resides, cancer associated deaths are expected to grow (Torre et al., 2015). In general, cancer rates are higher in more developed regions, for example, the number of all-sites cancer for both sexes in Western Europe is more than twice as high as that in Eastern Africa (Torre et al., 2015).

Cancer diseases can result from genetic or genomic alterations in DNA sequence, which can be related to copy number aberrations, chromosomal rearrangements and modifications in DNA methylation (McLendon et al., 2008). Some capabilities acquired during the multistep development of human tumors are designated as hallmarks of cancer (Hanahan et al., 2011). These hallmarks are some features related to the healthy cells transformation into cancer cells. These intrinsic characteristics are common traits that all cancer shares, such as the capacity of malignant cells to survive under conditions that could lead normal cells to growth arrest or apoptosis (Hanahan, 2000). During the cancer cells proliferation, the supply of oxygen and nutrients decrease, then cytokines and other signaling molecules are released from cells to develop new blood vessels, a process designated as angiogenesis (Allen et al., 2004). The new vascular network (angiogenesis process) will allow the uptake of oxygen and nutrients by the cancer cells, for the tumor survival and proliferation (Lammers et al., 2012; Maeda, 2001b). However, these new vessels are not similar to the blood vessels found in the normal tissues, since there are gaps from 600 to 800 nm between endothelial cells (Allen et al., 2004). This phenomenon is known as the enhanced permeability and retention (EPR) effect (Maeda, 2001b). Another physical distinction of tumor tissues lies in the absence of lymphatic system (**figure 1.1**) (Jain, 1987). Consequently, the clearance of macromolecules from tumor's interstitium is harder and slower, leading to a higher accumulation of molecules for an extended period of time.

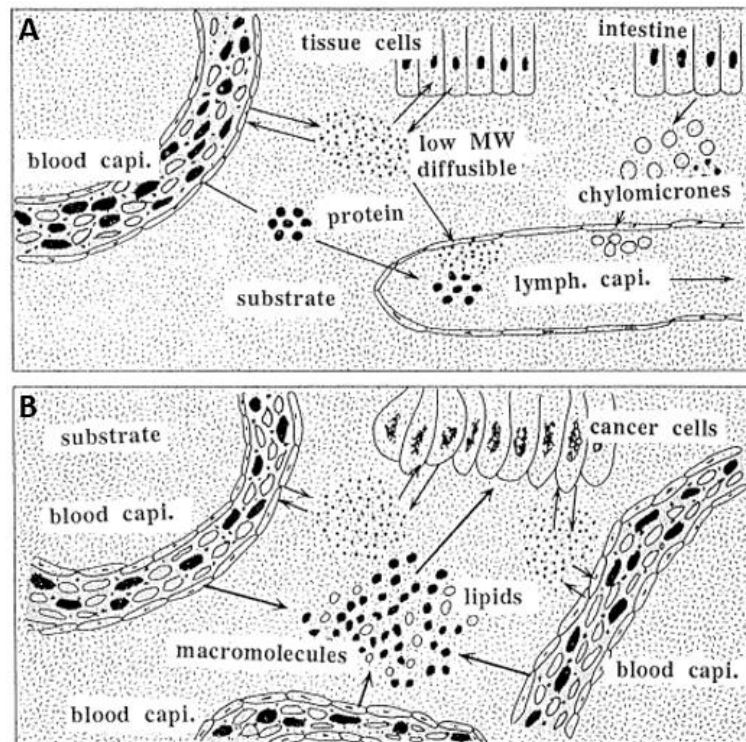


Figure 1.1: Schematic representation of differences between normal (A) and cancer tissue (B) (Maeda et al., 1989).

The improved understanding of tumorigenesis has been helpful to the development of new antitumor therapies (Lammers et al., 2008). Drug Delivery Systems (DDS) consist in the association of drugs and carriers to improve the pharmacological properties, when compared to a conventional drug (Allen et al., 2004). DDS can alter the pharmacokinetics (PKs) and biodistribution (BD) of the associated drugs (Allen et al., 2004), due to the small size and further physic-chemical features (Lammers et al., 2012).

DDS should balance the therapeutic activity and the toxicity of a drug, like chemotherapeutics that aim to avoid toxicity in healthy tissues but kill cancer cells (Allen et al., 2004; Davis et al., 2008; Jain et al., 2010, Lammers et al., 2008; Peer et al., 2007; Torchilin, 2000). Other important properties of DDS are the ability to overcome biological barriers and carry/deliver hydrophobic (poorly water-soluble) molecules to a specific site in the body (Desai, 2012).

DDS are being used to minimize drug degradation, instability upon administration, prevent harmful or undesirable side-effects, increase drug bioavailability and accumulation in the pathological site (Peer et al., 2007). Bioavailability is related to the presence of a drug in the pathological place, which for some drugs is very low, essentially due to the reduced drug's solubility, which should be increased using DDS for *in vivo* administrations (Amiji, 2006). The absence of lymphatic system combined with the increased gaps between the endothelial cells in the new blood vessels of the tumor could be useful for

the accumulation of DDS in the tumor's interstitium (Allen et al., 2004; Meada et al., 1989; Maeda, 2001a, 2001b), granting the possibility to an higher bioavailability. Nonetheless, the accumulation of DDS will depend on their size and in the degree of the tumor vascularization (Allen et al., 2004).

Drug targeting can be achieved by passive or active strategies (**figure 1.2**). The passive targeting is also designated as EPR effect and the vast majority of nanomedicines developed for drug targeting rely on them (**figure 1.2-A**) (Lammers et al., 2012). The active targeting (**figure 1.2-B**) strategy consists in the use of ligands to specifically bind receptors, such as peptides, antibodies or other molecules overexpressed by the target cells, which will improve the recognition and uptake from the cells (Lammers et al., 2012).

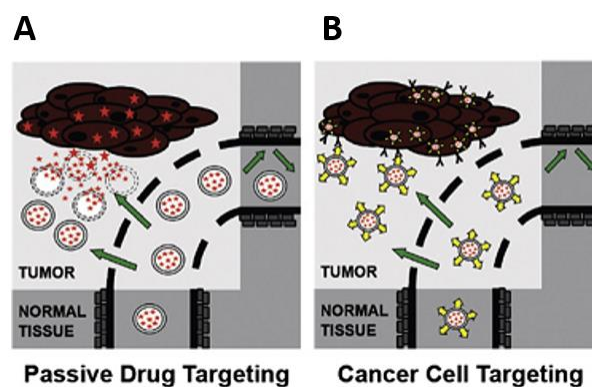


Figure 1.2: Schematics representation of passive targeting, by exploration of the EPR effect (**A**), and active targeting (**B**) using surface decoration (Lammers et al., 2012).

The use of high quantities of a carrier can lead to problems of toxicity, metabolism and biodegradation, however the carriers usually used are based on nontoxic and biodegradable polymers, presenting a minimal toxicity (Allen et al., 2004).

Polymeric nanoparticles are DDS, with potential when applied in tumor therapy. Their efficacy related with circulation time in the blood stream and accumulation in the target tissue before be cleared by the reticuloendothelial system (RES) will vary according to its characteristics, such as particle size, surface properties and particle shape (Duan et al., 2013). Nanoparticles size is similar to the size of biological entities such as proteins, antibodies and viruses (**figure 1.3**), which allows them to interact with biomolecules present on the cell surface and within the cell (van Rijt et al., 2014).

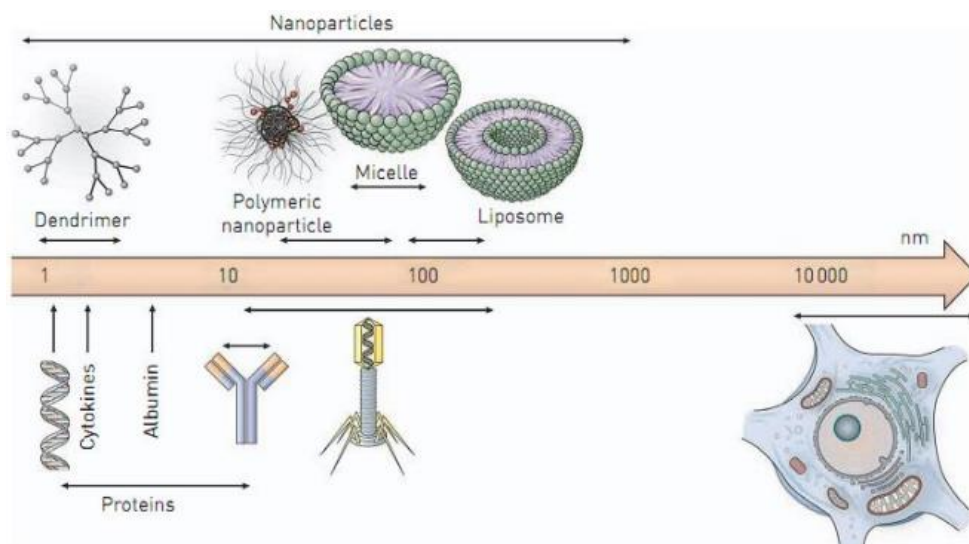


Figure 1.3: Schematic diagram showing the relative size of some nanoparticles, biological entities and cells (van Rijt, Bein, & Meiners, 2014)

Nanoparticle size should be between 20 to 150 nm (Lammers et al., 2012), since the ones with a size lower than 20 nm will pass through the glomerular capillary wall, being eliminated by the kidneys (Venturoli et al., 2005). Otherwise, the upper value should be smaller than 150 nm to avoid sequestration by sinusoids in spleen and fenestra of liver, which size is approximately 150 to 200 nm in diameter (Yuan, 1998) and also to prevent the uptake by the mononuclear phagocyte system (MPS) (Duan et al., 2013)

The surface properties, mainly surface charge and hydrophobicity can influence opsonization, phagocytosis, circulation time in the blood stream and BD of nanoparticles (Schipper et al., 2009). These properties can also affect the nanoparticles' stability and interaction with cells (Hillaireau et al., 2009; Verma et al., 2010). When negatively charged, nanoparticles present a lower phagocytic uptake, which leads to a longer of blood circulation time. In contrast when positively charged, the nanoparticles will present an increased phagocytosis (Duan et al., 2013). Nanoparticles with low positive charge present a promising potential as a long-circulating DDS, to deliver drugs into cancer cells with desirable biocompatibility and biofunctionality (Duan et al., 2013).

The shape of nanoparticle plays an important role in their *in vivo* behavior and interaction with cells, as non-spherical nanoparticles show superior properties when compared with spherical ones regarding escape from phagocytosis (Champion et al., 2006), circulation half-life (Geng et al., 2007) and target efficiency (Park et al., 2008).

Multidrug resistance is one obstacle that limits the efficacy of cancer therapies, which can be caused by physiological barriers or by alterations in the characteristics of the cancer cells (Davis, Chen, & Shin, 2008). There are two different mechanisms: non-cellular drug resistance which can have its origin

in the few blood vessels present in the tumor tissues, and cellular mechanisms, such as alteration of an enzyme, reduction of apoptosis, induction of the cellular repair system, mutation of the drug target or increasing drug efflux in tumor cells (Davis et al., 2008). The most common are changes in the drug-efflux pump (**figure 1.4**), whereby, the drug is removed out of the cell. DDS may help in circumventing this issue since they enter into the cell by endocytosis (Davis et al., 2008).

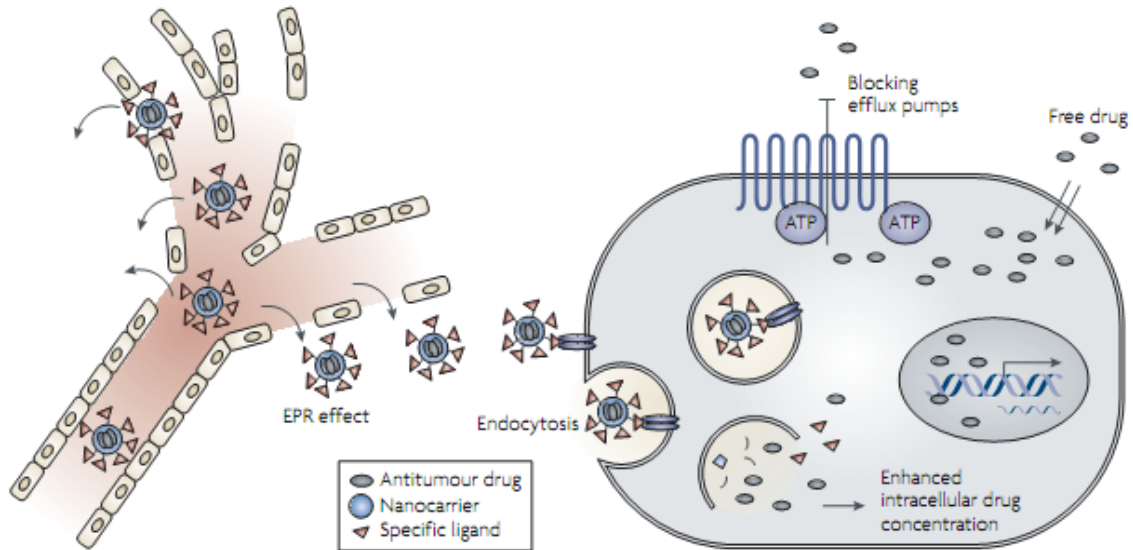


Figure 1.4: Schematic representation of free-drug elimination by a multidrug resistance process. The nanocarrier accumulates by the EPR effect and enters the cell, through endocytosis (mediated by the specific ligand). The increase of drug concentration inside the cell overcomes the efflux pump mediated by drug resistance (Davis et al., 2008).

Nanoparticles used as DDS have several relevant characteristics related to the improvement of anti-cancer therapy:

- large payload and drug protection from degradation, the loading depend on the size of the drug (smaller drugs allow higher loads) (Davis et al., 2008);
- nanoparticles' size permits the incorporation of multiple types of drug molecules, since the PKs of nanoparticles is not modified by the amount of drug loaded (Davis et al., 2008);
- nanoparticles' size allows multiple targeting, recognizing different cell-receptors (Hong et al., 2007), improving the affinity between the nanoparticle and the target cell;
- drug release kinetics from nanoparticles can be adjusted in order to match the mechanism of action (Davis et al., 2008);
- since nanoparticles enter cells by endocytosis, they can evade multidrug resistance mechanisms associated with the cell-surface protein pumps (Davis et al., 2008).

The association of these factors can minimize the side effects of anticancer drugs while maximizing the efficacy.

Nanoparticles can be divided in different types, such as liposome, polymer, micelle, antibody, protein-drug conjugate and nanogels (**figure 1.5**).

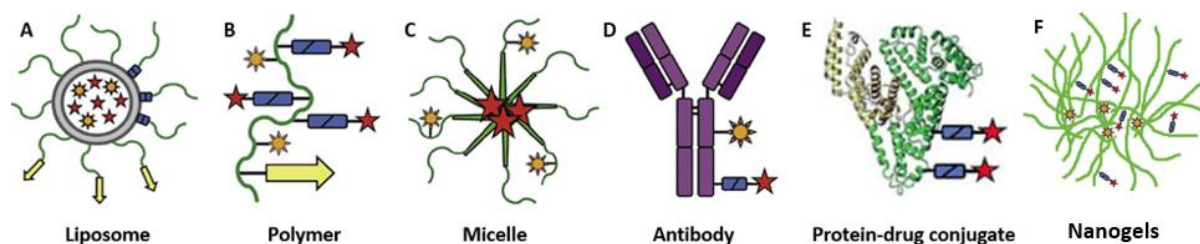


Figure 1.5: Representation of some examples of nanoparticles that can be used. In gray is represented the liposomal bilayer; polymers and polymer-coatings in green; linkers for drug release in blue rectangles; targeting ligands in yellow arrows; imaging agents in orange suns and conjugated or entrapped (chemo-) therapeutic agents in red stars. A-D from *Twan Lammers et al., 2012* and E from *T. Lammers et al., 2008*.

Liposomes (**figure 1.5-A**) are closed spherical vesicles, made from synthetic or natural phospholipids forming a lipid bilayer, which encapsulates an aqueous phase where a drug can be incorporated (Malam et al., 2009). Lipophilic drugs can also be incorporated in the lipid bilayer. The chemical properties of the liposome are based on the particular properties of the constituent phospholipids (Bawarski et al., 2008), such as permeability, charge density and steric hindrance. The liposome formation is spontaneous, resulting from the amphiphilic phospholipids self-associate into bilayers. Several commercial anticancer drugs based on liposomes are available, such as Doxil® (Malam, Loizidou, & Seifalian, 2009).

Polymer can be used as DDS conjugated with a drug (**figure 1.5-B**) or assembled with a drug forming micelles (**figure 1.5-C**). Micelles possess an hydrophobic core, that acts as a reservoir for lipophilic molecules surrounded by hydrophilic molecules, which confers aqueous solubility and steric stability to the ensemble (Gaucher et al., 2010).

More than 20 monoclonal antibodies (**figure 1.5-D**) have been approved for different applications, such as in cancer (Reichert, 2008), as targeting probes. Various approaches were made to enhance their activity, such as the production of antibody-drug conjugates (ADCs) (Alley et al., 2010). The ADCs have three principal components, the monoclonal antibodies, the drug and the linker between them (Alley, Okeley, & Senter, 2010). Obinutuzumab was recently approved by the FDA for the treatment of chronic lymphocytic leukemia. Bevacizumab showed to be effective in some clinical trials for different cancers as colorectal, lung, breast, renal, brain and ovarian cancer. There are over 30 ADCs in development and in clinical trials (Weiner, 2015).

Regarding protein-drug conjugates (**figure 1.5-E**), albumin is playing an increasing role as drug carrier and also improving the PK profile of peptides or protein-based drugs (Kratz, 2008). There are

different protein-based drugs being clinically evaluated and one is approved for treating metastatic breast cancer, Abraxane (Desai, 2012) and other is an albumin-binding prodrug of Doxorubicin (Kratz, 2007).

Nanogels (NG) are prepared from hydrophilic polymers, hydrophobically modified to produce amphiphilic polymers (Oh et al., 2008). Nanogels are produced by the self-assembly of the modified polymers when dispersed in water. The hydrophilic part of the polymer forms the outside surface, while the hydrophobic molecules form hydrophobic nanodomains within the nanogels (**figure 1.6-F**). Within these hydrophobic nanodomains, hydrophobic therapeutic molecules and/or imaging agents can be loaded (Peer et al., 2007).

In order to design and develop effective nanogel-based DDS for *in vivo* application several criteria must be met, such as:

- Nanogel stability for prolonged circulation time in the blood stream, since premature release of therapeutics, may result in adverse side effects and reduced therapy efficiency (Oh, Drumright, Siegwart, & Matyjaszewski, 2008);

- Specificity, using specific ligands that can recognize receptors on diseased cells, allowing active targeting (Oh et al., 2008);

- Small dimensions, less than 150 nm in diameter, as this can facilitate cellular uptake through receptor-mediated endocytosis and reduce the recognition by the mononuclear phagocyte system (MPS), increasing the nanogel circulation time in the blood stream (Seymour et al., 1987);

- Biodegradability of the nanogel, enabling the removal of the empty device after drug release (Oh et al., 2008).

Actually, there are already some anti-cancer nanomedicines in the market, such as RONDEL™ from Calando Pharmaceuticals, which is related with a nanoparticle-delivered clinical RNA interference (Davis et al., 2010). BIND-014, from BIND Biosciences, is a nanoparticle combined with a chemotherapeutic drug with prostate-specific membrane antigen (Hrkach et al., 2012). Other is Celgene's Abraxane, which consist of an albumin-functionalized paclitaxel formulation used approved for breast cancer therapy (Desai, 2012), and also for the treatment of lung and pancreatic cancers ("FDA Approval for Paclitaxel Albumin-stabilized Nanoparticle Formulation - National Cancer Institute," n.d.)

1.2 Hyaluronic Acid based nanogels

Different natural polymers (dextrin, glycol-chitosan, hyaluronic acid (HA), mannan) have been chemically modified leading to amphiphilic polymers that self-assemble, in an aqueous environment, originating nanogels. Dextrin nanogels were extensively characterized (Gonçalves et al., 2010a; Gonçalves et al., 2008; Gonçalves et al., 2010b; Gonçalves et al., 2007) and *in-vitro* studied as DDS of small size and poorly water soluble molecules such as curcumin (Gonçalves et al., 2012) or therapeutic proteins such as IL-10 (Carvalho et al., 2010). Another biomedical application explored concerned the loading of γ -Fe₂O₃ nanoparticles within the dextrin nanogels (nanomagnetogels) to produce a contrast agent for MRI. Its *in-vivo* performance was evaluated in a mouse model (Gonçalves et al., 2013). The major limitation with dextrin nanomagnetogels consists on the predominant accumulation in the MPS associated organs that difficult the tumor target.

The use of HA in the biomedical field has been explored by many researchers over the years. HA or hyaluronan is a high-molecular weight linear glycosaminoglycan (GAG) (Stern, 2004), composed by repeating units of glucuronic acid (GlcA) and N-acetylglucosamine (GlcNAc), connected by β -linkages, GlcA β -(1 \rightarrow 3)GlcNAc β -(1 \rightarrow 4) (**figure 1.6**) (Choi et al., 2012; Stern, 2004; Toole, 2004). HA is available in a wide range of molecular weight (MW), from 4000 Da to 10 MDa, which influences its biological functions (Mizrahy et al., 2011). Among the natural polymers, HA is the most abundant in the human body, being present in the extracellular matrix (ECM), connective tissues and body fluids. In physiological conditions. HA is in the form of a sodium salt, therefore negatively charged, referred as sodium hyaluronate. Chemical modifications of HA have been extensively reviewed, namely on the conjugation of cytotoxic drugs (Choi, Saravanakumar, Park, & Park, 2012) or grafting of hydrophobic molecules to obtain amphiphilic micelles (Liu et al., 2011) and stimuli responsive materials (Cheng et al., 2013). The chemical modification of HA can be performed on the carboxylic acid group or on the hydroxyl group.

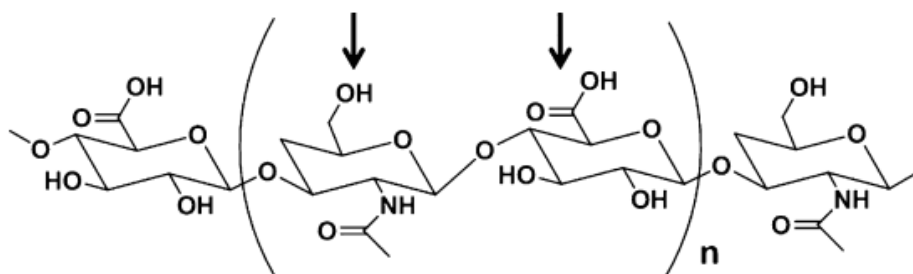


Figure 1.6: Chemical structure of HA, the arrows denote the principal places for modifications in the HA structure (Choi et al., 2012).

HA presents different cellular functions such as promotion of cell motility, regulation of cell-cell and cell-matrix adhesion, promotion of cellular proliferation and suppression of cellular differentiation

(Stern, 2004). Therefore, HA nanogels are expected to be poorly recognized by macrophages, therefore bearing lower liver and spleen accumulation and superior blood half-life.

In some tumors, the levels of HA is increased (Toole et al., 2002; Toole, 2002, 2004), comparing to normal tissues, therefore, the levels of HA can be related to malignancy (Toole et al., 2002) and stage of the tumor progression (Toole, 2004).

The enhanced expression or extracellular concentration of HA influence several signaling pathways related to tumor cell growth and survival, such as ErbB2, Ras, MAPK and PI3 kinase/ AKL (Bourguignon, 2001; Herrlich et al., 2000; Toole, 2002).

HA has received particular attention in the field of tumor-targeted delivery systems, due to its ability to specifically bind various cancer cells that overexpress CD44 receptor (Choi et al., 2012; Stern, 2004; Toole, 2004). HA can also bind the receptor for Hyaluronan-mediated motility (RHAMM) (Choi et al., 2012; Toole, 2004), lymphatic vessel endothelial Hyaluronan receptor 1 (LYVE-1) (Choi et al., 2012; Toole, 2004), TOLL4 (Toole, 2004) and tumor necrosis factor-simulator gene-6 (TSG-6) (Choi et al., 2012).

CD44 located in the cell-surface (Aruffo et al., 1990; Ponta et al., 2003; Stamenkovic et al., 1989), is the principal cell-surface receptor for HA in the cancer cells (Choi et al., 2012; Toole, 2004). It is a glycoprotein with significantly important roles, as the adhesion between cells from the same tissues (cell-cell and cell-matrix adhesion) (Toole, 2004), cell migration during morphogenesis, cell proliferation, cell migration, angiogenesis and tumor invasion and metastasis (Toole, 2004).

When CD44 interact with HA, there are diverse cellular responses, involving tyrosine kinases, protein kinase C, focal adhesion kinase, mitogen-activated protein kinase, nuclear factor- κ B, RAS and cytoskeletal components (Bourguignon, 2001; Ponta et al., 2003; Thorne et al., 2004). The HA endocytosis will lead to its degradation (Goodison et al., 1999; Kaya et al., 1997; Naor et al., 2002).

1.3 Doxorubicin

Doxorubicin (DOX) is one of the most frequently used drugs in chemotherapy, with the trade name of Adriamycin. DOX was discovered in the 1960s, showing a significant anti-cancer efficacy, being used as an anticancer drug, in the treatment of leukemia's, Hodgkin's lymphoma, bladder, stomach, lung, ovarian and thyroid cancers, soft tissue sarcoma, multiple myeloma and other types of cancer (Mohan et al., 2010). DOX is an anthracycline (Yang et al., 2014) and like daunorubicin, it was isolated from a soil bacterium, *Streptomyces peucetius* (Arcamone et al., 2000; DiMarco et al., 1969).

The structure of DOX (**figure 1.7**) is similar to the anthracycline antibiotic in which a flat anthraquinone nucleus of the molecule is linked through a glycosidic bond at ring atom 7 to an amino sugar (Mohan et al., 2010). DOX's structure is protonated, specifically in the amino group of the sugar forming a DOX hydrochloride, in order to increase aqueous solubility.

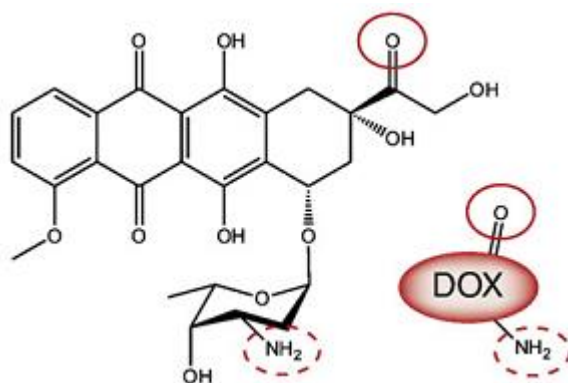


Figure 1.7: Chemical structure of DOX. Functional groups (amine and carbonyl), highlighted with red circles correspond to the coupling sites with the prodrugs (Bildstein et al., 2011).

The mechanism of the DOX antineoplastic activity is through the intercalation between two base pair of the DNA, which was evidenced by crystal structure (Frederick et al., 1990). This interaction will inhibit the progression of the enzyme topoisomerase II, which is responsible for unwinds DNA for transcription or replication, resulting in the arrest of the cells in G2-phase of the cell cycle or inducing apoptosis (Mohan et al., 2010). Other suggested mechanisms are related to free radical formation, lipid peroxidation and direct membrane effects. The binding between cell membranes and DOX results in the production of active oxygen species, especially hydroxyl radicals generated in DOX enzymatic reduction catalyzed by iron and/or copper ions (Aubel-Sadron et al., 1984; Marnett, 2002; Minotti et al., 2001; Minotti et al., 2004), which result in a decline of the mitochondrial oxidative phosphorylation. The severe

DOX cardiotoxicity can be related to the attack of reactive oxygen species on the myocytes (Berthiaume et al., 2007; Maejima et al., 2008; Minotti et al., 2004; Wallace, 2007).

The considerable DOX toxicity, especially when used in high dosages, limits the concentration range that can be used in the cancer treatment (Borst et al., 2000; Germann, 1996; Gottesman et al., 1993), for minimal side effects in the patient.

1.4 Theranostic formulations

Theranostic is a new tool used in the nanomedicine combining two different activities in the same formulation: therapy and diagnosis. The incorporation of an anticancer drug and an imaging agent in the same formulation allows the BD monitoring, as well as, the evaluation of the carrier and/or the drug accumulation at the target site, allowing an evaluation of the intervention in real-time (Lammers et al., 2011; Lammers et al., 2010; Sun et al., 2010). This information is useful for medical decisions respecting therapy (number, frequency and duration of the cycles of treatment) (Lammers et al., 2012).

The contrast agent incorporated into the theranostic system can be, for example, gold, iron-oxide or radiolabeled compounds, depending on the imaging technique used for diagnosis. Magnetic Resonance Imaging (MRI), uses iron oxide as a contrast agent, offering high resolution and the capacity of simultaneously obtaining physiological and anatomical information based on the interaction of contrast agents with the surrounding protons of the tissue (Merbach et al., 2013). Magnetic nanoparticles (MNPs) exhibit a unique contrast enhancement, which allows the MRI of cell trafficking, gene expression and cancer detection (Chen et al., 2010; Lalatonne et al., 2010). MNPs have been recognized as a promising tool for site-specific delivery through the application of an external magnetic field (Lalatonne et al., 2010).

Superparamagnetic iron oxide nanoparticles (SPION) are of considerable interest as contrast agents due to their nanoscale dimensions, non-toxic nature and magnetic properties. In medicine, their application in the nude form is limited by their aggregation in biological fluids, induced by their high surface energies and hydrophobicity, which lead to protein adsorption (Park et al., 2009). Polymer coating provides colloidal stability in water, through steric stabilization, giving well-dispersed formulations. Surface coating of iron nanoparticles with amphiphilic polymers has been described, primarily using synthetic polymers and experimental methodologies relying on organic solvents for phase transfer (Kim et al., 2011; Lin et al., 2008; Nasongkla et al., 2006). Such strategies are still limited regarding clinical applications, although considerable efforts have been devoted to the development of simple and efficient methods to prepare nanocarriers with high stability and narrow size distributions.

SPIONs have been clinically used as T_2 -type (negative) MRI contrast agents (Geraldes et al., 2009; Laurent et al., 2008). Superparamagnetic behavior means that the nanoparticles are highly magnetized in a magnetic field but lose their magnetization when the field is switched off. This behavior is necessary for injectable formulations because it reduces the risk of thrombosis from magnetically aggregated nanoparticles.

Currently, two SPION are clinically approved, namely: ferumoxides (Feridex in the USA, Endorem in Europe) and ferucarbotran (Resovist). Regarding the administration route, Resovist can be administered as a rapid bolus (used with both dynamic and delayed imaging), whereas Feridex needs to be administered by slow infusion (used only in delayed phase imaging). In the liver, these particles are sequestered by phagocytic Kupffer cells in normal tissues but are not retained in lesions lacking Kupffer cells. Consequently, significant differences in T_2/T_2^* relaxation enhances lesion detectability. Both Feridex and Resovist are approved specifically for MRI of the liver, namely for detection of hepatic metastases. After intravenous administration, clinically approved SPION are cleared from the blood by phagocytosis accomplished in the RES, so that uptake is observed in the normal liver, spleen, bone marrow, and lymph nodes. After the intracellular uptake, SPIONs are metabolized in the lysosomes into a soluble non superparamagnetic form of iron, that becomes part of the iron pool (e.g., ferritin, hemoglobin) (Wang, 2011).

2. OBJECTIVES

Cancer is the leading cause of death in the world. New antitumor therapies are much required, among them are the development of efficient drug delivery systems. In this work, nanogels will be used as drug carrier, since they are able to protect the drug in a stable way avoiding degradation before reaching the target. Besides that, nanogels allow the formation of labile linkages with the drug, namely pH-responsive systems. The pH-responsive linkage allows the drug release when a certain pH is reached and a specific release of the drug in the target, thereby reducing some undesirable side effects.

Natural polymers have been used in the development of new nanogels that allows the drug conjugation and loading of hydrophobic molecules and/or particles, such as $\gamma\text{-Fe}_2\text{O}_3$, to produce contrast agents for MRI. Hyaluronic acid was chosen since it is a natural polymer (the most abundant in the human body) and non-toxic, present in the extracellular matrix (ECM), connective tissues and body fluids. Besides that, hyaluronic acid can bind to various types of cancer cells that overexpress some of its receptors, as CD44.

Doxorubicin is one of the most used drugs in chemotherapy, however, it presents some toxicity when used in high dosages, especially in the cardiac tissue. This downside limits the concentration range that can be used in the cancer treatment.

One of the main objectives of this work consists in the development of pH-responsive nanogels for cancer therapy, using hyaluronic acid as carrier and doxorubicin as a bioactive agent. Another objective is the incorporation of $\gamma\text{-Fe}_2\text{O}_3$ into the nanogels, in order to obtain a theranostic formulation.

To achieve that goal, the hyaluronic acid will be chemically modified with hexadecylamine, yielding an amphiphilic hyaluronic acid. The most promising nanogels will be conjugated with doxorubicin, which will be chemically bound to the polymer molecule via hydrazone (pH-sensitive) or amide linkage. The release profile will be evaluated at different pH. $\gamma\text{-Fe}_2\text{O}_3$ will be stabilized into HA-DOX nanogels producing nanomagnetogels that will be characterized. Furthermore, *in vitro* cell studies with DOX nanogels will be performed to assess their cytotoxicity.

3. MATERIALS AND METHODS

3.1 Materials

For the development of this project, the reagents used were: 1-Ethyl-3-(3-dimethylaminopropyl)carbodiimide, EDC (Acros Organics); Adipic Acid Dihydrazide, ADH (Sigma-Aldrich); Dimethyl sulfoxide, DMSO (Fisher); Doxoubicin, DOX (Abcam-Biochemicals); Dulbecco's Modified Eagle Medium, DMEM (Millipore); Fetal bovine serum, FBS (Millipore); Hexadecylamine (Sigma-Aldrich); Hyaluronic Acid (7.48 kDa, LifeCore); N-Hydroxysuccinimide, NHS (Sigma-Aldrich); Penicillin/Streptomycin, PS (Millipore); Potassium Bromide, KBr (Agros Organic); sodium chloride, NaCl (Fisher Scientific); Tetra-n-butylammonium fluoride, TBA-F (Fluka Analytical); Triethylamine, TEA (Fluka); Trypsin/EDTA solution (Millipore) and ultrapure water (Millipore).

3.2 Chemical Reactions

3.2.1 Amphiphilic HA production

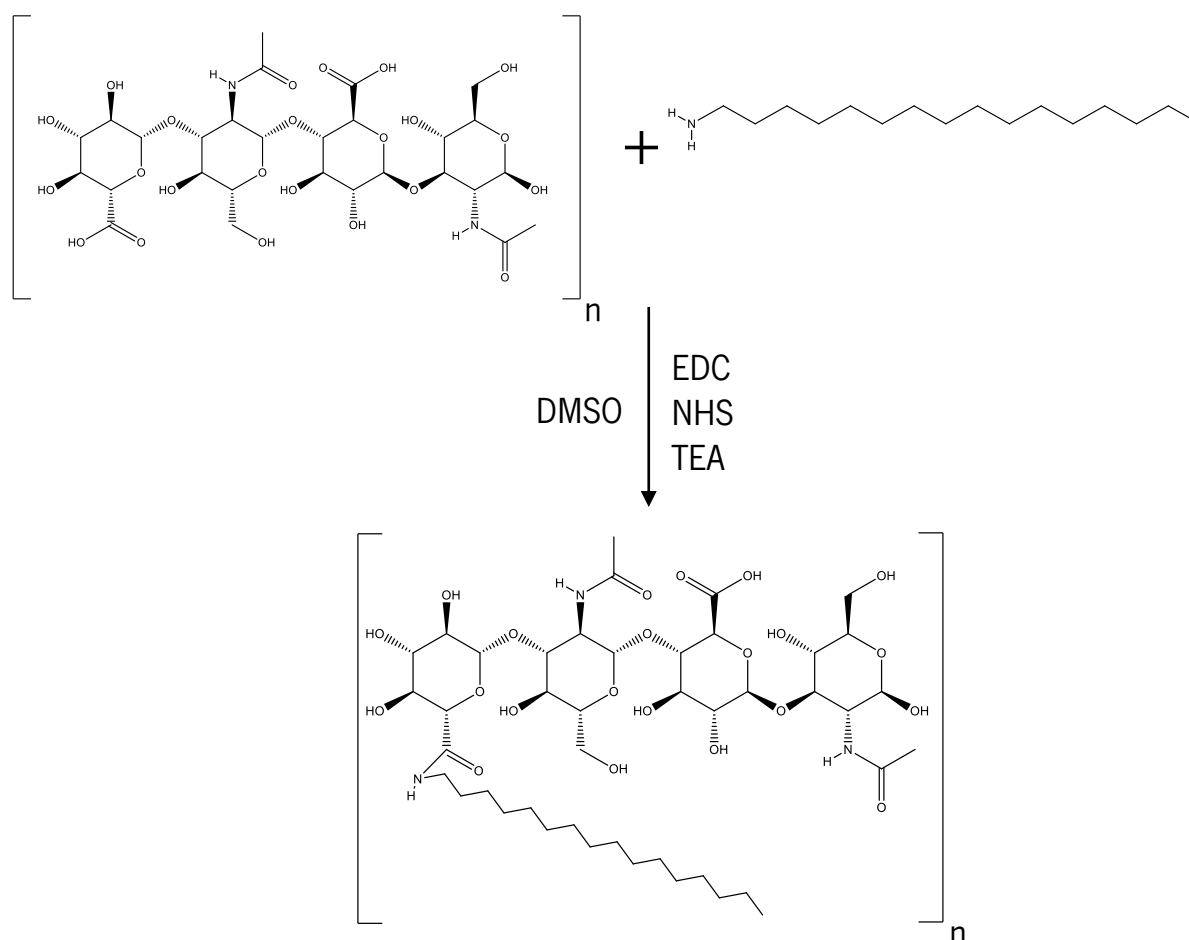
Ion Exchange

The ion exchange was performed to switch the sodium ion of HA by the tetra-n-butylammonium ion, TBA⁺, allowing the HA dissolution in DMSO, as described in the literature (Oudshoorn et al., 2007). Briefly, an excess of TBA-F (3.5 g) was used with a cation exchange resin AG 50W-X8 (BIO-RAD Laboratories) (1.0 g) in 12.5 mL of ultrapure water, incubated for 1 h at room temperature under rotational agitation. Then, the mixture was filtrated under pressure using a filter with a cut off 0.45 μm (Teknokroma). The HA, 250 mg, was dissolved in 25 mL of ultrapure water and added to the filtrated resin and left to react under rotational agitation for 2 h at room temperature. After that, the mixture was centrifuged for 2 min at 1000 g and the supernatant was removed, the obtained pellet was finally freeze-dried.

Amphiphilic HA production

Amphiphilic HA was produced grafting hexadecylamine, as shown in the **scheme 3.1**. Briefly, 100 mg of HA-TBA, 31.0 mg of EDC (molar ratio 1:1 of EDC to HA-TBA), 19.0 mg of NHS (molar ratio 1:1 of NHS to HA-TBA), 11.7 mg of hexadecylamine (molar ratio 0.3:1 of hexadecylamine to HA-TBA)

were dissolved in 12 mL of DMSO and 24 μ L of TEA (molar ratio 1:1.5 of hexadecylamine to TEA), were added to the obtained solution and incubated for 24 h at room temperature under rotational agitation. After that, two dialysis were carried out using a dialysis membrane with a molecular weight cut off (MWCO) of 1000 Da (OrDial D-Clean). The first one against sodium chloride, NaCl, solution (150 mM) for three days to replace TBA⁻ by the Na⁺, then against distilled water for two days. The final solution was freeze-dried.



Scheme 3.1: Representation of the reaction between HA and C₁₆NH₂ performed in DMSO with EDC, NHS and TEA.

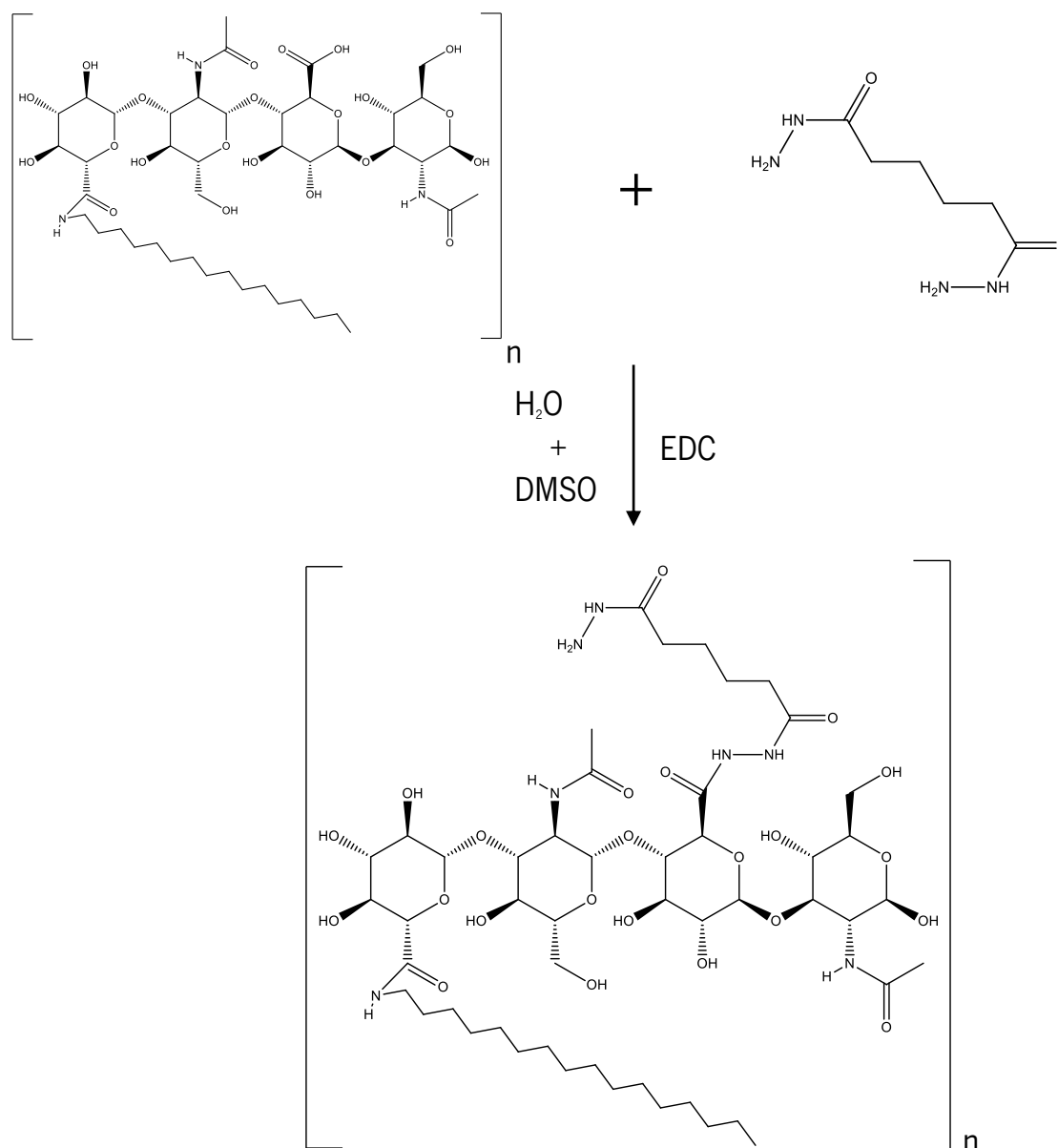
3.2.2 Doxorubicin conjugation

Via Hydrazone linkage

For the conjugation of the amphiphilic HA with DOX via hydrazone linkage, it was required to perform the conjugation of the amphiphilic HA with ADH, as shown in the **scheme 3.2**.

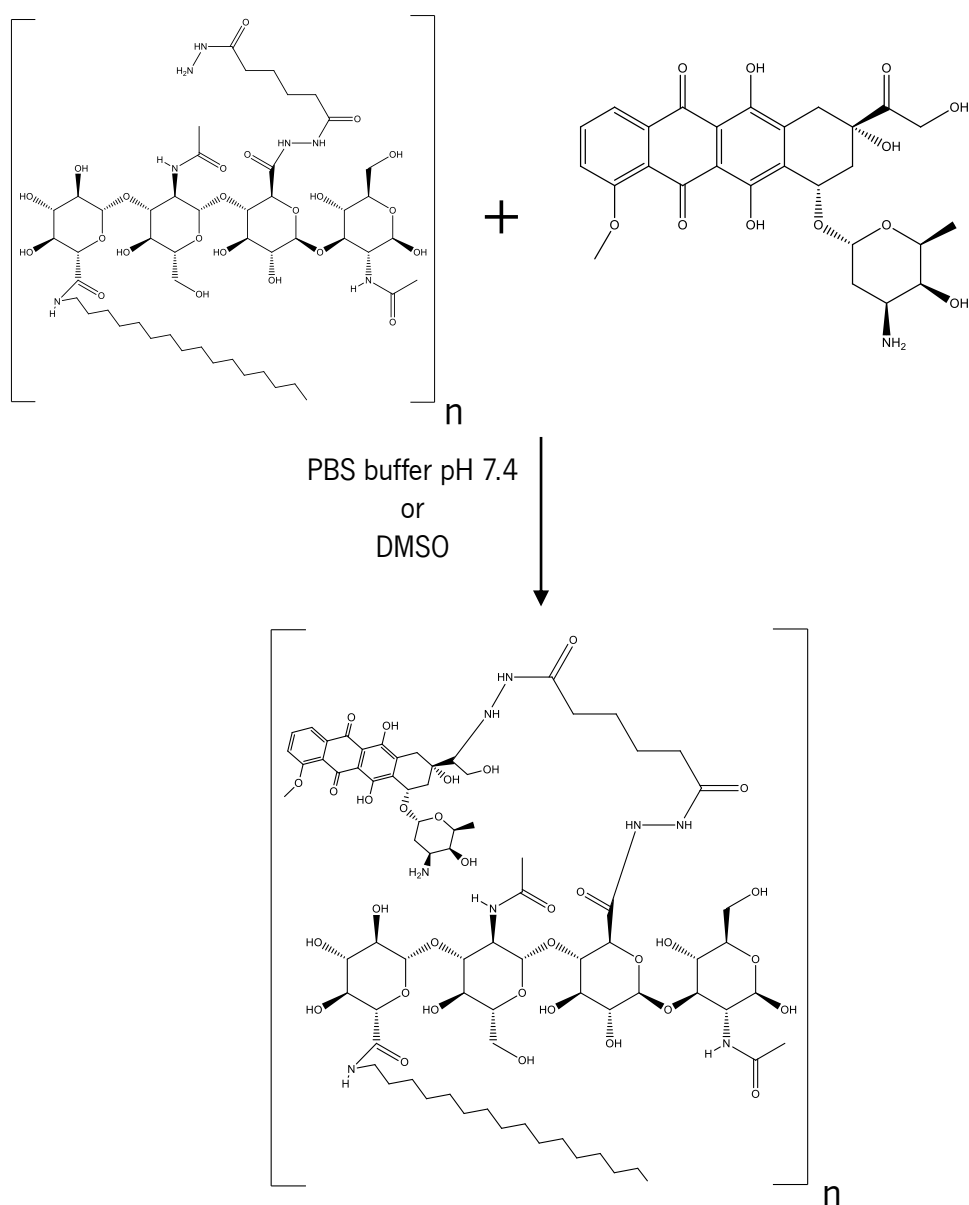
Briefly, 50.0 mg of amphiphilic HA, 24.0 mg of EDC, 22.0 mg of ADH were dissolved in 12 mL of distilled water and then 2.0 mL of DMSO were added to the previous solution and incubated for 24 h

at room temperature under rotational agitation. After that, a dialysis step was performed, against distilled water for three days using a dialysis membrane with an MWCO of 1000 Da (OrDial D-Clean). The final solution was freeze-dried.



Scheme 3.2: Representation of the reaction between the amphiphilic HA and ADH performed with EDC.

The conjugation between HA-ADH with DOX (**scheme 3.3**) was performed using different solvents: PBS buffer pH 7.4 or DMSO.



Scheme 3.3: Representation of the conjugation between HA-ADH and DOX through an hydrazone linkage.

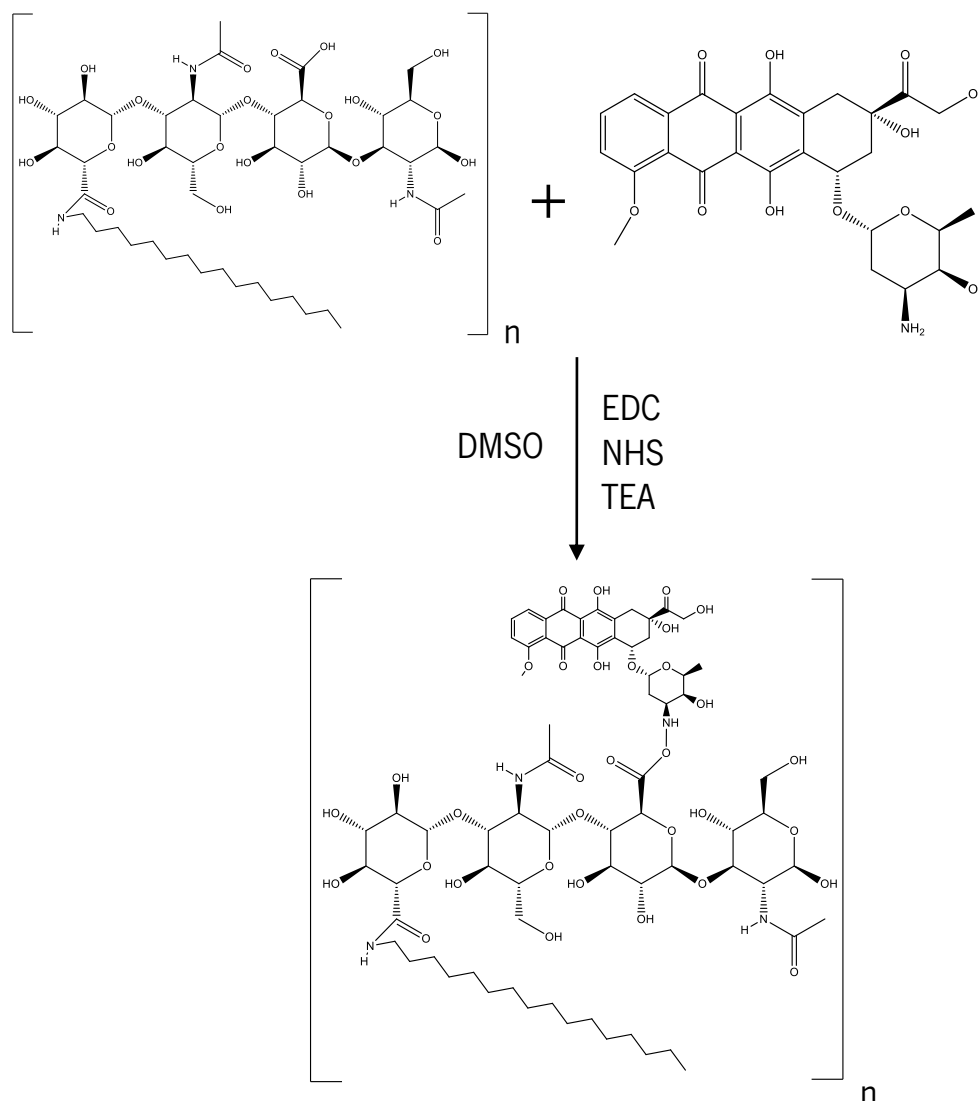
The reaction between DOX and HA-ADH in PBS pH 7.4 was performed using 30.0 mg of HA-ADH and 1.0 mg of DOX, dissolved in 9.0 mL PBS. The mixture was protected from light and incubated overnight at room temperature under rotational agitation. After that, dialysis was carried out against distilled water for 6 h with three water changes using a dialysis membrane with an MWCO 1000 Da (OrDial D-Clean). The final solution was freeze-dried.

For the conjugation of HA-ADH and DOX in DMSO, it was performed using 15.0 mg of HA-ADH, 0.5 mg of DOX, 0.34 mg of EDC (molar ratio 1:1 of ADH to EDC), 0.57 mg of NHS (molar ratio 1:1 of ADH to NHS) and 0.62 μL of TEA (molar ratio 1:1.5 of ADH to TEA) dissolved in 15.0 mL of DMSO. The

solution was protected from light and incubated overnight at room temperature under rotational agitation. After that, dialysis was carried out, against distilled water, for three days using a dialysis membrane with an MWCO of 1000 Da (OrDial D-Clean). The final solution was freeze-dried.

Via Amide linkage

The amphiphilic HA conjugation with DOX was produced as shown in the **scheme 3.4**. The reaction between the amphiphilic HA and DOX was performed using 30.0 mg of amphiphilic HA, 43.8 mg of EDC (molar ratio 1:1 of amphiphilic HA to EDC), 26.3 mg of NHS (molar ratio 1:1 of amphiphilic HA to NHS), 0.6 μ L of TEA (molar ratio 1:1.5 of DOX to TEA) and 1.8 mg of DOX dissolved in 3.2 mL of DMSO. The solution was protected from light and left reacting for 24 h at room temperature under magnetic agitation. After that, a dialysis was performed, against distilled water, for 3 days, using a dialysis membrane with a MWCO of 1000 Da (OrDial D-Clean) The final solution was freeze-dried.



Scheme 3.4: Representation of the conjugation of amphiphilic HA with DOX via amide linkage in DMSO with EDC, NHS and TEA.

3.3 ^1H NMR

The lyophilized material was dispersed in deuterium oxide (6.0 mg/mL) and then transferred to 5 mm NMR tubes. 1D ^1H NMR measurements were performed on a Varian Unity Plus 300 spectrometer operating at 299.94 MHz. The spectra were obtained at 298 K with 80 scans, a spectral width of 480 Hz, a relaxation delay of 1 s between scans, and an acquisition time of 3.75 s.

3.4 Size Distribution

The size distribution was determined by Dynamic Light Scattering (DLS) using a Malvern Zetasizer, model Nano ZS (Malvern Instruments), as previously described in the literature (Pedrosa et al., 2014). Briefly, samples were dispersed in distilled water or PBS pH 7.4 at 1.0 mg/ml and filtered with a 0.22 μm polyethersulfone (PES) syringe filter. Then each sample was analyzed at 25°C in a polystyrene cell, using a He-Ne laser – wavelength of 633 nm and a detector angle of 173°. In each analysis, the sample was measured 10 consecutive times, and in each measurement, the number of runs was determined by the Malvern software.

In each measurement, the correlation (correlogram profile) was evaluated in order to validate the measurement (values vary from 0 to 1). As a quality criteria of the results, the cut-off value of 0.7 was defined.

3.5 DOX quantification

The amount of DOX conjugated to the HA via hydrazone or amide linkage was obtained by acquiring the absorbance spectrum of the sample, from 400 nm to 600 nm, measuring at each 1 nm, with a normal read speed, 100 msec of delay and 8 measurements/data point. A microplates reader Cytation 3, Biotek was used. In the literature, the DOX is usually quantified at 480 nm (Fu et al., 2015) or 486 nm (Park et al., 2015), the wavelength used for the quantification was 488 nm. Samples were dispersed in distilled water or PBS buffer pH 7.4, at 1.0 mg/mL.

For the analysis of DOX concentration, absorbance was measured instead of fluorescence based on *Mohan et al.* results demonstrating that the optical absorbance shows a linear dependence on DOX's

concentration, while the fluorescence, above 25 $\mu\text{g}/\text{mL}$ of DOX, is essentially non-linear (Mohan et al., 2010), as shown in **figure 3.1**.

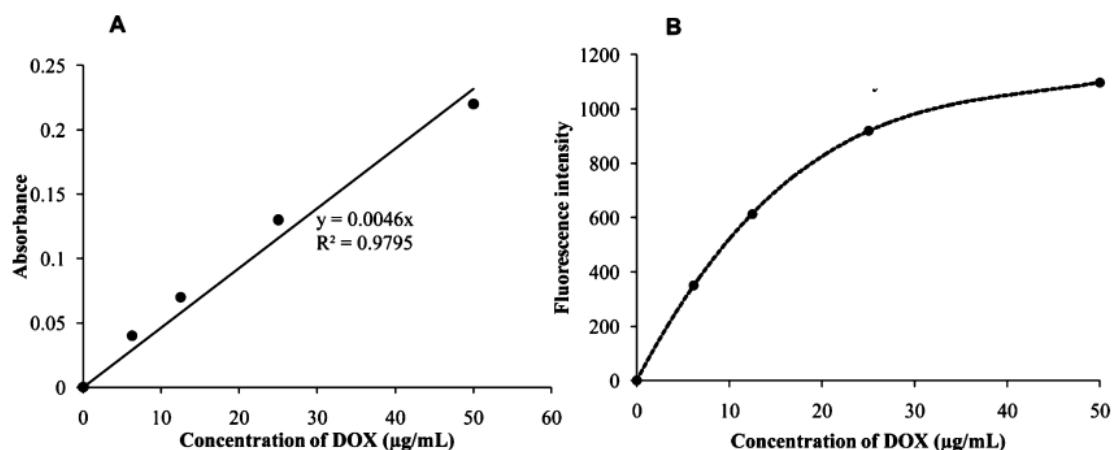


Figure 3.1: Relation between DOX concentration (PBS) and optical absorbance **(A)** or fluorescence intensity **(B)** (Mohan & Rapoport, 2010).

3.6 DOX release studies

The DOX release study was performed with free DOX or HA-DOX nanogels conjugated via amide or hydrazone linkage. The DOX concentration was fixed at 20 $\mu\text{g}/\text{mL}$, for both conjugates and free DOX. The assay was performed using a dialysis membrane with a cut-off of 2 kDa (OrDial D-Clean) and two different release mediums, PBS buffer pH 7.4 or sodium acetate buffer pH 5.0, at 37°C under magnetic agitation. 5 mL of the test sample was placed inside the dialysis membrane submersed in 1.0 L of the release medium. At each time point, the volume inside the dialysis membrane was evaluated and 350 μL were withdrawn for DOX quantification

The DOX quantification was performed as referred in section **3.5 - DOX quantification**.

3.7 $\gamma\text{-Fe}_2\text{O}_3$ incorporation

3.7.1 $\gamma\text{-Fe}_2\text{O}_3$ incorporation

The HA-DOX conjugates were dispersed in distilled water, 2.0 mg/mL, to allow the nanogels formation. The required volume of $\gamma\text{-Fe}_2\text{O}_3$ (stock solution 400 mM Fe) was added to the nanogels dispersion and pH adjusted to 7.4, using NaOH, 0.005 M, or HCl, 0.005 M. The formulation was kept

under circular stirring overnight to allow $\gamma\text{-Fe}_2\text{O}_3$ incorporation into the nanogel, through hydrophobic/hydrophobic interactions. After that, the formulation was centrifuged at 4000 g for 10 min at room temperature, to remove the non-stabilized $\gamma\text{-Fe}_2\text{O}_3$, while the supernatant was carefully collected and analyzed.

3.7.2 $\gamma\text{-Fe}_2\text{O}_3$ quantification

The quantification of the $\gamma\text{-Fe}_2\text{O}_3$ stabilized into the nanogels was performed by Inductively Coupled Plasma (ICP). The analysis was performed at a specific wavelength, 259.939 nm, radial view and the plasma was formed with Argon gas. The equipment used was a PerkinElmer Optima 8000. For the calibration curve, Iron Standard for ICP, 17.906 mM, dissolved in 2 % nitric acid, HNO_3 . All samples were prepared in a solution of 2 % HNO_3 and analyzed in triplicate.

3.7.3 Size Distribution and Zeta Potential

Size distribution of the nanomagnetogel ($\gamma\text{-Fe}_2\text{O}_3$ stabilized within NG) was evaluated without previous filtration. Five consecutive measurements for each sample were performed.

The Zeta Potential was determined by Dynamic Light Scattering (DLS) using a Zetasizer, model Nano ZS (Malvern Instruments), as previously described on **3.4 – Size Distribution**.

3.7.4 Magnetic Characterization

A vibrating sample magnetometer (VSM, Quantum Design, Versalab) was used for magnetic characterization. VSM measures the magnetization by cycling the applied field from -30 to $+30$ kOe with a step rate of 100 Oe s^{-1} . Measurements were performed on USPIO solutions at $1 \text{ g}\cdot\text{L}^{-1}$ at 300 K.

3.8 Cytotoxicity assay

A549 cells were grown in DMEM, supplemented with 10% Fetal Bovine Serum (FBS) and 1% Penicillin/Streptomycin (PS) in 75 cm^2 cell culture flasks, incubated in a humidified incubator with 5% CO_2 at 37°C . At confluence, cells were detached with trypsin/EDTA 0.25%/0.02% (Millipore), and diluted (1:5) and seeded in a new culture cell flask.

The HA-DOX nanogels cytotoxicity was evaluated, *in vitro*, using the 3-(4,5-dimethylthiazol-2-yl)-2,5-diphenyl-tetrazolium bromide (MTT) assay. The tetrazolium salt is widely used to quantify cytotoxicity, by colorimetry. The tetrazolium salts are metabolically reduced to highly colored end products, formazans (Mosmann, 1983). The colorless MTT is cleaved to formazan by the succinate-tetrazolium reductase system, which belongs to the mitochondrial respiratory chain and is active only in viable cells.

For the cytotoxicity assay, cells were seeded in 96 well plates (5000 cells/well) and incubated overnight for adhesion. The culture medium was removed, each sample (dispersed in PBS pH 7.4) was added to the respective well (diluted in culture medium: 20% v/v) and incubated for 24, 48 or 72 h.

At each time point, the culture medium was removed, cells were washed with PBS pH 7.4, and 50 μ L of MTT (1.0 mg/mL in DMEM without phenol red) was added and incubated at 37°C for 2 h. Then, the liquid was removed and MTT crystals were dissolved in 100 μ L of isopropanol incubating 30 min with smooth agitation. The absorbance was measured at 570 nm in a microplate reader Cytation 3 (Biotek). Isopropanol was used to measure the background. The test was performed in triplicate for all conditions.

4. RESULTS AND DISCUSSION

4.1 Synthesis of amphiphilic HA

4.1.1 Amphiphilic HA production with two different DS

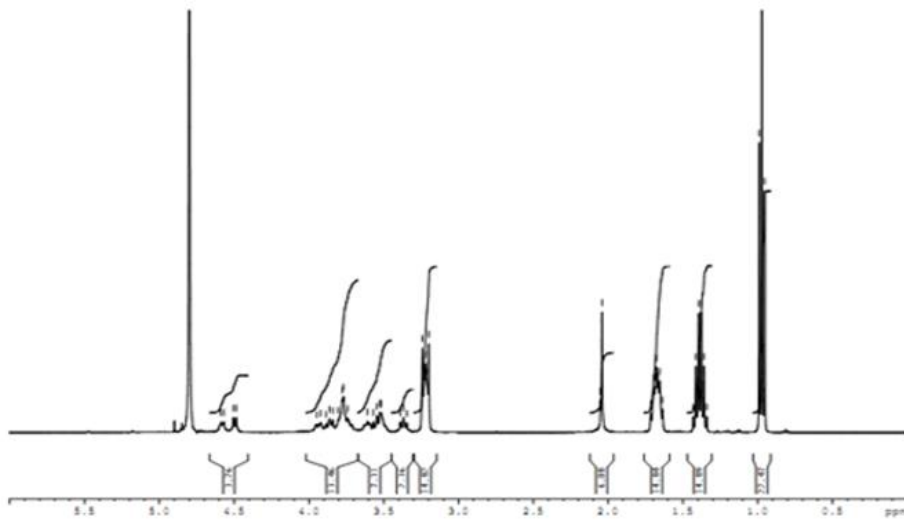
To render sodium hyaluronate soluble in DMSO, the sodium ions of HA were exchanged by the TBA ions as described in the literature (Oudshoorn, Rissmann, Bouwstra, & Hennink, 2007). After the ion exchange, the reaction between hexadecylamine, C₁₆NH₂, and HA-TBA was performed in DMSO. The synthesis of HA-C₁₆NH₂ with different degrees of substitution was accomplished by varying the molar ratio (theoretical DS) of NH₂ groups from hexadecylamine to COOH groups from HA, in the reaction mixture.

¹H NMR was used to calculate the degree of substitution (DS). The grafting of the hydrophobic chain and the respective DS, defined as the number of C₁₆NH₂ molecules per 100 disaccharide units of HA, was confirmed by ¹H NMR spectroscopy (**figure 4.1**). In the **Figure 4.1 A**, it is represented the ¹H NMR spectrum for HA-TBA and **figure 4.1 B** for the HA-C₁₆NH₂. When both are compared, there are two different peaks, at δ=0.915 and δ=2.046–2.057, present on the HA-C₁₆NH₂ spectrum, confirming the reaction success.

The peak correspondent to C₁₆NH₂, δ=0.915, is assigned to three protons present in the methyl group (-CH₃), which is identified in **figure 4.1 B**, with the letter **A**. The peaks corresponding to HA, with chemical shifts of δ=4.479-4.589, δ=3.604-3.924, δ=3.389-3.604 and δ=3.369-3.389, are assigned to the eleven protons present in the disaccharide, which are identified in **figure 4.1 B**, with the letter **B**. The C₁₆NH₂ degree of substitution (DS) was thus calculated according to equation 4.1:

$$DS (\%) = \frac{\text{number of H from peak B}}{\text{number of H from peak A}} * \frac{\int \text{peak area A}}{\int \text{peak area B}} * 100 \quad (\text{Equation 4.1})$$

A



B

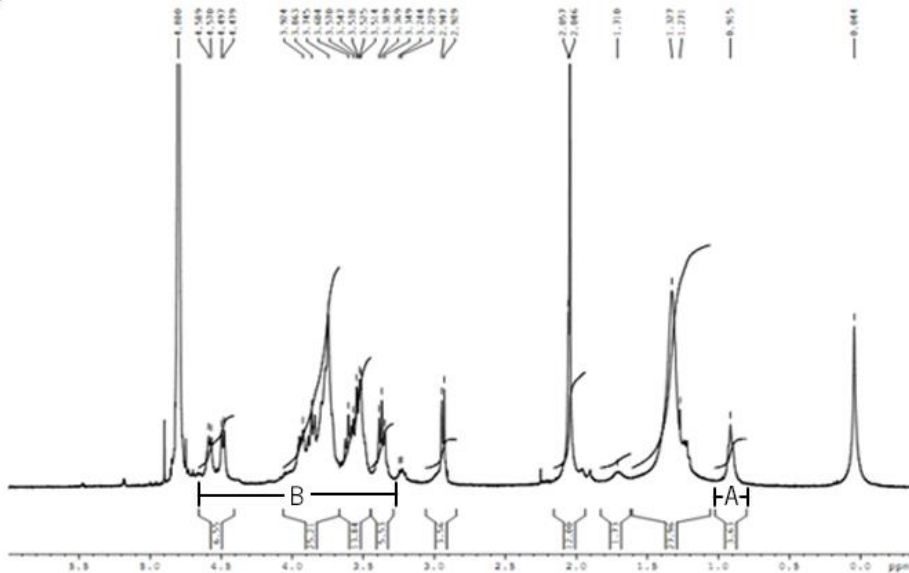


Figure 4.1: ^1H NMR spectra in D_2O of HA-TBA (A) and HA-C₁₈NH₂ (B) for the theoretical DS 30 %.

For a theoretical DS of 30 %, it was obtained a real DS of 26 %, as shown in **figure 4.1**, while for a theoretical DS 15 % the DS obtained was 10.5 %. Both results are presented in **table 4.1**.

Table 4.1: Results of the different productions of amphiphilic HA.

DS (%)		Material Designation
Theoretical	Real	
30.0	26.0	HA _{26.0}
15.0	10.5	HA _{10.5}

It is noticed that the obtained DS value is always lower than the theoretical one, meaning that the reaction efficiency is under 100 % of effectiveness. The efficiency obtained for the HA_{10.5} was 70.0 % while for the HA_{26.0} was 87.7 %.

The produced materials were dispersed in distilled water (1.0 mg/mL) and the size distribution was evaluated over time (more than 3 months) using DLS, as to assess the stability in aqueous medium.

The output of the DLS measurement consists on a distribution profile with an average size, and polydispersity index (Pdl), as shown in **figure 4.2**, and a correlogram graph, as shown in **figure 4.3**.

	Size (d.nm):	% Intensity:	St Dev (d.nm):
Z-Average (d.nm): 136,7	Peak 1: 178,3	100,0	78,56
Pdl: 0,224	Peak 2: 0,000	0,0	0,000
Intercept: 0,937	Peak 3: 0,000	0,0	0,000
Result quality : Good			

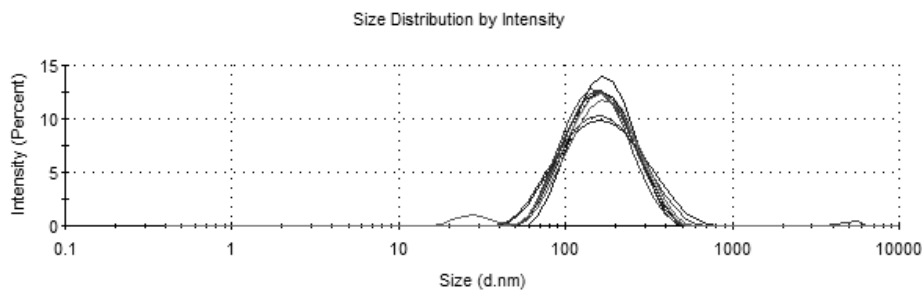


Figure 4.2: Average size distribution of a HA_{10.5} solution at 1 mg/mL, 10 consecutive measurements are represented.

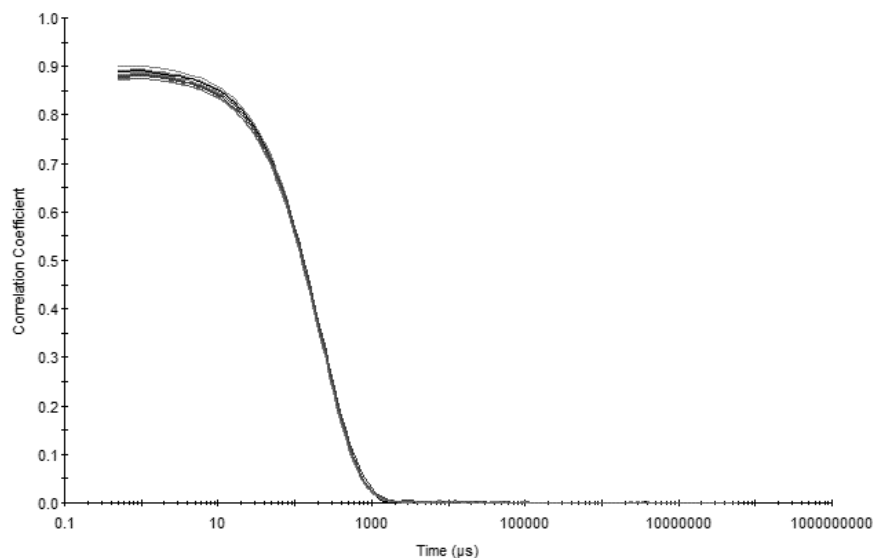


Figure 4.3: Correlogram of HA_{10.5} with 10 consecutive measurements are represented.

The DLS provides valuable information on the homogeneity of the dispersion. A single and sharp peak in the DLS profile implies the existence of a single and uniform particle population. The Pdl is an

indicator of the dispersion of the values measured. Pdl values above 0.3 are indicative of significant heterogeneity.

The stability of HA_{10.5%} and HA_{26.0%} nanogels were evaluated during a period of time, at least 3 months. Their average size and Pdl over time are represented in **figure 4.4**.

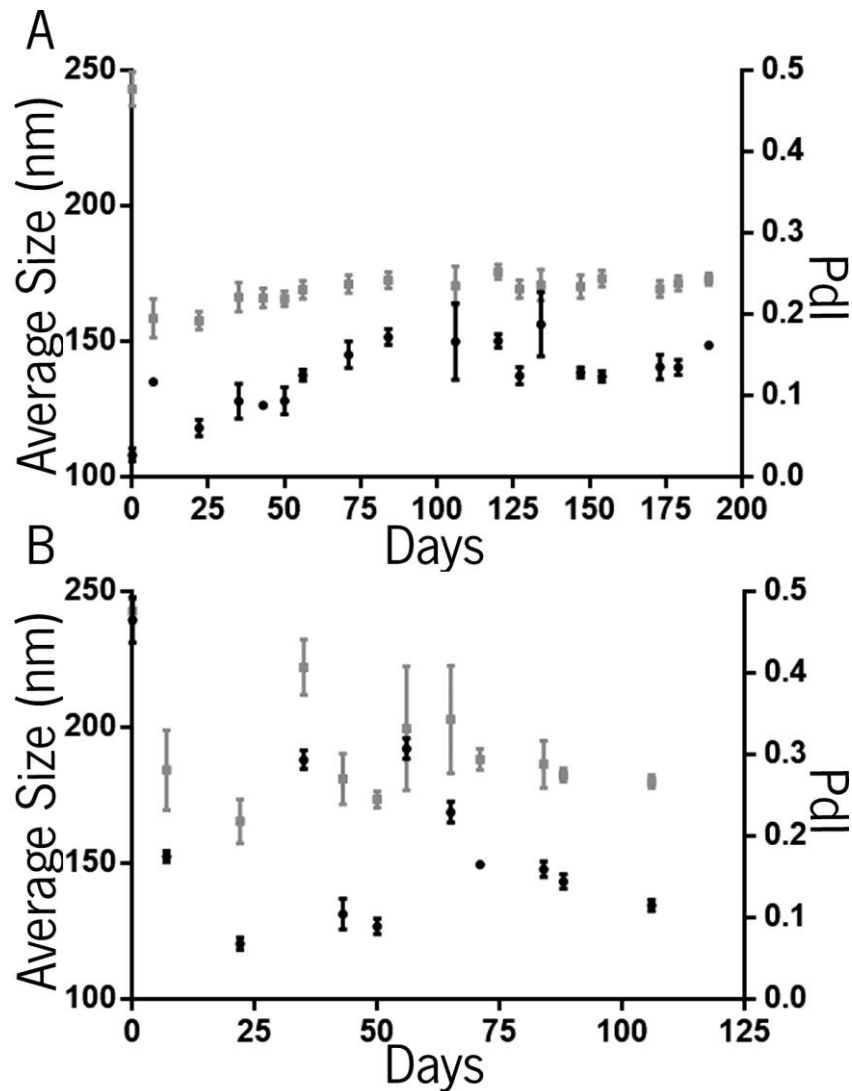


Figure 4.4: Average Size (●) and Pdl (■) values obtained for HA_{10.5%} (A) and HA_{26.0%} (B) over time, with the respective standard deviation (n=10).

The HA_{10.5%} is more stable than the HA_{26.0%} presenting fewer variations regarding the average size and maintaining low Pdl. Regarding the NG dispersion in water, the HA_{26.0%} was harder to disperse than the HA_{10.5%} sample, probably due to higher DS (higher density of hydrophobic chains). The DS should be balanced, since more substituted nanogels turns the dispersion more difficult and can present more cytotoxicity. Otherwise, DS can improve the nanogels stability due to the increase of hydrophobic interactions that are the driving force on the nanogels formation. In that way, theoretical DS 15 % was chosen to proceed for the following work.

4.1.2 Production of amphiphilic HA using theoretical DS 15 %

Amphiphilic HA was produced using 15 mol of hexadecylamine per 100 disaccharide units of HA (theoretical DS 15 %). Different batches were produced and the real DS obtained for each one is presented in **table 4.2**.

Table 4.2: Different batches of amphiphilic HA produced with a theoretical DS of 15 %.

DS (%)		Material Designation
Theoretical	Real	
15.0	8.0	HA _{8.0}
	10.5	HA _{10.5}
	12.6	HA _{12.6}

Although the same theoretical DS and reaction conditions were used, the result of each batch was different, resulting in three different real DS: 8.0 %, 10.5 % and 12.6 %. The efficiency obtained for the HA_{8.0} was 53.3 %, HA_{10.5} was 70 % and HA_{12.6} was 84 %. The results obtained suggest that the real DS of amphiphilic HA can be controlled through the molar ratio of hexadecylamine to disaccharide units of HA in the reaction mixture (theoretical DS), although some variations probably also associated with the DS quantification technique.

The size distribution of each material was also evaluated to understand the DS influence on average size and Pdl. Results are shown in **figure 4.5**.

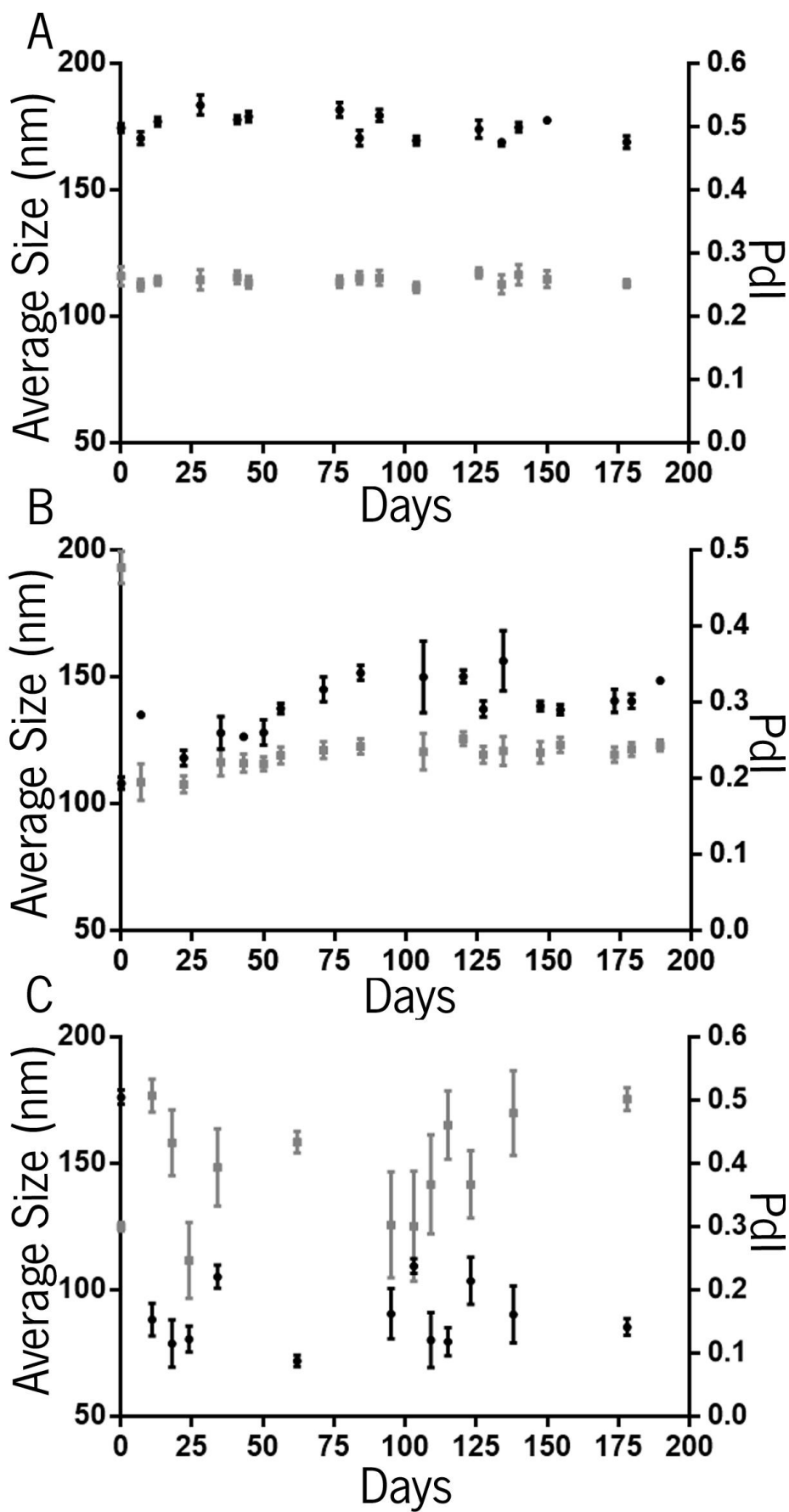


Figure 4.5: Average size (●) and Pdl (■) values obtained for HA₆₀ (A), HA_{10.5} (B) and for HA_{12.6} (C) over time, with the respective standard deviation (n=10).

Generally, when increasing the real DS, the average size tends to decrease, while the Pdl value tend to increase. HA_{8.0} and HA_{10.5} show high stability in the timeframe studied with interesting average size for DDS (< 200 nm) and low polydispersity. Regarding dispersion in water, no differences were observed between materials, all dispersing easily. For the upcoming work, HA_{12.6} was chosen due to its smaller average size, below 120 nm, which is suitable for the upcoming work.

4.2 Production of HA-DOX nanogels

HA-DOX nanogels were produced through two different approaches: via hydrazone linkage or amide linkage. The analysis of the results obtained using each approach will be done separately.

4.2.1 Hydrazone Linkage

In this approach, the doxorubicin grafting is mediated by the ADH molecule.

The ADH linkage and the respective DS_{ADH} , defined as the number of ADH molecules per 100 disaccharide units of HA, was confirmed by 1H NMR, as shown in **figure 4.6**. Comparing the 1H NMR spectrum of amphiphilic HA (**figure 4.6 A**) and HA-ADH (**figure 4.6 B**) two new peaks appear, after the reaction, at $\delta=2.107-2.299$ and $\delta=1.691$.

The ADH peaks used in the calculation of DS_{ADH} are assigned to eight protons from methylene groups ($H_2N-NH-(CH_2)_4-NH-NH_2$), $\delta=2.107-2.299$ and $\delta=1.691$, identified in **figure 4.6 B**, with the letter **A**. The HA peaks are assigned to the eleven protons present in the disaccharide, $\delta=4.592-4.484$, $\delta=3.949-3.756$, $\delta=3.756-3.529$ and $\delta=3.412-3.3352$, are identified in **figure 4.6 B**, with the letter **B**. The DS_{ADH} (%) was calculated using the equation 4.1.

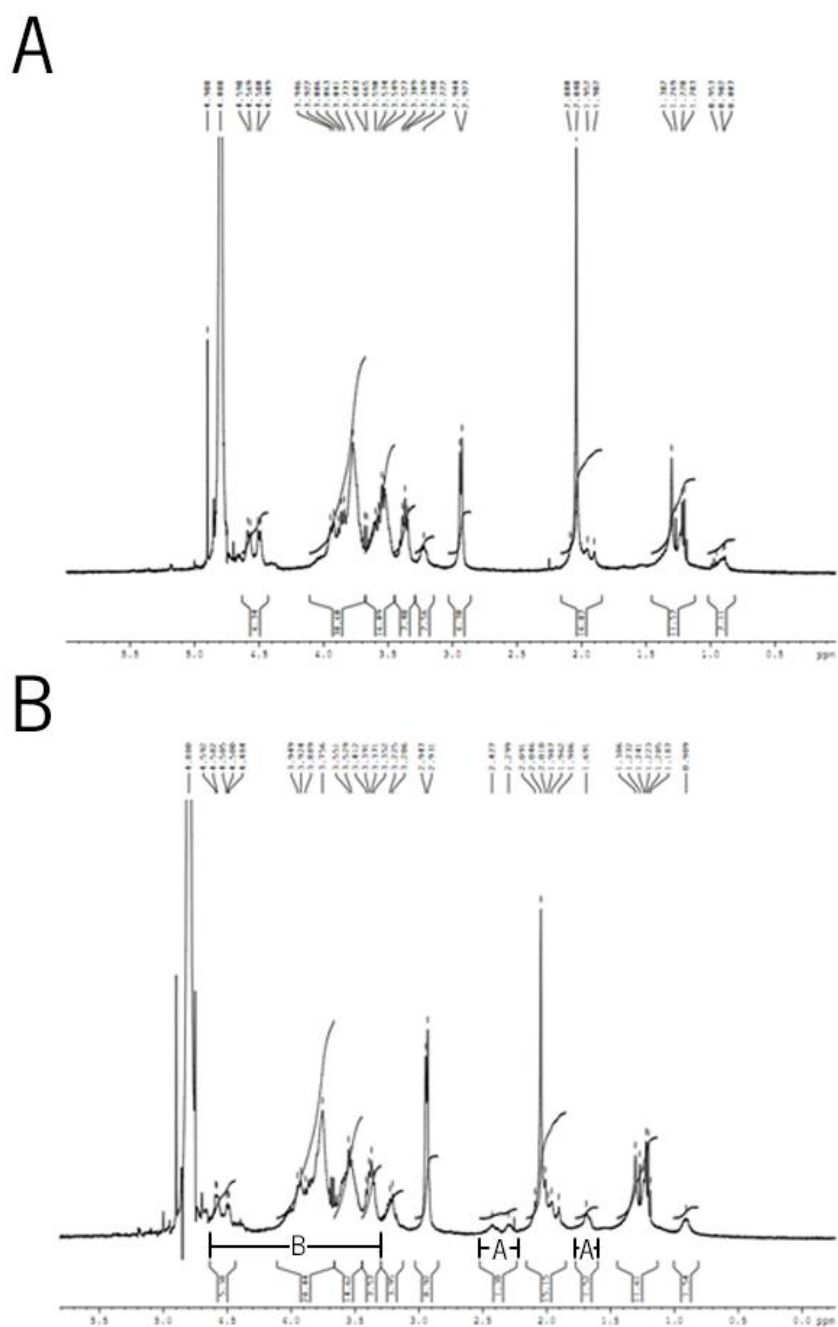


Figure 4.6: ^1H NMR of HA_{126} (A) and $\text{HA}_{126}\text{-ADH}$ (B), in D_2O .

DS_{ADH} (%) obtained for HA-ADH conjugation was 6.9 %. The average size and Pdl values obtained over time are shown in **figure 4.7**.

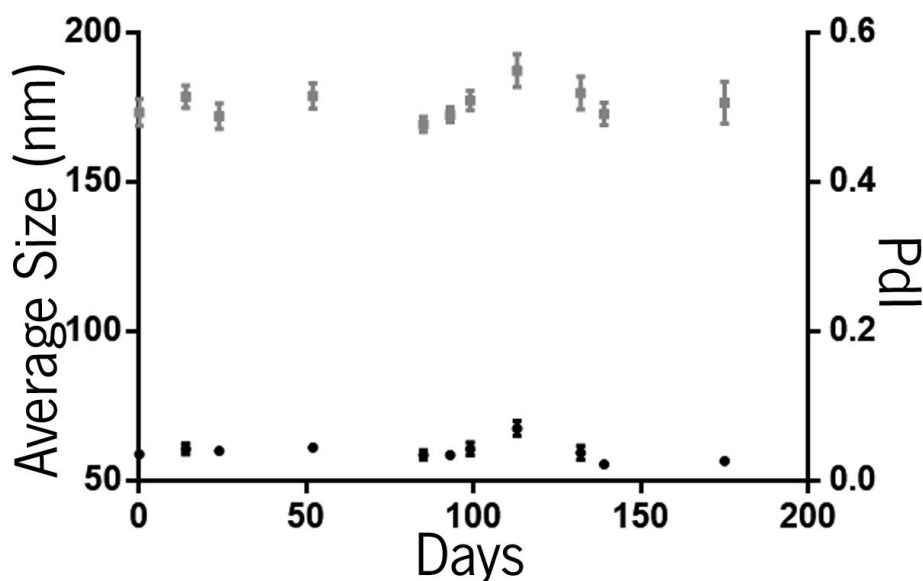


Figure 4.7: Average size (●) and PDI (■) values obtained for HA-ADH_{6,9} over time, with the respective standard deviation (n=10).

The HA-ADH_{6,9}, produced from the amphiphilic HA_{12,6}, exhibits a smaller average size (< 70 nm) when compared with HA_{12,6}. The stability seems enhanced after ADH reaction, while the PDI slightly increased (around 0.5).

The next step is the conjugation between DOX and HA-ADH by reacting the ketone group of DOX and the amine group of ADH, obtaining a pH-sensitive linkage. The reaction was performed using different solvents, DMSO or PBS. The results obtained regarding reaction efficiency are present in **Table 4.3**.

Table 4.3: Results obtained for HA-DOX nanogels, via hydrazone.

	HA _{Hidra1}	HA _{Hidra2}	HA _{Hidra3}
Solvent	DMSO	PBS	PBS
DS _{C₁₆NH₂} (%)	8.0	8.0	12.6
DS _{ADH} (%)	8.7	8.7	6.9
DOX Concentration (µg/mg)	49	25	22
% DOX theoretical (mol/mol)	36.1	37.2	30.1
% DOX real (mol/mol)	39.6	20.5	22.5
Reaction Efficiency (%)	109.5	55.1	74.6

Absorbance spectrum of the HA-DOX conjugates, free DOX (25 µg/mL and 50 µg/mL) and HA-ADH dissolved with 25 µg/mL of DOX (without reaction) are present in **figure 4.8**. All materials were dispersed in PBS buffer pH 7.4.

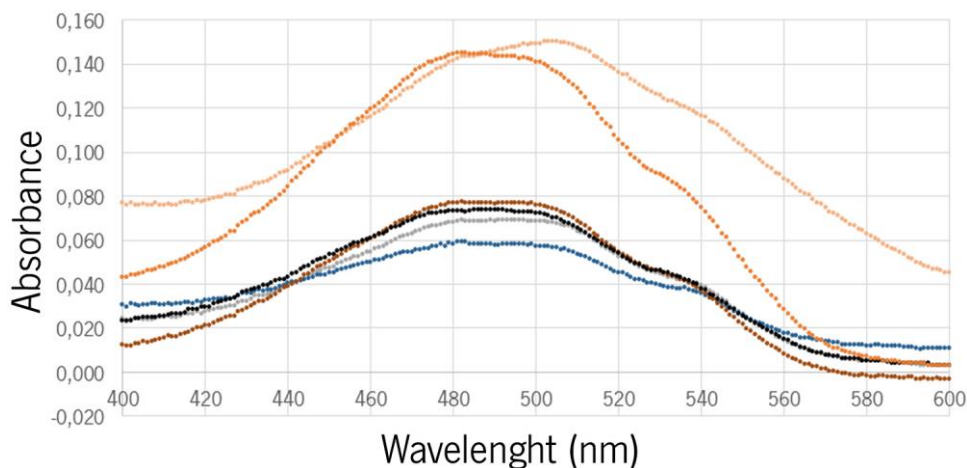


Figure 4.8: Absorbance spectra of free DOX at 25 µg/mL (●) and 50 µg/mL (○), HA_{Hidra1} 1.0 mg/mL (○), HA_{Hidra2} 1.0 mg/mL (●), HA_{Hidra3} 1.0 mg/mL (●) and HA-ADH 1.0 mg/mL with free DOX at 25 µg/mL (●) when dispersed at PBS buffer pH 7.4.

The DOX concentration was obtained from the calibration curve, shown in the **Supplementary Data section, figure S.1 (DOX Calibration Curve)**. All calculations are exemplified at **Calculation Example I** in the **Supplementary Data section**.

DS_{C16NH2} might affect the DS_{ADH}, since as DS_{C16NH2} value increases, the DS_{ADH} tends to decrease, as it was confirmed from the results presented in **table 4.3**. Since both compounds bond to the carboxyl groups available in the HA, the inverse relation between the grafted amount of each one could be expected.

The solvent used might have some influence in the DOX conjugation. The NG produced in DMSO, presented a higher DOX concentration when compared with the two NG produced in PBS, suggesting that DMSO could be a better option as solvent for the conjugation reaction. The two NG samples produced in PBS presented similar DOX concentration, probably because the DS_{ADH} values were similar and the amount of ADH present in the HA will directly influence the DOX concentration obtained.

Absorbance spectra show that all conjugates present a very similar spectra, exhibiting a peak at 488 nm and a shoulder at 540 nm. The exception is HA_{Hidra1}, which presented a peak at 510 nm and a shoulder at 540 nm. The peak shift is not related with other reagents that can be present, such as: NHS presents a strong absorbance at 260 nm (Hermanson, 2013), EDC shows a high absorbance between 213/214 nm (Wrobel et al., 2002) and the volume of TEA used was too low to have any interference.

The average size and Pdl values, over time, for these conjugates are shown in **figure 4.9**.

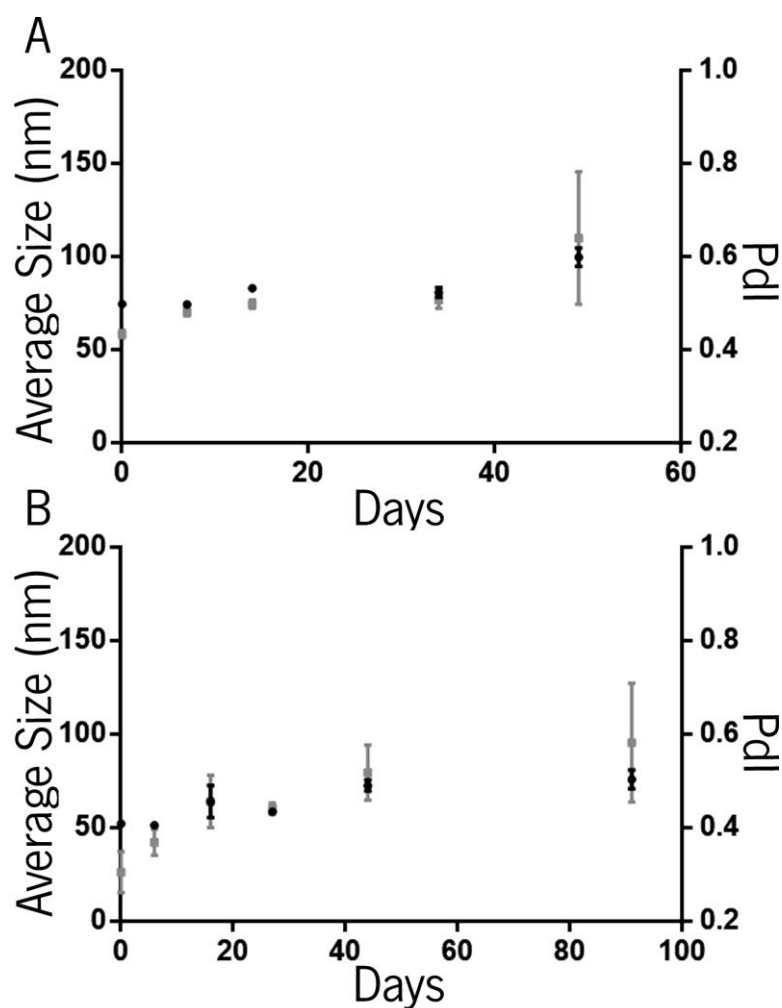


Figure 4.9: Average size (●) and PDI (■) obtained for the HA-DOX nanogels over time, HA_{Hidra2} (A) and HA_{Hidra3} (B), with the respective standard deviation (n=10).

Although the promising results regarding the DOX incorporation of HA_{Hidra1} (produced in DMSO), as seen in **table 4.3**, this material proved to be unstable, in the DLS evaluation (data not shown).

The materials produced in PBS buffer present an average size suitable for DDS, below 100 nm, although presenting some polydispersity, around 0.5.

HA_{Hidra3} presented an average size of 70 nm, an average polydispersity index of 0.45 and DOX concentration of 22 µg/mg. This NG presents some interesting features and will be used on the upcoming work.

4.2.2 Amide Linkage

In this approach, the doxorubicin grafting was performed directly to the amphiphilic HA, between the amine group of DOX and the carboxyl group present in HA. The results obtained regarding this reaction are presented in **table 4.4**.

Table 4.4: Results obtained for HA-DOX nanogels, via amide.

	HA _{Am1}	HA _{Am2}
DS _{C₁₆NH₂} (%)	10.5	12.6
DOX Concentration (µg/mg)	22	29
% DOX theoretical (mol/mol)	4.6	3.3
% DOX real (mol/mol)	1.7	2.3
Reaction Efficiency (%)	37.1	71.3

Absorbance spectrum of each conjugate, free DOX (25 µg/mL) and HA-C₁₆NH₂ dissolved with 25 µg/mL of free DOX (without reaction) are presented in **figure 4.10**. All materials were dispersed in PBS buffer pH 7.4.

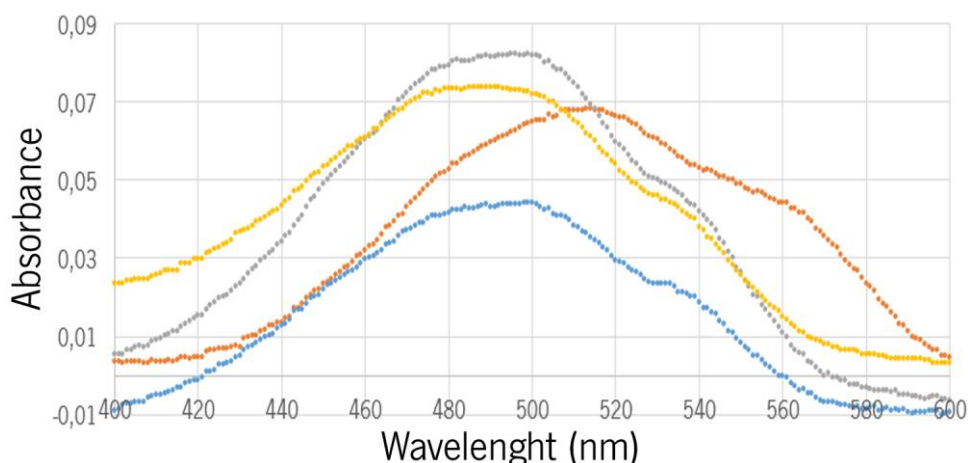


Figure 4.10: Absorbance spectra of free DOX at 25 µg/mL (●), HA_{Am1} (●), HA_{Am2} (●) and HA-C₁₆NH₂ 1.0 mg/mL with free DOX 25 µg/mL (●) when dispersed at PBS buffer pH 7.4.

The DOX concentration was obtained from the calibration curve, shown in the **Supplementary Data section, figure S.1 (DOX Calibration Curve)**. All calculations are exemplified at **Calculation example II** in the **Supplementary Data section**.

DS_{C₁₆NH₂} was expected to influence the conjugation of DOX to the HA backbone, considering that C₁₆NH₂ and DOX compete to the carboxyl groups in HA molecule. However, that was not verified according to the obtained results, probably due to the low DS_{C₁₆NH₂} (15 %) used, which means that 85 % of carboxyl groups in HA disaccharides are free for reaction with DOX. The DOX concentrations obtained are similar,

although the reaction efficiency is very different, being higher for HA_{Ami2}. That could suggest that the higher DS_{C16NH2}, the higher conjugation with DOX may be obtained, probably due to the higher hydrophobicity present in the NG.

The absorbance spectrum of HA_{Ami2} presents a peak at 488 nm and a shoulder at 540 nm, as happened for the free DOX and the HA-C₁₆NH₂ solution with free DOX. These results suggest that probably the DOX is not grafted to the HA. The HA_{Ami1} presents a different peak, at 513 nm, and a shoulder at 560 nm. These variations are not related to the use of NHS, TEA and EDC due to the previously reported reasons.

These materials were evaluated regarding their average size and Pdl values over time, the results obtained are shown in **figure 4.11**.

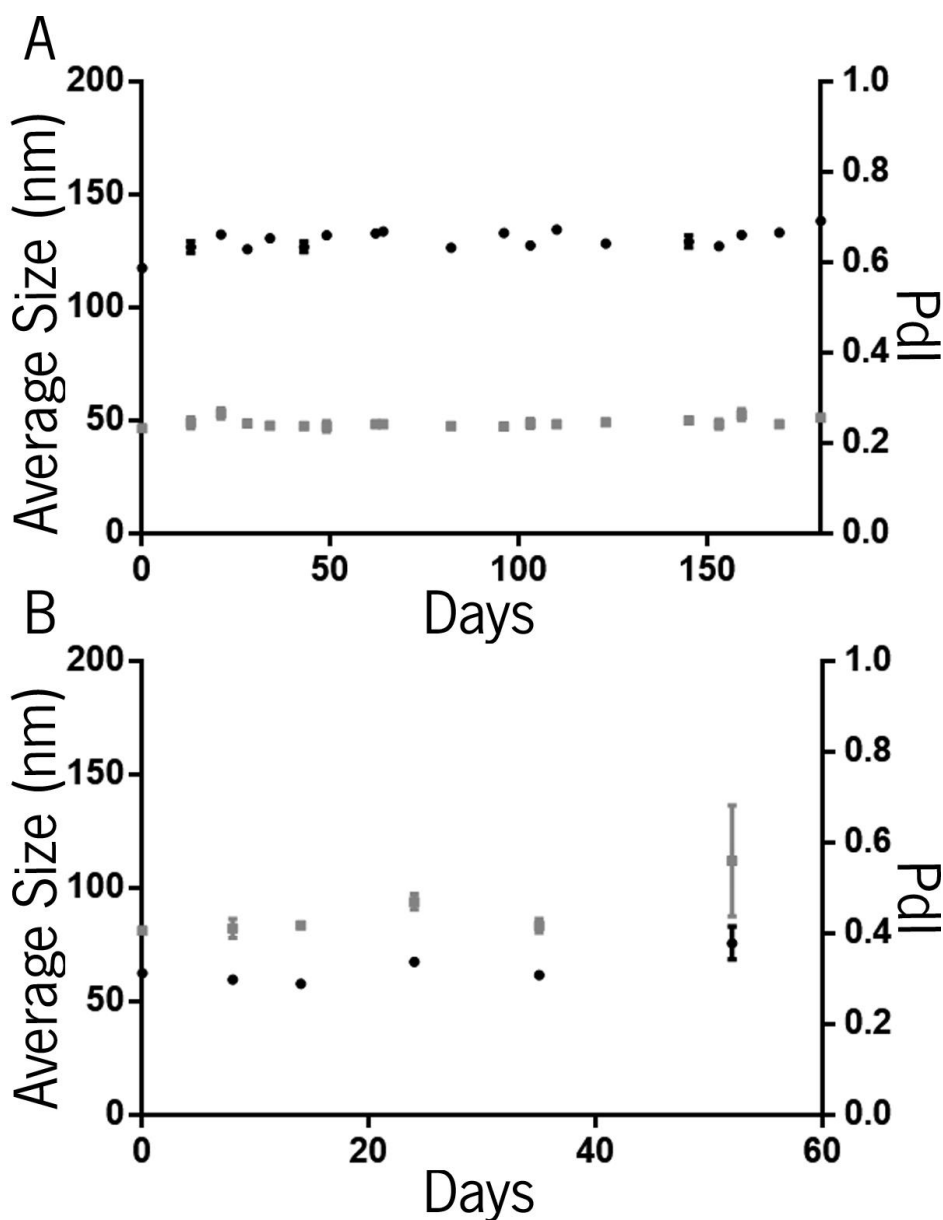


Figure 4.11: Average size (●) and Pdl values (■) for the HA-DOX nanogels, HA_{Ami1} (A), HA_{Ami2} (B), with the respective standard deviation (n=10).

Both NG present an interesting average size for DDS (< 150 nm), although the HA_{A_{mi2}} has the smallest average size (< 70 nm), however its polydispersity value is higher (around 0.45). As HA_{A_{mi2}} presented the smallest average size and highest DOX concentration, 29 µg/mg, this NG may present some interesting features when associated with γ -Fe₂O₃.

4.3 Release Studies

The release studies were performed using two different pH values: 5.0, mimicking lysosomal pH (Cooper, 2000; Mindell, 2012) and 7.4, mimicking extracellular pH.

It is important to study the kinetics of DOX release from the NG. It should not happen too fast, enabling the nanogel to reach the target site. On the other hand, it should not be too slow, enabling the nanogel recognition and remotion by the Mononuclear Phagocytic System. Ideally, the release kinetics should be controlled by the microenvironmental pH. A higher DOX release at pH 5.0 from the nanogels conjugated via hydrazone linkage is expected, due to the pH-sensitive linkage, unlike nanogels produced via amide linkage, a stable linkage. Both NG should present low release at pH 7.4, avoiding the release of DOX before reaching the target site.

The **figure 4.12** presents the cumulative release profiles for HA_{Ami2y}, HA_{Hidra3} and free DOX at pH 5.0 or 7.4. All related calculations are presented at **Release Data** in the **Supplementary Data section**.

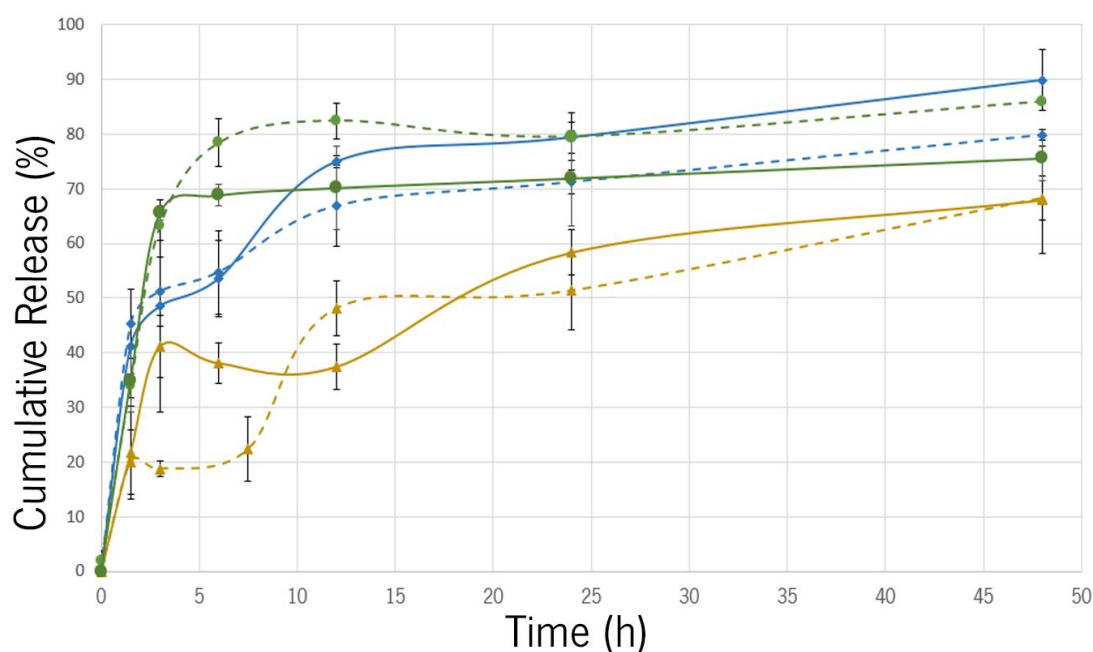


Figure 4.12: Cumulative release (%) profiles for HA_{Ami2y} (◆), HA_{Hidra3} (▲) and free DOX (●), at pH 7.4 (solid line) or pH 5.0 (dashed line), (n=3).

As expected, free DOX is quickly released in the first 6 h: 78.4 % at pH 5.0 and 68.8 % at pH 7.4.

In the case of nanogels, different release profiles are observed regarding linkage type and pH value. HA_{Hidra3} presented different releases profiles at each pH, essentially in the first 9 h. Surprisingly, the release of DOX occurs faster at pH 7.4 than at pH 5.0, suggesting that the HA_{Hidra3} obtained does not bear pH responsive properties.

Unexpectedly, the HA_{Amt2} nanogels presented higher % of cumulative release, at both pHs, than HA_{Hdra3}, which was not expected considering the stability of the amide linkage. It could be hypothesized that DOX is not conjugated to the HA, as it was observed 54 % of DOX release in the first 6 h, for both pHs.

From the literature, DOX has been used to develop different pH-responsive drug release systems. One example is the one performed by *Gillies et al.* (Gillies & Fréchet, 2005), in which, DOX-loaded micelles were developed. For the release study of DOX-loaded micelles, different pH values (4.0-7.4) were used, while for free DOX pH 5.0 or 7.4 were used. The results showed that free DOX achieved higher releases (100 % for pH 5.0 and 90 % for pH 7.4) after 18 h, while for the DOX-loaded micelles only achieved releases near 100 % after 72 h (at pH 4.0). These results demonstrated that the carriers used by *Gillies et al.* decrease the release rate of DOX when compared to free DOX. In the present study, the DOX release was also retarded by conjugation with nanogels, mainly in the first 12 h, however the conjugation procedure should be optimized.

4.4 $\gamma\text{-Fe}_2\text{O}_3$ incorporation

$\gamma\text{-Fe}_2\text{O}_3$ incorporation into HA-DOX NGs was performed according to *Gonçalves et al.* (Gonçalves et al., 2013). The concentration of the amphiphilic HA was 1.3 mg/mL and a concentration of 13.3 mM of Fe was added.

Two formulations were prepared using HA_{Ami2} and HA_{Hidra3} for $\gamma\text{-Fe}_2\text{O}_3$ stabilization. The results obtained are presented in **figure 4.13**.

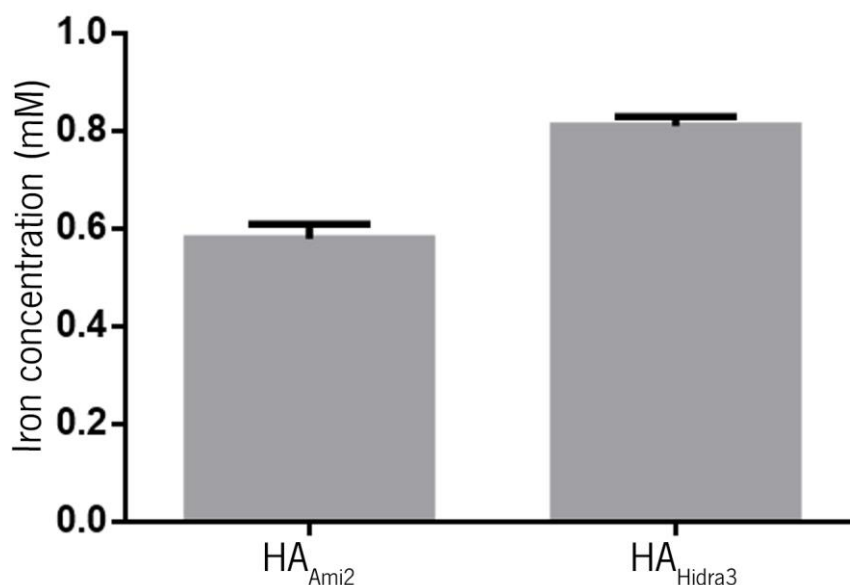


Figure 4.13: Result of the iron quantification after the incorporation of $\gamma\text{-Fe}_2\text{O}_3$ into different NG, with the respective standard deviation (n=6).

The $\gamma\text{-Fe}_2\text{O}_3$ quantification was performed using a calibration curve, which is presented at **$\gamma\text{-Fe}_2\text{O}_3$ incorporation** in the **Supplementary Data section**, as well as all associated calculations. After the $\gamma\text{-Fe}_2\text{O}_3$ incorporation into the NG, the nanosystem is designed nanomagnetogels.

HA_{Ami2} presented 0.6 mM of incorporated $\gamma\text{-Fe}_2\text{O}_3$, while HA_{Hidra3} incorporated 0.8 mM of $\gamma\text{-Fe}_2\text{O}_3$. *Gonçalves et al.* (Gonçalves et al., 2013) achieved higher iron incorporation with dextrin nanogels (about 4.0 mM of $\gamma\text{-Fe}_2\text{O}_3$ incorporated). The presence of anionic charges in the HA-based NG may influence the incorporation of $\gamma\text{-Fe}_2\text{O}_3$ NPs.

The average size and Pdl of nanomagnetogels were measured. The results are presented in the **figure 4.14**.

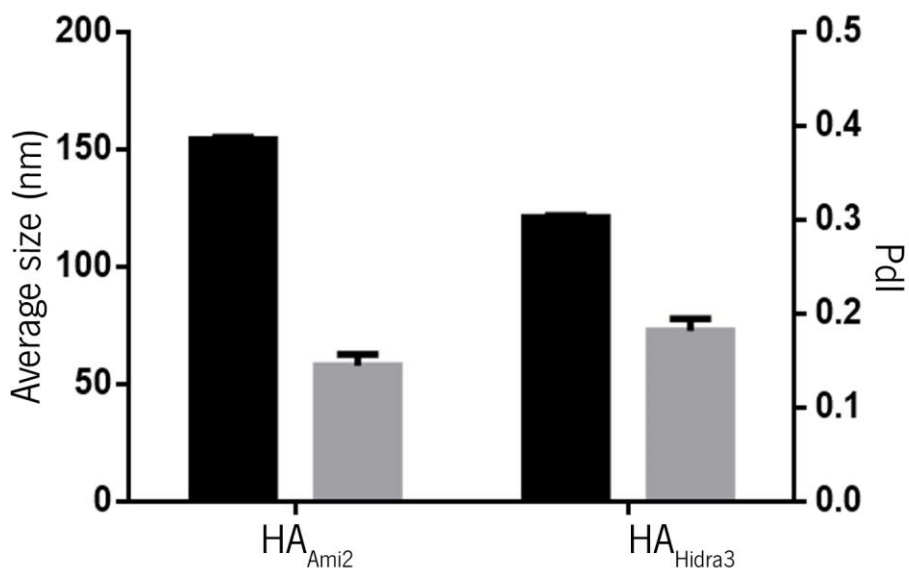


Figure 4.14: Average size (■) and Pdl (■) distribution for HA-DOX conjugates after the incorporation with $\gamma\text{-Fe}_2\text{O}_3$, (nanomagnetogels), with the respective standard deviation (n=5).

All nanomagnetogels present very similar average size (100-160 nm). The incorporation of $\gamma\text{-Fe}_2\text{O}_3$ increased the average size of the nanogels, which remains interesting for DDS. Regarding the polydispersity index, lower values were obtained for the nanomagnetogels.

Zeta Potential of nanomagnetogels was evaluated. The results are presented in **figure 4.15**.

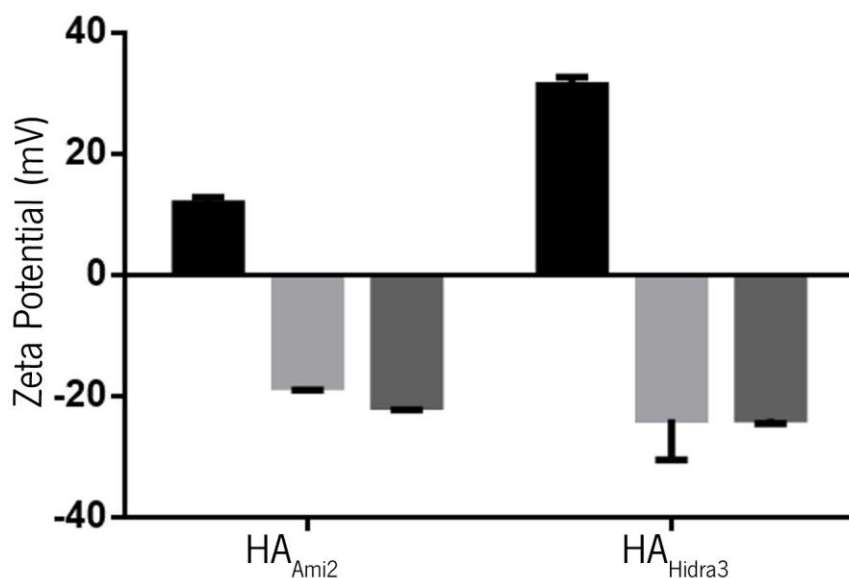


Figure 4.15: Zeta Potential of free $\gamma\text{-Fe}_2\text{O}_3$ (■), NG (■) and the nanomagnetogels (■), each value presents its standard deviation, (n=5).

The zeta potential values are positive for bare $\gamma\text{-Fe}_2\text{O}_3$ and negative for empty nanogels. The zeta potential remains negative after the iron incorporation (nanomagnetogels). Similar zeta potential values

are obtained for nanogels and nanomagnetogels, therefore it can be concluded that the iron nanoparticles were incorporated into the nanogels. According to the literature, negatively charged nanoparticles present a lower phagocytic uptake, leading to a longer blood circulation time, in contrast to positively charged nanoparticles (Duan et al., 2013). Therefore, it could be expected improved and satisfactory circulation time for nanomagnetogels.

The magnetic properties of HA_{Ami2} and HA_{Hidra3} were measured and the results are presented in **figure 4.16**.

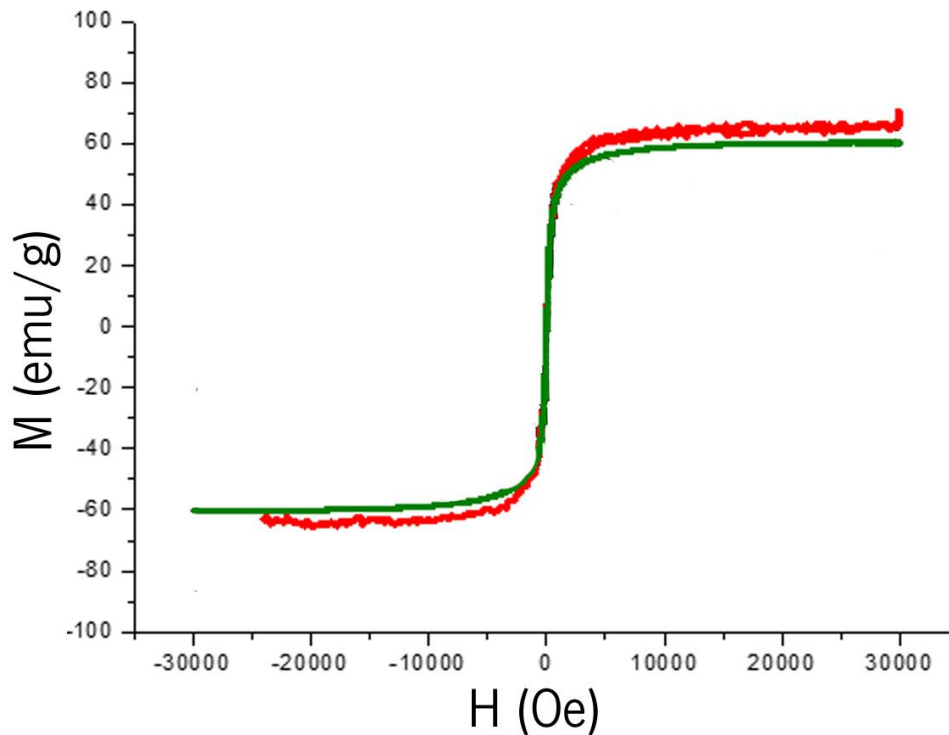


Figure 4.16: Magnetization versus magnetic applied field of HA_{Hidra3} (red) and free $\gamma-Fe_2O_3$ (green). Nanomagnetogels were dispersed in distilled water pH 7.4, while bare $\gamma-Fe_2O_3$ in distilled water pH 2.0.

The magnetization obtained for bare $\gamma-Fe_2O_3$ was 62 emu/g, while for the nanomagnetogel HA_{Hidra3} was 65 emu/g. The magnetization measurement of HA_{Ami2} was not possible. The magnetic properties of bare $\gamma-Fe_2O_3$ are conserved after their stabilization within nanogels, since the magnetization profile of bare $\gamma-Fe_2O_3$ is similar to the one obtained for HA_{Hidra3} . This result confirms that the $\gamma-Fe_2O_3$ NPs are incorporated into the NG, otherwise $\gamma-Fe_2O_3$ NPs would not be stable in aqueous solution losing their magnetization profile.

4.5 Cytotoxicity

HA is classified according to its Molecular Weight (MW). High MW HA (> 1000 kDa) may induce a possible inhibition of cell proliferation, while low MW HA (< 50 kDa) did not induce a similar result (Boeckel et al., 2014; Kunze et al., 2010; Pilloni et al., 1998). As the HA used in this work has an MW of 7.68 kDa, it is not expected to reveal any cytotoxicity.

HA-DOX nanogels were incubated with cells using two different DOX concentrations, 15 and 10 µg/mL, which determined the NG concentration of both amide and hydrazone linkage. Besides the HA-DOX nanogels, the reagents used in the nanogels production were also tested individually: HA_{12.6}, HA-ADH_{6.9}, C₁₆NH₂, ADH and free DOX as controls, to assess cytotoxicity. To evaluate the number of viable cells after different incubation times, MTT assay was used.

The % cell viability was calculated using equation 4.2:

$$\% \text{ cell viability} = \frac{\text{Absorbance of each condition}_{tn}}{\text{Absorbance medium control}_{tn}} * 100 \quad (\text{Equation 4.2}),$$

The absorbance of cells growth in the culture medium (negative control) at each incubation time was compared to the absorbance of each test condition, for the calculation of the % of cell viability. The results are presented in **figure 4.17**.

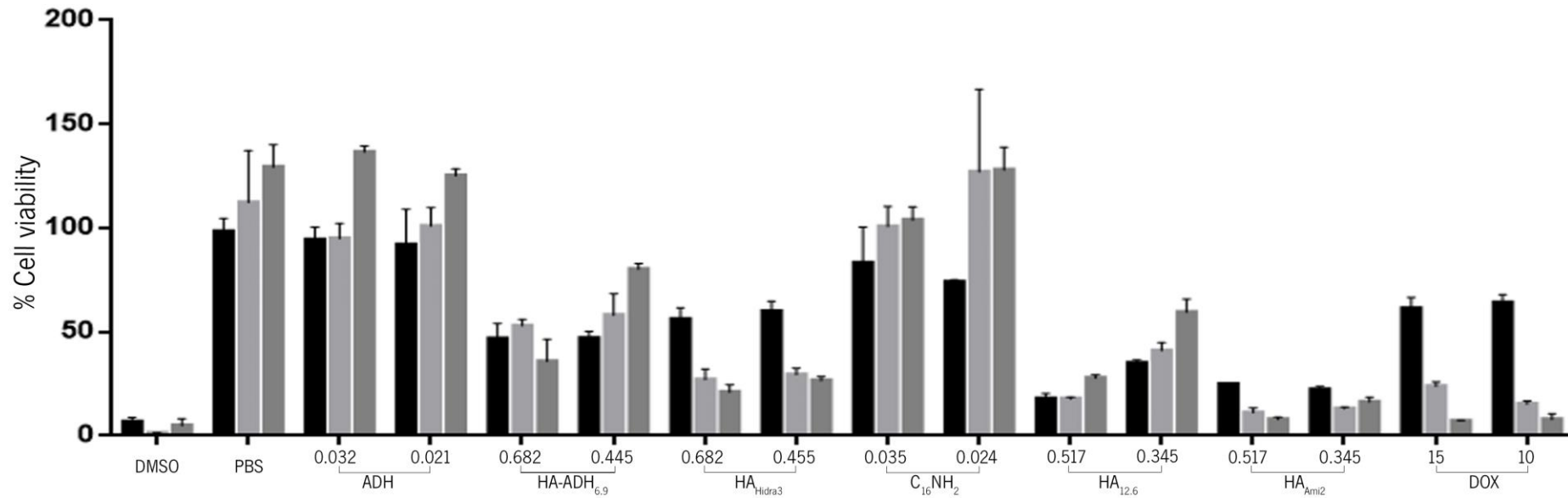


Figure 4.17: Cell viability of A549 cells was determined by MTT assay at 24 h (■), 48 h (▒) and 72 h (▓). For all nanogels the concentration is represented in mg/mL while for free DOX is expressed in $\mu\text{g/mL}$.

The PBS, ADH and C₁₆NH₂ controls did not exhibit much influence on cell viability up to 72 h of incubation, revealing a percentage of cell viability close to 100 % or superior.

HA-ADH_{6,9} and HA_{12,6} presented strong toxicity to the A549 cell line at all time points, with values of cell viability (%) below 50 %. These are surprising results demonstrating cytotoxicity of modified HA. In the literature, other modified HA has been produced, such as the HA-AT (HA grafted via amide with a C11 alkyl chain) produced by *Pedrosa et al.* (Pedrosa, Gonçalves, David, & Gama, 2014). The HA-AT's cytotoxicity was assessed by MTT assay and it was observed that the nanogel did not affect the cell viability for the tested cell lines (3T3, HMEC and RAW 264.7); however, a reduced cell proliferation was observed in 3T3 and RAW for a longer incubation time (72 h) (Pedrosa et al., 2016). The HA_{12,6} used in the present study is very similar to the one produced by *Pedrosa et al.*, being the main difference the length of the alkyl chain (C11 vs C16) that probably is not enough to explain the present results. The unexpected HA cytotoxicity can be related with the HA modification that requires a previous ion exchange using a resin that is removed by centrifugation and could be contaminating the material, supposing an inefficient removal.

Free DOX presented the expected cytotoxicity that increases along time. HA_{Hidra3} and HA_{Ami2} also have a cytotoxic effect, time-dependent, more pronounced for HA_{Ami2}.

The cytotoxic results for HA_{Ami2} supported the ones obtained in the release assay, where HA_{Ami2} presented the highest release, which could suggest a good therapeutic effect.

5. CONCLUSIONS AND FUTURE PERSPECTIVES

In the present work, two different HA-DOX nanogels were produced, via hydrazone linkage (pH-sensitive linkage) or via amide linkage from an amphiphilic HA. In addition, γ -Fe₂O₃ was incorporated physically into both nanogels without using any organic solvent or salt.

The degree of substitution should be balanced, in order to have enough hydrophobic chains for nanogels formation and on the other hand, maintain water dispersibility and prevent cytotoxicity eventually associated with long alkyl chains. Nanogels with DS_{15%} were selected for further characterization, since HA_{12.6} presented an average size lower than 150 nm and a polydispersity index lower than 0.5, that are interesting features for the development of a new DDS.

HA_{Hidra3} nanogels produced via hydrazone linkage were produced in PBS pH 7.4, as it showed to be a more appropriate solvent for the reaction. HA_{Hidra3} nanogels were produced with a DOX concentration of 22 μ g/mg, an average size of 100 nm, a polydispersity index around 0.5, presenting good stability up to 40 days, evaluated by DLS.

HA_{Ami2} nanogels produced via amide linkage in DMSO presented a DOX concentration of 29 μ g/mg, an average size of 70 nm and a polydispersity index around 0.45.

The DOX release studies were performed at two different pH values: 5.0, mimicking lysosomal pH or pH 7.4, mimicking the extracellular pH. Sink conditions were verified for free DOX. Unexpectedly, the amide nanogels revealed a faster release than the hydrazone nanogels, and the pH-responsiveness was not verified.

The incorporation of γ -Fe₂O₃ within nanogels was achieved resulting 0.6 mM γ -Fe₂O₃ for HA_{Ami2} and 0.8 mM γ -Fe₂O₃ for HA_{Hidra3}. The incorporation of γ -Fe₂O₃ led to an increased average size and a decrease of polydispersity values.

The zeta potential is negative and similar for empty nanogels and nanomagnetogels, while bare γ -Fe₂O₃ presents positive values, suggesting γ -Fe₂O₃ incorporation within nanogels.

The magnetization studies performed for HA_{Hidra3} demonstrated similar profiles for bare γ -Fe₂O₃ nanoparticles and for nanomagnetogels indicating that the magnetic properties are preserved after γ -Fe₂O₃ incorporation. This result also supports that the γ -Fe₂O₃ particles are incorporated into the HA_{Hidra3} nanogel.

Regarding cytotoxicity evaluation, HA-ADH_{6.9} and HA_{12.6} presented strong toxicity to the A549 cell line, revealing cytotoxicity of modified HA (without DOX), in opposition to the expected results. This result

may be related to the iron exchange performed previously to the HA modification. Free DOX presented the expected cytotoxicity that increases along time. HA_{Hidra3} and HA_{Ami2} also demonstrated time-dependent cytotoxic effect, more pronounced for HA_{Ami2}.

As future work, it would be interesting to study some of the following aspects:

- Guarantee the biocompatibility of modified HA;
- Optimize the HA-DOX conjugation to obtain higher efficiency and ascertain DOX linkage to achieve higher stability for amide linkage and pH-responsiveness for hydrazone;
- Study the HA-DOX nanogels internalization by CD44 responsive cells, with and without blocking receptors with HA;
- Test the nanogels in different cells lines (non-tumor), such as epithelial cells;
- Study nanomagnetogel stability after intravenous injection in animal models.

REFERENCES

- Allen, T. M., & Cullis, P. R. (2004). Drug delivery systems: entering the mainstream. *Science (New York, N.Y.)*, *303*(5665), 1818–1822. <http://doi.org/10.1126/science.1095833>
- Alley, S. C., Okeley, N. M., & Senter, P. D. (2010). Antibody-drug conjugates: Targeted drug delivery for cancer. *Current Opinion in Chemical Biology*. <http://doi.org/10.1016/j.cbpa.2010.06.170>
- Amiji, M. M. (Ed.). (2006). *Nanotechnology for Cancer Therapy*. CRC Press. Retrieved from <https://books.google.com/books?hl=pt-PT&lr=&id=y9TLBQAAQBAJ&pgis=1>
- Arcamone, F., Cassinelli, G., Fantini, G., Grein, A., Orezzi, P., Pol, C., & Spalla, C. (2000). Adriamycin, 14-hydroxydaunomycin, a new antitumor antibiotic from *S. peucetius* var. *caesius*. *Biotechnology and Bioengineering*, *67*(6), 704–713. [http://doi.org/10.1002/\(SICI\)1097-0290\(20000320\)67:6<704::AID-BIT8>3.0.CO;2-L](http://doi.org/10.1002/(SICI)1097-0290(20000320)67:6<704::AID-BIT8>3.0.CO;2-L)
- Aruffo, A., Stamenkovic, I., Melnick, M., Underhill, C. B., & Seed, B. (1990). CD44 is the principal cell surface receptor for hyaluronate. *Cell*, *61*(7), 1303–1313. [http://doi.org/10.1016/0092-8674\(90\)90694-A](http://doi.org/10.1016/0092-8674(90)90694-A)
- Aubel-Sadron, G., & Londos-Gagliardi, D. (1984). Daunorubicin and doxorubicin, anthracycline antibiotics, a physicochemical and biological review. *Biochimie*, *66*(5), 333–52. [http://doi.org/http://dx.doi.org/10.1016/0300-9084\(84\)90018-X](http://doi.org/http://dx.doi.org/10.1016/0300-9084(84)90018-X)
- Bawarski, W. E., Chidlow, E., Bharali, D. J., & Mousa, S. A. (2008). Emerging nanopharmaceuticals. *Nanomedicine: Nanotechnology, Biology, and Medicine*. <http://doi.org/10.1016/j.nano.2008.06.002>
- Berthiaume, J. M., & Wallace, K. B. (2007). Adriamycin-induced oxidative mitochondrial cardiotoxicity. *Cell Biology and Toxicology*, *23*(1), 15–25. <http://doi.org/10.1007/s10565-006-0140-y>
- Bildstein, L., Dubernet, C., & Couvreur, P. (2011). Prodrug-based intracellular delivery of anticancer agents. *Advanced Drug Delivery Reviews*. <http://doi.org/10.1016/j.addr.2010.12.005>
- Boeckel, D. G., Shinkai, R. S. A., Grossi, M. L., & Teixeira, E. R. (2014). In vitro evaluation of cytotoxicity of hyaluronic acid as an extracellular matrix on OFCOL II cells by the MTT assay. *Oral Surgery, Oral Medicine, Oral Pathology and Oral Radiology*, *117*(6). <http://doi.org/10.1016/j.oooo.2012.07.486>
- Borst, P., Evers, R., Kool, M., & Wijnholds, J. (2000). A family of drug transporters: the multidrug resistance-associated proteins. *Journal of the National Cancer Institute*, *92*(16), 1295–1302. <http://doi.org/10.1093/jnci/92.16.1295>
- Bourguignon, L. Y. W. (2001). CD44-mediated oncogenic signaling and cytoskeleton activation during mammary tumor progression. *Journal of Mammary Gland Biology and Neoplasia*. <http://doi.org/10.1023/A:1011371523994>
- Carvalho, V., Castanheira, P., Faria, T. Q., Gonçalves, C., Madureira, P., Faro, C., ... Gama, M. (2010). Biological activity of heterologous murine interleukin-10 and preliminary studies on the use of a dextrin nanogel as a delivery system. *International Journal of Pharmaceutics*, *400*(1-2), 234–42. <http://doi.org/10.1016/j.ijpharm.2010.08.040>
- Champion, J. A., & Mitragotri, S. (2006). Role of target geometry in phagocytosis. *Proceedings of the National Academy of Sciences of the United States of America*, *103*(13), 4930–4934. <http://doi.org/10.1073/pnas.0600997103>
- Chen, S., Wang, L., Duce, S. L., Brown, S., Lee, S., Melzer, A., ... André, P. (2010). Engineered biocompatible nanoparticles for in vivo imaging applications. *Journal of the American Chemical Society*, *132*(42), 15022–15029. <http://doi.org/10.1021/ja106543j>
- Cheng, R., Meng, F., Deng, C., Klok, H.-A., & Zhong, Z. (2013). Dual and multi-stimuli responsive polymeric nanoparticles for programmed site-specific drug delivery. *Biomaterials*, *34*(14), 3647–57. <http://doi.org/10.1016/j.biomaterials.2013.01.084>
- Choi, K. Y., Saravanakumar, G., Park, J. H., & Park, K. (2012). Hyaluronic acid-based nanocarriers for intracellular targeting: Interfacial interactions with proteins in cancer. *Colloids and Surfaces B: Biointerfaces*, *99*, 82–94. <http://doi.org/10.1016/j.colsurfb.2011.10.029>
- Cooper, G. M. (2000). Lysosomes.
- Davis, M. E., Chen, Z. G., & Shin, D. M. (2008). Nanoparticle therapeutics: an emerging treatment modality for cancer. *Nature Reviews Drug Discovery*, *7*(9), 771–782. <http://doi.org/10.1038/nrd2614>
- Davis, M. E., Zuckerman, J. E., Choi, C. H. J., Seligson, D., Tolcher, A., Alabi, C. A., ... Ribas, A. (2010). Evidence of RNAi in humans from systemically administered siRNA via targeted nanoparticles. *Nature*, *464*(7291), 1067–1070. <http://doi.org/10.1038/nature08956>
- Desai, N. (2012). Challenges in Development of Nanoparticle-Based Therapeutics. *The AAPS Journal*. <http://doi.org/10.1208/s12248-012-9339-4>
- DiMarco, A., Gastani, M., & Scarpinato, B. (1969). Adriamycin: A new antibiotic with antitumor activity. *Cancer Chemotherapy Reports*.
- Duan, X., & Li, Y. (2013). Physicochemical characteristics of nanoparticles affect circulation, biodistribution, cellular internalization, and trafficking. *Small*. <http://doi.org/10.1002/smll.201201390>

- FDA Approval for Paclitaxel Albumin-stabilized Nanoparticle Formulation - National Cancer Institute. (n.d.). Retrieved June 26, 2015, from <http://www.cancer.gov/about-cancer/treatment/drugs/fda-nanoparticle-paclitaxel>
- Frederick, C. a, Williams, L. D., Ughetto, G., van der Marel, G. a, van Boom, J. H., Rich, a, & Wang, a H. (1990). Structural comparison of anticancer drug-DNA complexes: adriamycin and daunomycin. *Biochemistry*, *29*(10), 2538–2549. <http://doi.org/10.1021/bi00462a016>
- Fu, C., Li, H., Li, N., Miao, X., Xie, M., Du, W., & Zhang, L.-M. (2015). Conjugating an anticancer drug onto thiolated hyaluronic acid by acid liable hydrazone linkage for its gelation and dual stimuli-response release. *Carbohydrate Polymers*, *128*, 163–70. <http://doi.org/10.1016/j.carbpol.2015.04.024>
- Gaucher, G., Satturwar, P., Jones, M.-C., Furtos, A., & Leroux, J.-C. (2010). Polymeric micelles for oral drug delivery. *European Journal of Pharmaceutics and Biopharmaceutics: Official Journal of Arbeitsgemeinschaft Für Pharmazeutische Verfahrenstechnik e.V.*, *76*(2), 147–58. <http://doi.org/10.1016/j.ejpb.2010.06.007>
- Geng, Y., Dalhaimer, P., Cai, S., Tsai, R., Tewari, M., Minko, T., & Discher, D. E. (2007). Shape effects of filaments versus spherical particles in flow and drug delivery. *Nature Nanotechnology*, *2*(4), 249–255. <http://doi.org/10.1038/nnano.2007.70>
- Geraldes, C. F. G. C., & Laurent, S. Classification and basic properties of contrast agents for magnetic resonance imaging. *Contrast Media & Molecular Imaging*, *4*(1), 1–23. <http://doi.org/10.1002/cmimi.265>
- Germann, U. A. (1996). P-glycoprotein—a mediator of multidrug resistance in tumour cells. *European Journal of Cancer (Oxford, England: 1990)*, *32A*(6), 927–44. Retrieved from <http://www.ncbi.nlm.nih.gov/pubmed/8763334>
- Gillies, E. R., & Fréchet, J. M. J. (2005). pH-responsive copolymer assemblies for controlled release of doxorubicin. *Bioconjugate Chemistry*, *16*(2), 361–368. <http://doi.org/10.1021/bc049851c>
- Gonçalves, C., Ferreira, M. F. M., Santos, A. C., Prata, M. I. M., Geraldes, C. F. G. C., Martins, J. A., & Gama, F. M. (2010). Studies on the biodistribution of dextrin nanoparticles. *Nanotechnology*, *21*(29), 295103. <http://doi.org/10.1088/0957-4484/21/29/295103>
- Gonçalves, C., & Gama, F. M. (2008). Characterization of the self-assembly process of hydrophobically modified dextrin. *European Polymer Journal*, *44*(11), 3529–3534. <http://doi.org/10.1016/j.eurpolymj.2008.08.034>
- Gonçalves, C., Lalatonne, Y., Melro, L., Badino, G., Ferreira, M. F. M., David, L., ... Gama, F. M. (2013). New dextrin nanomagnetogels as contrast agents for magnetic resonance imaging. *Journal of Materials Chemistry B*, *1*(42), 5853. <http://doi.org/10.1039/c3tb21063d>
- Gonçalves, C., Martins, J. A., & Gama, F. M. (2007). Self-assembled nanoparticles of dextrin substituted with hexadecanethiol. *Biomacromolecules*, *8*(2), 392–8. <http://doi.org/10.1021/bm060993e>
- Gonçalves, C., Pereira, P., Schelleberg, P., Coutinho, P., & Gama, F. M. (2012). Self-assembled dextrin nanogel as curcumin delivery system. Retrieved July 2, 2015, from <http://www.ceb.uminho.pt/funcarb/Publications/Details/9174>
- Gonçalves, C., Torrado, E., Martins, T., Pereira, P., Pedrosa, J., & Gama, M. (2010). Dextrin nanoparticles: studies on the interaction with murine macrophages and blood clearance. *Colloids and Surfaces. B, Biointerfaces*, *75*(2), 483–9. <http://doi.org/10.1016/j.colsurfb.2009.09.024>
- Goodison, S., Urquidi, V., & Tarin, D. (1999). CD44 cell adhesion molecules. *Mol.Pathol.*, *52*(1366-8714 SB - IM), 189–196.
- Gottesman, M. M., & Pastan, I. (1993). Biochemistry of multidrug resistance mediated by the multidrug transporter. *Annual Review of Biochemistry*, *62*, 385–427. <http://doi.org/10.1146/annurev.bi.62.070193.002125>
- HANAHAN, D. (2000). The Hallmarks of Cancer. *Cell*, *100*(1), 57–70. [http://doi.org/10.1016/S0092-8674\(00\)81683-9](http://doi.org/10.1016/S0092-8674(00)81683-9)
- Hanahan, D., & Weinberg, R. A. (2011). Hallmarks of cancer: The next generation. *Cell*. <http://doi.org/10.1016/j.cell.2011.02.013>
- Hermanson, G. T. (2013). *Bioconjugate Techniques*. *Bioconjugate Techniques*. <http://doi.org/10.1016/B978-0-12-382239-0.00004-2>
- Herrlich, P., Morrison, H., Sleeman, J., Orian-Rousseau, V., König, H., Weg-Remers, S., & Ponta, H. (2000). CD44 acts both as a growth- and invasiveness-promoting molecule and as a tumor-suppressing cofactor. *Annals of the New York Academy of Sciences*, *910*, 106–118; discussion 118–120.
- Hillaireau, H., & Couvreur, P. (2009). Nanocarriers' entry into the cell: Relevance to drug delivery. *Cellular and Molecular Life Sciences*. <http://doi.org/10.1007/s00018-009-0053-z>
- Hong, S., Leroueil, P. R., Majoros, I. J., Orr, B. G., Baker, J. R., & Banaszak Holl, M. M. (2007). The Binding Avidity of a Nanoparticle-Based Multivalent Targeted Drug Delivery Platform. *Chemistry and Biology*, *14*(1), 107–115. <http://doi.org/10.1016/j.chembiol.2006.11.015>
- Hrkach, J., Von Hoff, D., Ali, M. M., Andrianova, E., Auer, J., Campbell, T., ... Zale, S. (2012). Preclinical Development and Clinical Translation of a PSMA-Targeted Docetaxel Nanoparticle with a Differentiated Pharmacological Profile. *Science Translational Medicine*. <http://doi.org/10.1126/scitranslmed.3003651>
- Jain, R. K. (1987). Transport of molecules across tumor vasculature. *CANCER AND METASTASIS REVIEW*, *6*(4), 559–593. <http://doi.org/10.1007/BF00047468>
- Jain, R. K., & Stylianopoulos, T. (2010). Delivering nanomedicine to solid tumors. *Nature Reviews. Clinical Oncology*, *7*(11), 653–664. <http://doi.org/10.1038/nrclinonc.2010.139>

- Kaya, G., Rodriguez, I., Jorcano, J. L., Vassalli, P., & Stamenkovic, I. (1997). Selective suppression of CD44 in keratinocytes of mice bearing an antisense CD44 transgene driven by a tissue-specific promoter disrupts hyaluronate metabolism in the skin and impairs keratinocyte proliferation. *Genes and Development*, *11*(8), 996–1007. <http://doi.org/10.1101/gad.11.8.996>
- Kim, D., Yu, M. K., Lee, T. S., Park, J. J., Jeong, Y. Y., & Jon, S. (2011). Amphiphilic polymer-coated hybrid nanoparticles as CT/MRI dual contrast agents. *Nanotechnology*, *22*(15), 155101. <http://doi.org/10.1088/0957-4484/22/15/155101>
- Kim, S. W., Oh, K. T., Youn, Y. S., & Lee, E. S. (2014). Hyaluronated nanoparticles with pH- and enzyme-responsive drug release properties. *Colloids and Surfaces B: Biointerfaces*, *116*, 359–364. <http://doi.org/10.1016/j.colsurfb.2014.01.017>
- Kratz, F. (2007). DOXO-EMCH (INNO-206): the first albumin-binding prodrug of doxorubicin to enter clinical trials. *Expert Opinion on Investigational Drugs*, *16*(6), 855–866. <http://doi.org/10.1517/13543784.16.6.855>
- Kratz, F. (2008). Albumin as a drug carrier: Design of prodrugs, drug conjugates and nanoparticles. *Journal of Controlled Release*, *132*(3), 171–183. <http://doi.org/10.1016/j.jconrel.2008.05.010>
- Kunze, R., R?ssler, M., M?ller, S., Schnabelrauch, M., Riemer, T., Hempel, U., & Dieter, P. (2010). Sulfated hyaluronan derivatives reduce the proliferation rate of primary rat calvarial osteoblasts. *Glycoconjugate Journal*, *27*(1), 151–158. <http://doi.org/10.1007/s10719-009-9270-9>
- Lalatonne, Y., Monteil, M., Jouni, H., Serfaty, J. M., Sainte-Catherine, O., Lièvre, N., ... Motte, L. (2010). Superparamagnetic bifunctional bisphosphonates nanoparticles: a potential MRI contrast agent for osteoporosis therapy and diagnostic. *Journal of Osteoporosis*, *2010*, 747852. <http://doi.org/10.4061/2010/747852>
- Lammers, T., Aime, S., Hennink, W. E., Storm, G., & Kiessling, F. (2011). Theranostic nanomedicine. *Accounts of Chemical Research*, *44*(10), 1029–1038. <http://doi.org/10.1021/ar200019c>
- Lammers, T., Hennink, W. E., & Storm, G. (2008). Tumour-targeted nanomedicines: principles and practice. *British Journal of Cancer*, *99*(3), 392–397. <http://doi.org/10.1038/sj.bjc.6604483>
- Lammers, T., Kiessling, F., Hennink, W. E., & Storm, G. (2010). Nanotheranostics and image-guided drug delivery: Current concepts and future directions. *Molecular Pharmaceutics*. <http://doi.org/10.1021/mp100228v>
- Lammers, T., Kiessling, F., Hennink, W. E., & Storm, G. (2012). Drug targeting to tumors: Principles, pitfalls and (pre-) clinical progress. *Journal of Controlled Release*. <http://doi.org/10.1016/j.jconrel.2011.09.063>
- Laurent, S., Forge, D., Port, M., Roch, A., Robic, C., Vander Elst, L., & Muller, R. N. (2008). Magnetic iron oxide nanoparticles: synthesis, stabilization, vectorization, physicochemical characterizations, and biological applications. *Chemical Reviews*, *108*(6), 2064–110. <http://doi.org/10.1021/cr068445e>
- Lin, C.-A. J., Sperling, R. A., Li, J. K., Yang, T.-Y., Li, P.-Y., Zanella, M., ... Parak, W. J. (2008). Design of an amphiphilic polymer for nanoparticle coating and functionalization. *Small (Weinheim an Der Bergstrasse, Germany)*, *4*(3), 334–41. <http://doi.org/10.1002/smll.200700654>
- Liu, Y., Sun, J., Zhang, P., & He, Z. (2011). Amphiphilic polysaccharide-hydrophobicized graft polymeric micelles for drug delivery nanosystems. *Current Medicinal Chemistry*, *18*(17), 2638–48. Retrieved from <http://www.ncbi.nlm.nih.gov/pubmed/21568897>
- Maeda, H. (2001a). SMANCS and polymer-conjugated macromolecular drugs: Advantages in cancer chemotherapy. *Advanced Drug Delivery Reviews*. [http://doi.org/10.1016/S0169-409X\(00\)00134-4](http://doi.org/10.1016/S0169-409X(00)00134-4)
- Maeda, H. (2001b). The enhanced permeability and retention (EPR) effect in tumor vasculature: The key role of tumor-selective macromolecular drug targeting. *Advances in Enzyme Regulation*, *41*, 189–207. [http://doi.org/10.1016/S0065-2571\(00\)00013-3](http://doi.org/10.1016/S0065-2571(00)00013-3)
- Maeda, H., & Matsumura, Y. (1989). Tumorotropic and lymphotropic principles of macromolecular drugs. *Critical Reviews in Therapeutic Drug Carrier Systems*, *6*(3), 193–210.
- Maejima, Y., Adachi, S., Ito, H., Hirao, K., & Isobe, M. (2008). Induction of premature senescence in cardiomyocytes by doxorubicin as a novel mechanism of myocardial damage. *Aging Cell*, *7*(2), 125–136. <http://doi.org/10.1111/j.1474-9726.2007.00358.x>
- Malam, Y., Loizidou, M., & Seifalian, A. M. (2009). Liposomes and nanoparticles: nanosized vehicles for drug delivery in cancer. *Trends in Pharmacological Sciences*. <http://doi.org/10.1016/j.tips.2009.08.004>
- Marnett, L. J. (2002). Oxy radicals, lipid peroxidation and DNA damage. *Toxicology*, *181-182*, 219–222. [http://doi.org/10.1016/S0300-483X\(02\)00448-1](http://doi.org/10.1016/S0300-483X(02)00448-1)
- McLendon, R., Friedman, A., Bigner, D., Van Meir, E. G., Brat, D. J., M. Mastrogiannis, G., ... Thomson, E. (2008). Comprehensive genomic characterization defines human glioblastoma genes and core pathways. *Nature*. <http://doi.org/10.1038/nature07385>
- Merbach, A. S., Helm, L., & Tóth, E. (2013). *The Chemistry of Contrast Agents in Medical Magnetic Resonance Imaging*. (A. S. Merbach, L. Helm, & E. Tóth, Eds.) (2nd editio). John Wiley & Sons, Inc.
- Mindell, J. A. (2012). Lysosomal Acidification Mechanisms*. <http://dx.doi.org/10.1146/annurev-Physiol-012110-142317>
- Minotti, G., Menna, P., Salvatorelli, E., Cairo, G., & Gianni, L. (2004). Anthracyclines: molecular advances and pharmacologic developments in antitumor activity and cardiotoxicity. *Pharmacological Reviews*, *56*(2), 185–229.

<http://doi.org/10.1124/pr.56.2.6>

- Minotti, G., Ronchi, R., Salvatorelli, E., Menna, P., & Cairo, G. (2001). Doxorubicin irreversibly inactivates iron regulatory proteins 1 and 2 in cardiomyocytes: Evidence for distinct metabolic pathways and implications for iron-mediated cardiotoxicity of antitumor therapy. *Cancer Research*, *61*(23), 8422–8428.
- Mizrahy, S., Raz, S. R., Hasgaard, M., Liu, H., Soffer-Tsur, N., Cohen, K., ... Peer, D. (2011). Hyaluronan-coated nanoparticles: the influence of the molecular weight on CD44-hyaluronan interactions and on the immune response. *Journal of Controlled Release: Official Journal of the Controlled Release Society*, *156*(2), 231–8. <http://doi.org/10.1016/j.jconrel.2011.06.031>
- Mohan, P., & Rapoport, N. (2010). Doxorubicin as a molecular nanotheranostic agent: Effect of doxorubicin encapsulation in micelles or nanoemulsions on the ultrasound-mediated intracellular delivery and nuclear trafficking. *Molecular Pharmaceutics*, *7*(6), 1959–1973. <http://doi.org/10.1021/mp100269f>
- Mosmann, T. (1983). Rapid colorimetric assay for cellular growth and survival: application to proliferation and cytotoxicity assays. *Journal of Immunological Methods*, *65*(1-2), 55–63. Retrieved from <http://www.ncbi.nlm.nih.gov/pubmed/6606682>
- Naor, D., Nedvetzki, S., Golan, I., Melnik, L., & Faitelson, Y. (2002). CD44 in cancer. *Critical Reviews in Clinical Laboratory Sciences*, *39*(6), 527–579. <http://doi.org/10.1080/10408360290795574>
- Nasongkla, N., Bey, E., Ren, J., Ai, H., Khemtong, C., Guthi, J. S., ... Gao, J. (2006). Multifunctional polymeric micelles as cancer-targeted, MRI-ultrasensitive drug delivery systems. *Nano Letters*, *6*(11), 2427–30. <http://doi.org/10.1021/nl061412u>
- Oh, J. K., Drumright, R., Siegwart, D. J., & Matyjaszewski, K. (2008). The development of microgels/nanogels for drug delivery applications. *Progress in Polymer Science (Oxford)*. <http://doi.org/10.1016/j.progpolymsci.2008.01.002>
- Oudshoorn, M. H. M., Rissmann, R., Bouwstra, J. A., & Hennink, W. E. (2007). Synthesis of methacrylated hyaluronic acid with tailored degree of substitution. *Polymer*, *48*(7), 1915–1920. <http://doi.org/10.1016/j.polymer.2007.01.068>
- Park, H.-K., Lee, S. J., Oh, J.-S., Lee, S.-G., Jeong, Y.-I., & Lee, H. C. (2015). Smart Nanoparticles Based on Hyaluronic Acid for Redox-Responsive and CD44 Receptor-Mediated Targeting of Tumor. *Nanoscale Research Letters*, *10*(1), 981. <http://doi.org/10.1186/s11671-015-0981-5>
- Park, J. H., Von Maltzahn, G., Zhang, L., Schwartz, M. P., Ruoslahti, E., Bhatia, S. N., & Sailor, M. J. (2008). Magnetic iron oxide nanoworms for tumor targeting and imaging. *Advanced Materials*, *20*(9), 1630–1635. <http://doi.org/10.1002/adma.200800004>
- Park, J., Yu, M. K., Jeong, Y. Y., Kim, J. W., Lee, K., Phan, V. N., & Jon, S. (2009). Antibiofouling amphiphilic polymer-coated superparamagnetic iron oxide nanoparticles: synthesis, characterization, and use in cancer imaging in vivo. *Journal of Materials Chemistry*, *19*(35), 6412–6417. Retrieved from <Go to ISI>://000269289300024
- Patil, R., Portilla-Arias, J., Ding, H., Konda, B., Rekechenetskiy, A., Inoue, S., ... Ljubimova, J. Y. (2012). Cellular delivery of doxorubicin via pH-controlled hydrazone linkage using multifunctional nano vehicle based on poly(L-malic acid). *International Journal of Molecular Sciences*, *13*(9), 11681–11693. <http://doi.org/10.3390/ijms130911681>
- Pedrosa, S. S., Gonçalves, C., David, L., & Gama, M. (2014). A Novel Crosslinked Hyaluronic Acid Nanogel for Drug Delivery. *Macromolecular Bioscience*. <http://doi.org/10.1002/mabi.201400135>
- Pedrosa, S. S., Pereira, P., Correia, A., Moreira, S., Rocha, H., & Gama, F. M. (2016). Biocompatibility of a Self-Assembled Crosslinkable Hyaluronic Acid Nanogel. *Macromolecular Bioscience*. <http://doi.org/10.1002/mabi.201600221>
- Peer, D., Karp, J. M., Hong, S., Farokhzad, O. C., Margalit, R., & Langer, R. (2007). Nanocarriers as an emerging platform for cancer therapy. *Nature Nanotechnology*, *2*(12), 751–760. <http://doi.org/10.1038/nnano.2007.387>
- Pilloni, A., & Bernard, G. W. (1998). The effect of hyaluronan on mouse intramembranous osteogenesis in vitro. *Cell and Tissue Research*, *294*(2), 323–333. <http://doi.org/10.1007/s004410051182>
- Ponta, H., Sherman, L., & Herrlich, P. A. (2003). CD44: from adhesion molecules to signalling regulators. *Nature Reviews. Molecular Cell Biology*, *4*(1), 33–45. <http://doi.org/10.1038/nrm1004>
- Reichert, J. M. (2008). Monoclonal antibodies as innovative therapeutics. *Current Pharmaceutical Biotechnology*, *9*(6), 423–430. <http://doi.org/10.2174/138920108786786358>
- Schipper, M. L., Iyer, G., Koh, A. L., Cheng, Z., Ebenstein, Y., Aharoni, A., ... Gambhir, S. S. (2009). Particle size, surface coating, and PEGylation influence the biodistribution of quantum dots in living mice. *Small (Weinheim an Der Bergstrasse, Germany)*, *5*(1), 126–34. <http://doi.org/10.1002/smll.200800003>
- Seymour, L. W., Duncan, R., Strohm, J., & Kopecek, J. (1987). Effect of molecular weight (Mw) of N-(2-hydroxypropyl)methacrylamide copolymers on body distribution and rate of excretion after subcutaneous, intraperitoneal, and intravenous administration to rats. *Journal of Biomedical Materials Research*, *21*(11), 1341–1358. <http://doi.org/10.1002/jbm.820211106>
- Silva, J. P., Gonçalves, C., Costa, C., Sousa, J., Silva-Gomes, R., Castro, A. G., ... Gama, F. M. (2016). Delivery of LLKKK18 loaded into self-assembling hyaluronic acid nanogel for tuberculosis treatment. *Journal of Controlled Release*, *235*, 112–124. <http://doi.org/10.1016/j.jconrel.2016.05.064>
- Stamenkovic, I., Amiot, M., Pesando, J. M., & Seed, B. (1989). A lymphocyte molecule implicated in lymph node homing is a

- member of the cartilage link protein family. *Cell*, 56(6), 1057–1062. [http://doi.org/10.1016/0092-8674\(89\)90638-7](http://doi.org/10.1016/0092-8674(89)90638-7)
- Stern, R. (2004). Hyaluronan catabolism: a new metabolic pathway. *European Journal of Cell Biology*, 83(7), 317–325. <http://doi.org/10.1078/0171-9335-00392>
- Sun, D. (2010). Nanotheranostics: integration of imaging and targeted drug delivery. *Molecular Pharmaceutics*, 7(6), 1879. <http://doi.org/10.1021/mp1003652>
- Thorne, R. F., Legg, J. W., & Isacke, C. M. (2004). The role of the CD44 transmembrane and cytoplasmic domains in coordinating adhesive and signalling events. *Journal of Cell Science*, 117(Pt 3), 373–380. <http://doi.org/10.1242/jcs.00954>
- Toole, B. P. (2002). Hyaluronan promotes the malignant phenotype. *Glycobiology*, 12(3), 37R–42R. <http://doi.org/10.1093/glycob/12.3.37R>
- Toole, B. P. (2004). Hyaluronan: from extracellular glue to pericellular cue. *Nature Reviews. Cancer*, 4(7), 528–539. <http://doi.org/10.1038/nrc1391>
- Toole, B. P., & Hascall, V. C. (2002). Hyaluronan and tumor growth. *The American Journal of Pathology*, 161(3), 745–7. [http://doi.org/10.1016/S0002-9440\(10\)64232-0](http://doi.org/10.1016/S0002-9440(10)64232-0)
- Toole, B. P., Wight, T. N., & Tammi, M. I. (2002). Hyaluronan-cell interactions in cancer and vascular disease. *Journal of Biological Chemistry*. <http://doi.org/10.1074/jbc.R100039200>
- Torchilin, V. P. (2000). Drug targeting. *European Journal of Pharmaceutical Sciences: Official Journal of the European Federation for Pharmaceutical Sciences*, 11 Suppl 2, S81–S91. [http://doi.org/10.1016/S0928-0987\(00\)00166-4](http://doi.org/10.1016/S0928-0987(00)00166-4)
- Torre, L. A., Bray, F., Siegel, R. L., Ferlay, J., Lortet-Tieulent, J., & Jemal, A. (2015). Global cancer statistics, 2012. *CA: A Cancer Journal for Clinicians*, 65(2), 87–108. <http://doi.org/10.3322/caac.21262>
- van Rijt, S. H., Bein, T., & Meiners, S. (2014). Medical nanoparticles for next generation drug delivery to the lungs. *The European Respiratory Journal*, 1–10. <http://doi.org/10.1183/09031936.00212813>
- Venturoli, D., & Rippe, B. (2005). Ficoll and dextran vs. globular proteins as probes for testing glomerular permselectivity: effects of molecular size, shape, charge, and deformability. *American Journal of Physiology. Renal Physiology*, 288(4), F605–F613. <http://doi.org/10.1152/ajprenal.00171.2004>
- Verma, A., & Stellacci, F. (2010). Effect of surface properties on nanoparticle-cell interactions. *Small*. <http://doi.org/10.1002/smll.200901158>
- Wallace, K. B. (2007). Adriamycin-induced interference with cardiac mitochondrial calcium homeostasis. *Cardiovascular Toxicology*, 7(2), 101–7. <http://doi.org/10.1007/s12012-007-0008-2>
- Wang, Y.-X. J. (2011). Superparamagnetic iron oxide based MRI contrast agents: Current status of clinical application. *Quantitative Imaging in Medicine and Surgery*, 1(1), 35–40. <http://doi.org/10.3978/j.issn.2223-4292.2011.08.03>
- Weiner, G. J. (2015). Building better monoclonal antibody-based therapeutics. *Nature Reviews Cancer*, 15(6), 361–370. <http://doi.org/10.1038/nrc3930>
- World Health Organization, N. (2008). *The Global Burden of Disease: 2004 update. Update* (Vol. 2010). Retrieved from http://www.who.int/healthinfo/global_burden_disease/2004_report_update/en/index.html
- Wrobel, N., Schinkinger, M., & Mirsky, V. M. (2002). A novel ultraviolet assay for testing side reactions of carbodiimides. *Analytical Biochemistry*, 305(2), 135–8. <http://doi.org/10.1006/abio.2002.5646>
- Yang, F., Teves, S. S., Kemp, C. J., & Henikoff, S. (2014). Doxorubicin, DNA torsion, and chromatin dynamics. *Biochimica et Biophysica Acta - Reviews on Cancer*. <http://doi.org/10.1016/j.bbcan.2013.12.002>
- Yuan, F. (1998). Transvascular drug delivery in solid tumors. *Seminars in Radiation Oncology*, 8(3), 164–75. Retrieved from <http://www.ncbi.nlm.nih.gov/pubmed/9634493>

SUPPLEMENTARY DATA

- **Production of HA-DOX nanogels**

- DOX Calibration curve

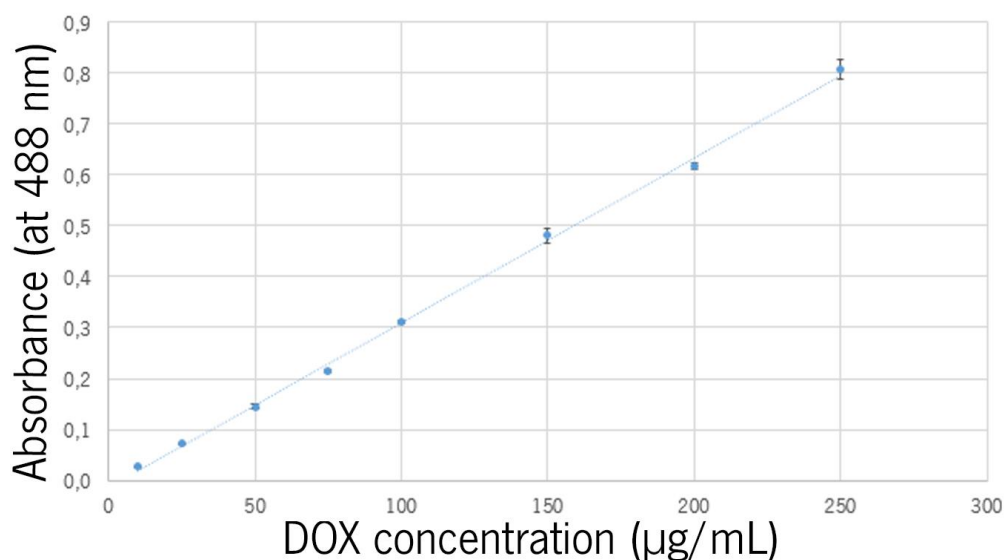


Figure S.1: Calibration curve for DOX dissolved in PBS buffer pH 7.4. Absorbance quantified at 488 nm. The curve obtained is $y = 0.0032x - 0,0135$, associated with a square error of 0.9986.

- Calculations examples I

The example calculation presented here uses HA_{Hidra1} results.

% DOX theoretical was calculated using the relation between the number of DOX moles used in the reaction mixture and the ADH moles presented in the HA. For this quantification the HA moles are multiplied by DS_{ADH} .

$$n_{Dox} = \frac{0.670 * 10^{-3} g}{620.52 g/mol} = 1.67974 * 10^{-6} mol$$

$$n_{ADH} = \frac{15 * 10^{-3} g}{435.41 g/mol} * \left(\frac{8.68}{100}\right) = 2.99029 * 10^{-6} mol$$

$$\% \text{ DOX theoretical } \left(\frac{\text{mol of Dox}}{\text{mol of ADH}} \right) = \frac{1.67974 * 10^{-6} mol}{2.99029 * 10^{-6} mol} * 100 = 36.1 \%$$

% DOX practical was calculated by using the same equations, although it was used the real DOX effectively conjugated to the HA, which was calculated by the amount of DOX present in each mg of NG and the mass of HA recovered, which was used to calculate the moles of ADH.

$$n_{Dox} = \frac{0.621 * 10^{-3} g}{620.52 g/mol} = 1.00122 * 10^{-6} mol$$

$$n_{ADH} = \frac{12.7 * 10^{-3} g}{435.41 g/mol} * \left(\frac{8.68}{100}\right) = 2.53177 * 10^{-6} mol$$

$$\% DOX \text{ practical} \left(\frac{\text{mol of Dox}}{\text{mol of ADH}}\right) = \frac{1.00122 * 10^{-6} mol}{2.53177 * 10^{-6} mol} * 100 = 39.6 \%$$

The Reaction Efficiency was calculated through the relation between % DOX practical and % DOX theoretical.

$$\text{Reaction Efficiency (\%)} = \frac{\% DOX \text{ practical}}{\% DOX \text{ theoretical}} = \frac{39.6}{36.1} * 100 = 109.5 \%$$

○ Calculations examples II

The calculation presented here uses HA_{Aml} results.

% DOX theoretical was obtained by calculating the relation between the moles of DOX used and the moles of free HA that would be able to react, for this it is needed to multiple by 100 less the DS % of the C₁₆NH₂.

$$n_{Dox} = \frac{1.8 * 10^{-3} g}{620.53 g/mol} = 2.90079 * 10^{-6} mol$$

$$n_{HA} = \frac{30 * 10^{-3} g}{426.55 g/mol} * \left(\frac{100 - 10.52}{100}\right) = 6.29325 * 10^{-5} mol$$

$$\% DOX \text{ theoretical} \left(\frac{\text{mol of Dox}}{\text{mol of free HA}}\right) = \frac{2.90079 * 10^{-6} mol}{6.29325 * 10^{-5} mol} * 100 = 4.6\%$$

% DOX practical was calculated using the same equations, although it was used the real DOX effectively conjugated to the HA, which was calculated by the amount of DOX present in each mg of NG and the mass of HA recovered, and the free HA was calculated by the total mass recovered after the process of freeze-dried multiplied by 100 less the DS % of the C₁₆NH₂.

$$n_{Dox} = \frac{0.488 * 10^{-3} g}{620.53 g/mol} = 7.86924 * 10^{-7} mol$$

$$n_{HA} = \frac{21.93 * 10^{-3} g}{426.55 g/mol} * \left(\frac{100 - 10.52}{100}\right) = 4.60039 * 10^{-5} mol$$

$$\% DOX \text{ practical} \left(\frac{\text{mol of Dox}}{\text{mol of free HA}}\right) = \frac{7.86924 * 10^{-7} mol}{4.60039 * 10^{-5} mol} * 100 = 1.7\%$$

The Reaction Efficiency was calculated through the relation between % DOX practical and % DOX theoretical.

$$\text{Reaction Efficiency (\%)} = \frac{\% DOX \text{ practical}}{\% DOX \text{ theoretical}} = \frac{1.7}{4.6} * 100 = 37.1 \%$$

- **Release Studies**

DOX concentration was calculated using the absorbance at 488 nm and the equation presented at **DOX calibration curve** in the **Supplementary Data section**. For each measurement, the volume present inside the dialysis bag was measured, and considering the DOX concentration, the DOX mass was calculated by the following equation:

$$DOX\ mass = DOX\ concentration * Volume$$

After the calculation of the DOX mass present at each time point, the % of cumulative release was quantified through the following equation:

$$\% \text{ of cumulative release} = \left(1 - \frac{m_{DOX\ t_n}}{m_{DOX\ t_0}}\right) * 100,$$

where $m_{DOX\ t_n}$ is the DOX mass in the respective time point, while $m_{DOX\ t_0}$ is the mass of DOX present at the beginning, t_0 , of the release study.

- $\gamma\text{-Fe}_2\text{O}_3$ incorporation

Calibration curve used for the quantification of the Fe incorporation represented in the **Figure**

S.2.

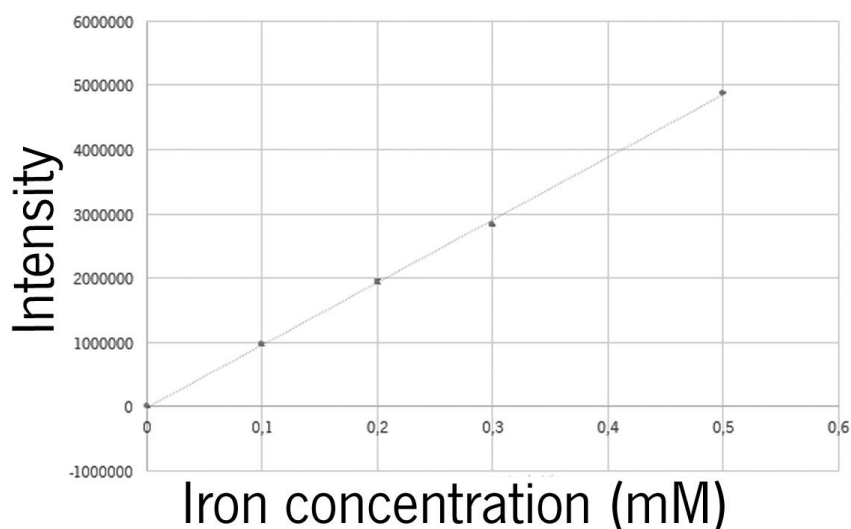


Figure S.2: Calibration curve obtained for Fe dissolved in HNO_3 2%. Absorbance quantified at 260 nm. The curve obtained is $y = 9708192,1x - 12347,638$, associated with a square error of 0.9999.

From the **figure S.2**, it was possible to calculate the iron concentrations for the NG, as presented at **Table S.1**.

Table S.1: Table containing the results for each NG used in the incorporation of the $\gamma\text{-Fe}_2\text{O}_3$.

Material Designation	Intensity	Dilution factor	Iron Concentration (mM)	Standard Deviation
HA _{Hidra3}	575669.09	13,3	0.81	0.02
HA _{Ami2}	270851.42	20	0.58	0.03

The iron concentrations, from the **table S.1**, were obtained by the following equation:

$$\text{Iron concentration (mM)} = \left(\frac{\text{Absorbance} - (-12347,638)}{9708192,1} \right) * \text{dilution factor}$$

- **HA 4.0 kDa**

The reactions performed with the HA 4.0 kDa followed the methods described above, with the exception of temperature, which was 37 °C and the dialysis membrane MWCO, which was 2.0 kDa.

- **Amphiphilic HA**

The synthesis of HA-C₁₆NH₂, using HA 4.0 kDa, was performed for a theoretical DS (%) of 15 % and ¹H RMN was used to quantify the degree of substitution.

The DS_{C₁₆NH₂} (%) obtained for this modification was 11.0 %, and the material was designated HA_{11.0}.

The average size and Pdl were also evaluated over time. The results are presented in the **figure**

S.3.

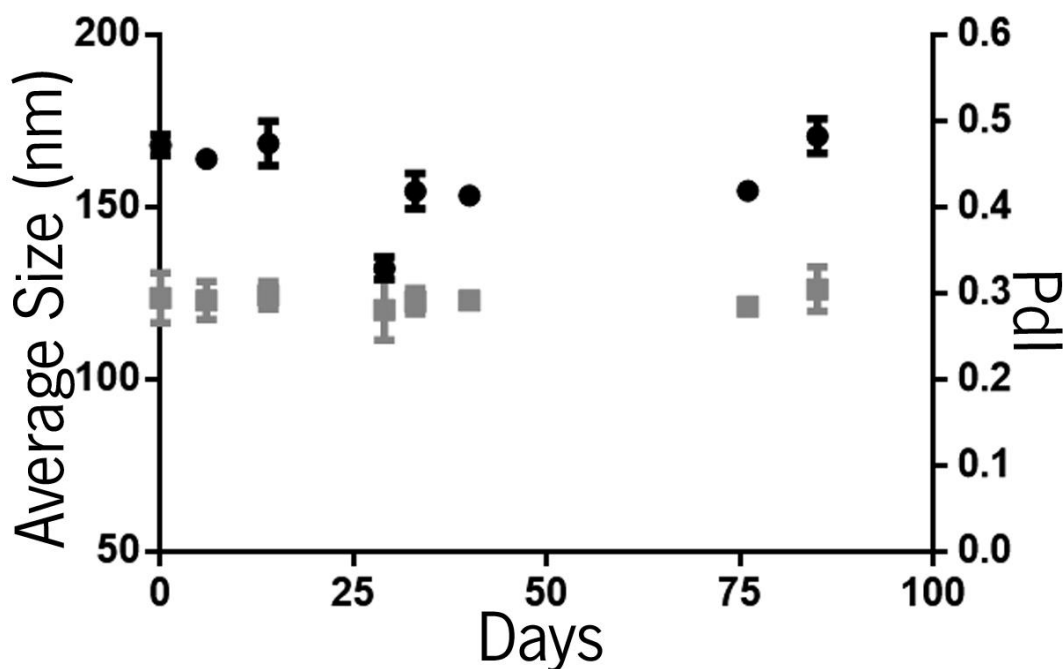


Figure S.3: Average size (●) and Pdl (■) values obtained for HA_{11.0}, over time, with the respective standard deviation (n=10).

HA_{11.0} presents a higher average size when compared to HA_{12.6}, which could be originated by the difference regarding the DS_{C₁₆NH₂} or due to the MW of the HA, although its average size is interesting for DDS (< 200 nm). The HA_{11.0} have an associated Pdl value around 0.3, which is smaller than the one from HA 7.68 kDa, HA_{12.6}.

- **Production of HA-DOX nanogels**

As performed to the HA 7.68 kDa, the conjugation of amphiphilic HA with DOX was performed via hydrazone or amide linkage.

- **Hydrazone Linkage**

As for HA 7.68 kDa, it was required to perform a conjugation between HA_{11.0} and ADH. The grafting of the hydrophobic chain and the respective DS was confirmed by ¹H NMR spectroscopy.

The DS (%) obtained for the HA-ADH was 16.1 %, and the material was designated as HA-ADH_{16.1}. Then it was performed a conjugation with DOX, to obtain an hydrazone linkage (HA_{Hidra4}). The results are presented in the **table S.2**.

Table S.2: Results from the conjugation of HA-ADH with DOX.

	HA _{Hidra4}
DS _{C16NH2} (%)	11,0
DS _{ADH} (%)	16,1
DOX Concentration (µg/mg)	29
% DOX theoretical (mol/mol)	21,7
% DOX real (mol/mol)	13,4
Reaction Efficiency (%)	61,7

Absorbance spectra of HA_{Hidra4}, free DOX (25 µg/mL) and HA-ADH dissolved with 25 µg/mL of DOX (without reaction) are present in **figure S.4**. All materials were dispersed in PBS buffer pH 7.4.

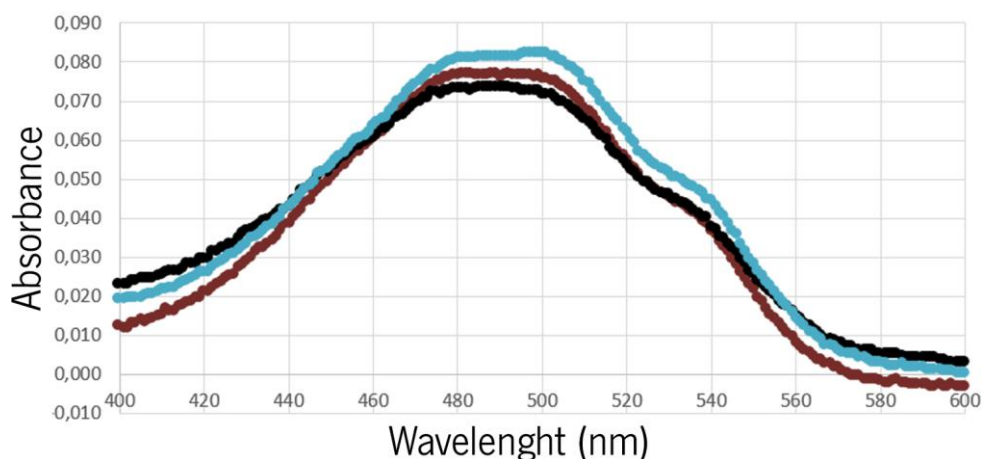


Figure S.4: Absorbance spectra of free DOX at 25 µg/mL (●), HA_{Hidra4} 1.0 mg/mL (●) and HA-ADH 1.0 mg/mL with free DOX at 25 µg/mL (●) when dispersed at PBS buffer pH 7.4.

The DOX concentration obtained was 29 $\mu\text{g}/\text{mg}$, which was higher than the one obtained for the HA_{Hidra3}. The absorbance spectra show that the HA_{Hidra4} presents a peak around 500 nm while maintaining its shoulder at 540 nm, as free DOX or HA-ADH solution with free DOX.

The average size and Pdl over time of this material are shown in **figure S.5**.

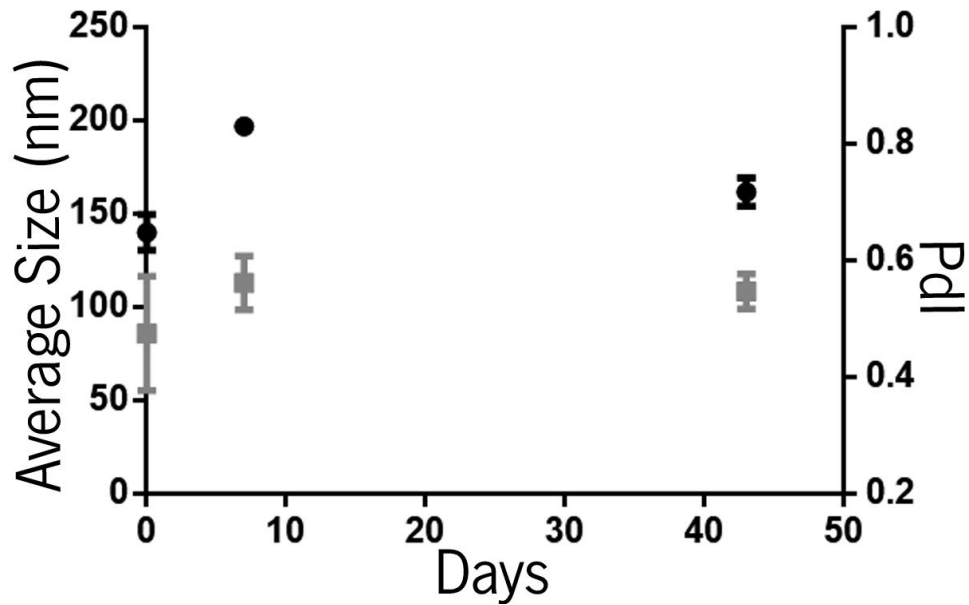


Figure S.5: Average size (●) and Pdl (■) values distribution for HA_{Hidra4}, with the respective standard deviation (n=10).

The HA_{Hidra4} exhibit an average size below 200 nm and Pdl value around 0.6, suggesting that this NG is suitable for the development of DDS, however, more measurements would be required.

➤ Amide Linkage

The DOX grafting was performed directly to the amphiphilic HA between the reaction of amine group in DOX and the carboxyl group present in HA. The results obtained for this reaction (HA_{Ami3}) are presented in **table S.3**.

Table S.3: Different conjugations of amphiphilic HA with DOX.

	HA _{Ami3}
DS _{C₁₆NH₂} (%)	11,0
DOX Concentration (ug/mg)	98,4
% DOX theoretical (mol/mol)	5,2
% DOX real (mol/mol)	7,6
Reaction Efficiency (%)	147,6

Absorbance spectra of HA_{Ami3}, free DOX (150 µg/mL) and HA-C₁₆NH₂ dissolved with 25 µg/mL of free DOX (without reaction) are presented in **figure S6**. All materials were dispersed in PBS buffer pH 7.4.

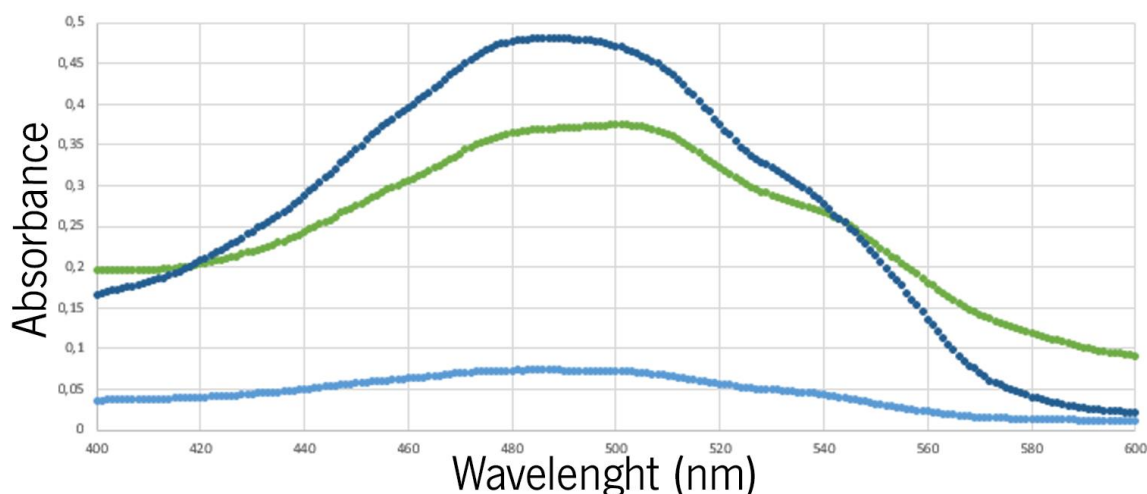


Figure S.6: Absorbance spectra of free DOX at 150 µg/mL (●), HA_{Ami3} (●) and HA-C₁₆NH₂ 1.0 mg/mL with free DOX 25 µg/mL (●) when dispersed at PBS buffer pH 7.4.

HA_{Ami3} presented a higher concentration of DOX grafted in the HA, although the reaction efficiency value is higher than 100 %. This efficiency value was not expected, since it was used a dialysis membrane with a MWCO of 2.0 kDa, that would allow the removal of all free DOX (MW of 620.52). The DOX concentration obtained was 98.4 µg/mg, which was the highest one from all NG produced.

Absorbance spectra show that the HA_{Ami3} presents its peak around 513 nm and its shoulder around 545 nm, while the free DOX and HA-C₁₆NH₂ with free DOX present their peak at 488 nm and a shoulder at 540 nm.

The average size and Pdl over time of this material are shown in **figure S.7**.

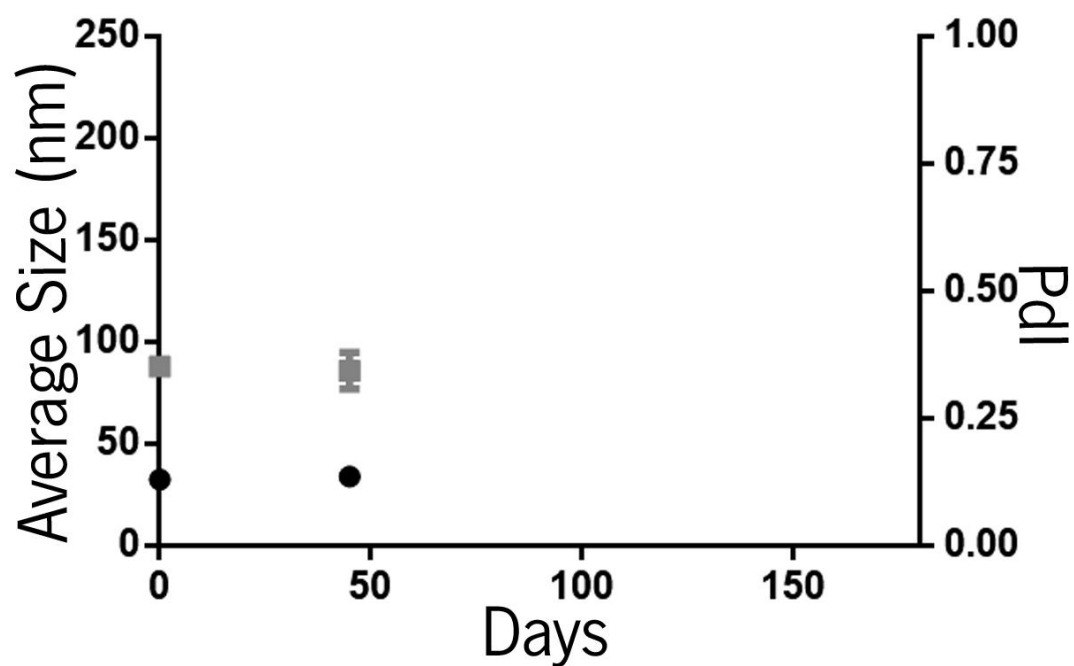


Figure S.7: Average size (●) and Pdl values (■) values distribution for HA_{Ami3}, with the respective standard deviation (n=10).

HA_{Ami3} presents a very interesting average size (< 50 nm), however, more assays should be performed. This NG has a smaller average size and Pdl than the HA_{Ami2} produced with HA 7.68 kDa.

○ Release Studies

The same release study, using the same conditions, was performed for conjugates produced with HA 4.0 kDa. The obtained results are presented in the **figure S.8**.

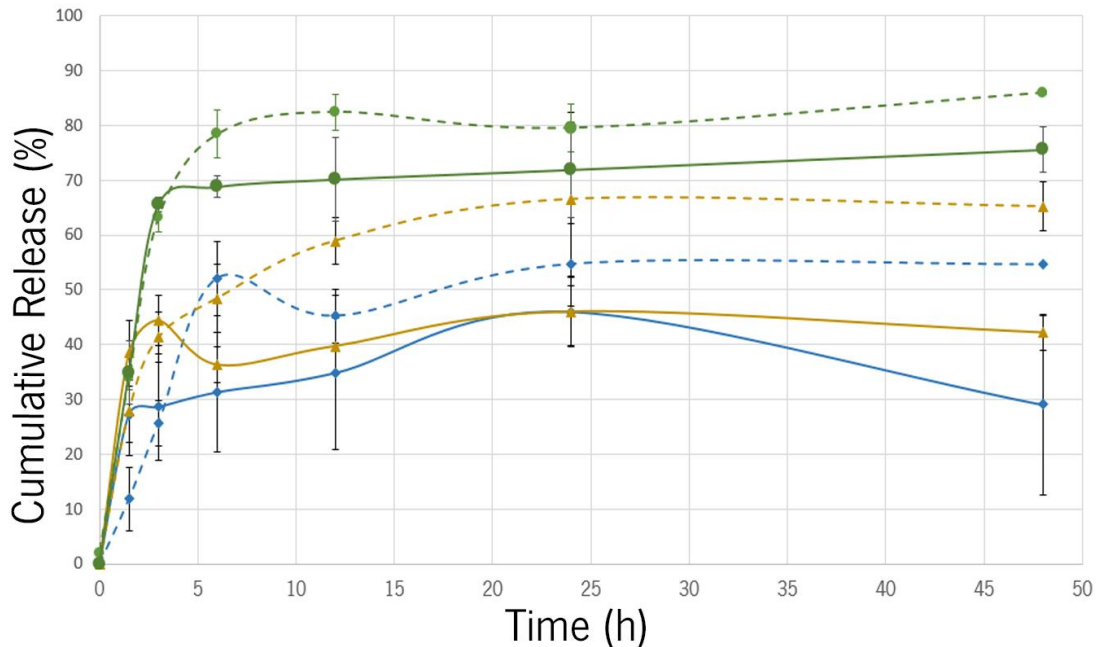


Figure S.8: Cumulative release (%) profiles for HA_{Ami3} (◆), HA_{Hidra4} (▲) and free DOX (●), at pH of 7.4 (solid line) or pH 5.0 (dashed line), (n=3).

The release of free DOX is faster, as in the previous assay.

In this study, the HA_{Hidra4} at pH 5.0 showed higher release than at pH 7.4, as expected due to its labile linkage (Patil et al., 2012). A higher release at pH 5.0 could indicate an effective pH-responsive formulation and more effective, since the release at this pH would occur inside the cells. Comparing different linkages, HA_{Hidra4}, released 65 % of DOX, while HA_{Ami3} released of 55 % after 48h, at pH 5.0. From the literature, different responsive systems, to pH and/or to enzyme, have been developed, as the one developed by *Kim et al.* (Kim, Oh, Youn, & Lee, 2014). For their release study, they associate to the pH 5.0 an enzyme, named hyaluronidase, which cleaves the HA and when used it lead to an increase of the DOX release.

At physiologic pH, both amide and hydrazone linkage presented low release, 27.5 % and 44 % respectively, after 48 h. This is a huger difference compared to free DOX release, and indicate that nanogels could be stable at the extracellular pH, allowing an efficient therapy.

In conclusion, these results suggested that it was possible to produce a pH-sensitive nanogel, HA_{Hidra4}, which present a higher release at pH 5.0 than at pH 7.4, as expected. The produced nanogels affectively decrease the release rate of DOX when compared to free DOX.

○ $\gamma\text{-Fe}_2\text{O}_3$ incorporation

The $\gamma\text{-Fe}_2\text{O}_3$ incorporation was performed as for the HA 7.68 kDa. The results of the iron incorporation in the NG from HA 4 kDa are presented in **figure S.9**.

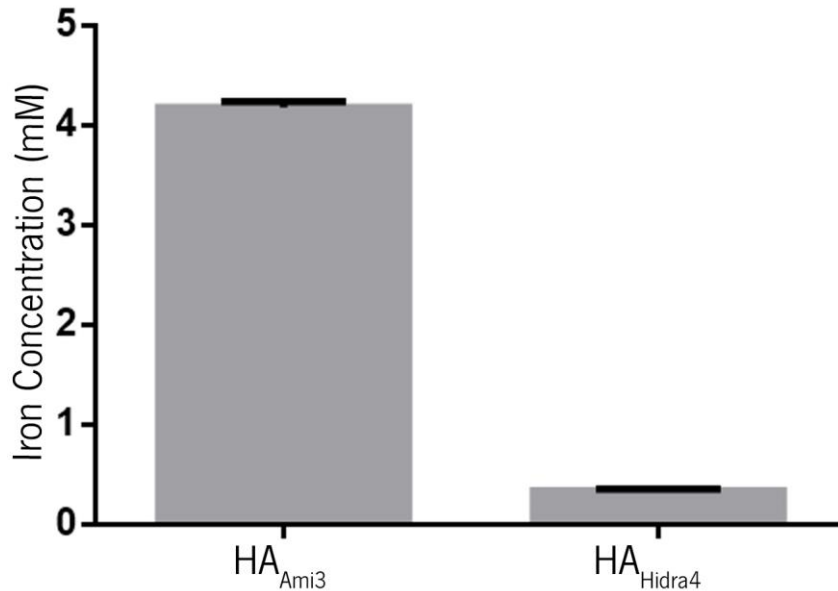


Figure S.9: Results for the iron quantification after $\gamma\text{-Fe}_2\text{O}_3$ incorporation into the different NG using HA 4.0 kDa, with the respective standard deviation (n=6).

HA_{Ami3} exhibited 4.2 mM of $\gamma\text{-Fe}_2\text{O}_3$ incorporated, seven times more than HA_{Ami2} produced with HA 7.68 kDa. On the other hand, HA_{Hidra4} exhibited 0.3 mM, less than the value obtained for HA 7.68 kDa.

For these materials, average size and Pdl values were evaluated. The results are presented at **figure S.10**.

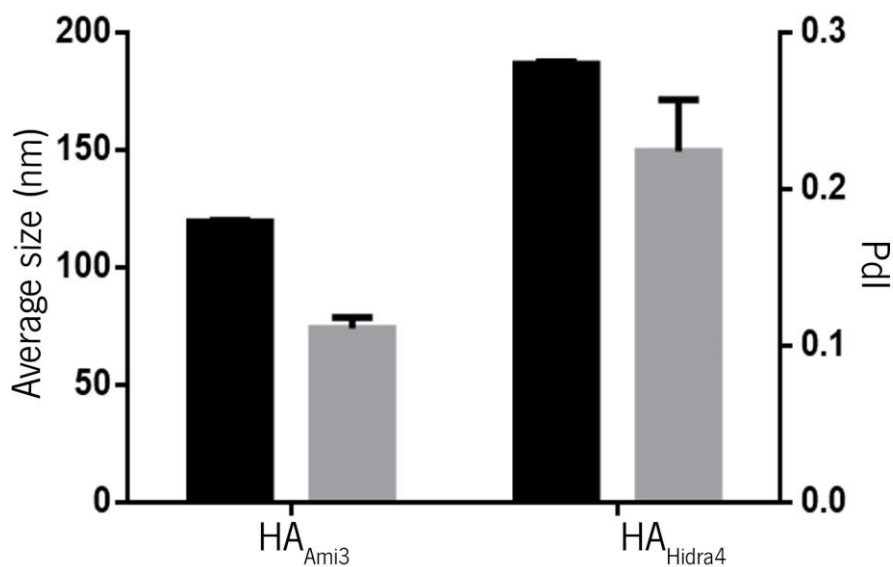


Figure S.10: Average size (■) and Pdl (■) distribution for the nanomagnetogels, with the respective standard deviation (n=5).

Regarding the average size of the nanomagnetogels, HA_{Hidra4} showed a similar average size, while HA_{Ami3} had an increased size. The polydispersity index decreased.

The Zeta Potential was also evaluated for these nanomagnetogels. The results are presented in **figure S.11**.

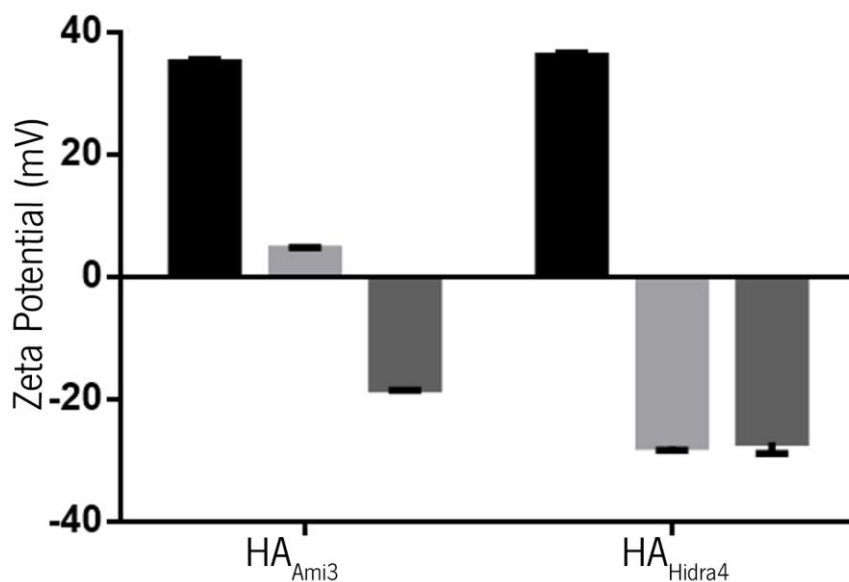


Figure S.11: Results from the Zeta Potential for the free $\gamma\text{-Fe}_2\text{O}_3$ (■), for the nanogel (■) and for the nanomagnetogels (■), each value presents its own standard deviation, (n=5)

The HA_{Ami3} nanogel presents an unexpected positive zeta potential value. All nanomagnetogels present negative zeta potential, as expected.

For HA_{Ami3}, magnetic properties were studied. The results are presented in **figure S.12**.

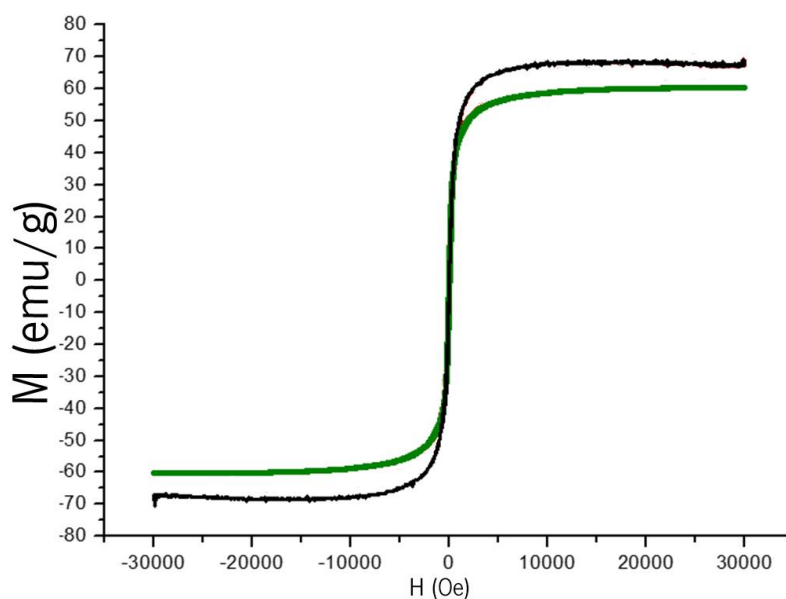


Figure S.12: Magnetization versus magnetic applied field of HA_{Ami3} (■) and free $\gamma\text{-Fe}_2\text{O}_3$ (■). Nanomagnetogel was dispersed in distilled water pH 7.4, while bare $\gamma\text{-Fe}_2\text{O}_3$ in distilled water pH 2.0.

The magnetization result for free $\gamma\text{-Fe}_2\text{O}_3$ was 62 emu/g, while for the nanomagnetogel, HA_{Ami3} was 65 emu/g. The magnetic properties of bare $\gamma\text{-Fe}_2\text{O}_3$ are conserved after their stabilization, since the magnetization profile of bare $\gamma\text{-Fe}_2\text{O}_3$ is similar to the one obtained for HA_{Ami3} , confirming the incorporation of the $\gamma\text{-Fe}_2\text{O}_3$ NPs into the NG, otherwise $\gamma\text{-Fe}_2\text{O}_3$ NPs would not be stable in aqueous solution losing their magnetization profile.

- **Cytotoxicity**

The NG produced from HA 4.0 kDa were incubated with cells in the same conditions that were used for the HA 7.68 kDa. MTT assay was used to evaluate the number of viable cells at each time point. The % cell viability was calculated using equation 4.2 presented before. The results are presented in **figure S.13**.

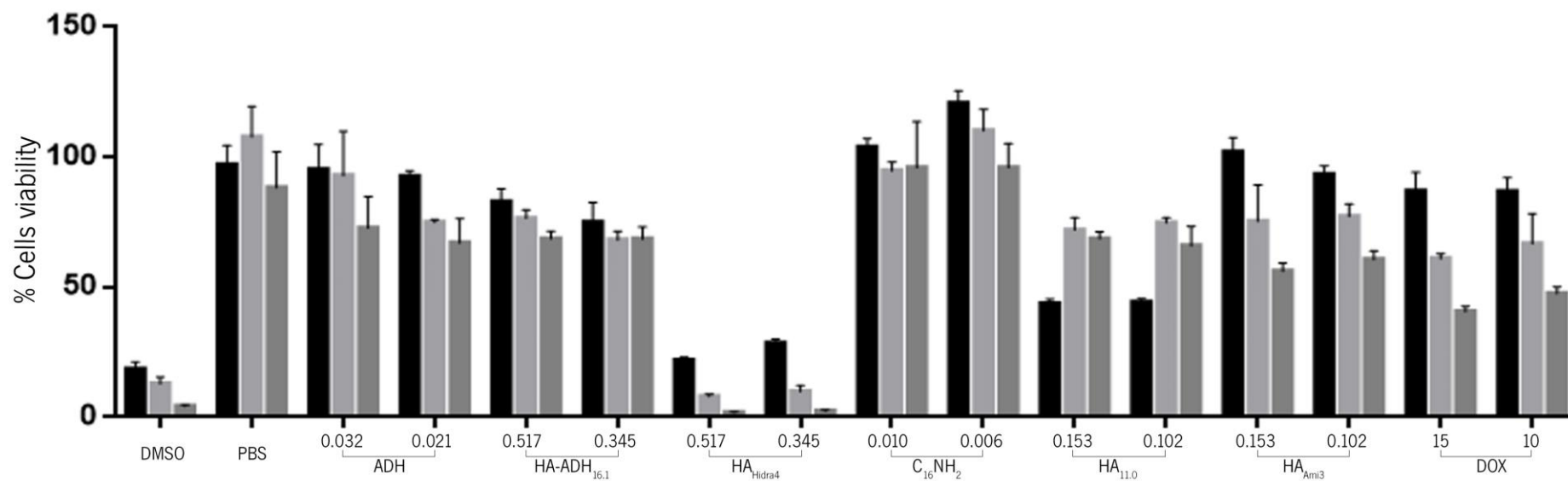


Figure S.13: Cell viability of A549 cells was determined by MTT assay at 24 h (■), 48 h (▒) and 72 h (▓). For all nanogels the concentration is represented in mg/mL while for free DOX is expressed in $\mu\text{g/mL}$.

As for the HA 7.68 kDa assay, PBS, ADH and C₁₆NH₂ controls did not exhibit much influence on cell viability up to 72 h of incubation, revealing % cell viability close to 100 % or superior.

HA_{11.0} presented pronounced toxicity to the A549 cell line at 24 h, 50 % of cell viability, on the other hand, HA-ADH_{16.1} did not present so significant toxicity, since cell viability is higher than 50 % at all time points. Lower cytotoxicity was observed than for HA 7.68 kDa. Free DOX presented a lower cytotoxicity than the one observed for the assay with HA 7.68 kDa, however, it was decreased along time. HA_{Ami3} exhibited low toxicity, although a decrease on the % cell viability was verified. This result was not expected since this nanogel presented the highest DOX grafted. While HA_{Hidra3} exhibit a cytotoxic effect and time-dependent, more pronounced than free DOX in this assay

The cytotoxic results for HA_{Hidra4} supported the ones obtained in the release assay, where HA_{Hidra4} presented the highest release, which could suggest a good therapeutic efficacy.